Leibniz Universität Hannover

B-Spline based Uncertainty Quantification for Stochastic Analysis

Von der Fakultät für Bauingenieurwesen und Geodäsie
der Gottfried Wilhelm Leibniz Universität Hannover
zur Erlangung des Grades

Doktor-Ingenieur
Dr.-Ing.

genehmigte Dissertation von
M. Sc. Christoph Eckert

2022

Referent:	Prof. Dr.-Ing. Michael Beer
Korreferent:	Prof. Dr.-Ing. Dominik Schillinger
Tag der Promotion:	13.12.2021

Kurzfassung

In der modernen Wissenschaft und Technik ist die Berücksichtigung von Unsicherheiten unverzichtbar geworden. Die Forschung im Bereich der Unsicherheitsquantifizierung hat in den letzten Dekaden stark an Bedeutung gewonnen. Dabei stehen im Wesentlich die Identifizierung von unsicheren Quellen, die Bestimmung und Hierachisierung von Unsicherheiten, sowie die Untersuchung ihrer Einflüsse auf Systemantworten im Fokus der Wissenschaftler. Für diesen Zweck eignet sich unter anderem die Polynomial-Chaos-Expansion, die sich als vielseitiges und mächtiges Werkzeug in verschiedenen Forschungsbereichen behauptet hat. In den letzten Jahren wurde die Kombination mit jeglichen Arten von Dimensionsreduktionsmethoden intensiv untersucht und unterstützt so die Verarbeitung von hoch-dimensionalen Eingabegrößen bis heute. Dies wird auch als Fluch der Dimensionen bezeichnet und dessen Aufhebung würde als Meilenstein in der Unsicherheitsquantifizierung gelten.
An diesem Punkt setzt die vorliegende Doktorarbeit an und untersucht Spline-Räume im Bereich der Unsicherheitsquantifizierung, die als natürliche Erweiterung von Polynomen gelten. Die neu entwickelte Methode 'Spline-Chaos', möchte die komplexere, aber dadurch auch flexiblere, Struktur von Splines ausnutzen, um härteren realen Problemen zu begegnen, an denen das Polynomial-Chaos scheitert.
Normalerweise sind die Basen der Poynomial-Chaos-Expansion orthogonale Polynome, die hier durch B-Spline-Basisfunktionen ersetzt werden. Ferner wird die Konvergenz der neuen Methode bewiesen und durch numerische Beispiele unterstrichen, die auf eine Genauigkeitsanalyse mit mehr-dimensionaler Eingabe ausgeweitet werden. Außerdem wird durch das Lösen mehrerer stochastischer Proleme gezeigt, dass das Spline-Chaos eine Verallgemeinerung des Multi-Element-Legendre-Chaos ist und ihr überlegen ist. Schließlich trägt das Spline-Chaos zur Lösung partieller Differentialgleichungen bei und führt zu einer auf dem Galerkin-Ansatz basierenden stochastischen isogeometrischen Analyse, die zur effizienten Unsicherheitsquantifizierung von elliptischen partiellen Differentialgleichungen beiträgt. Es wird ein allgemeiner Ansatz in Kombination mit einer a-priori-Fehlerabschätzung der erwarteten Lösung vorgestellt.

Schlagworte: Unsicherheitsquantifizierung, Spline Chaos, Stochastik Galerkin isogeometrische Analysis, stochastische Galerkin Methode, Representation von Zufallsfeldern

Abstract

The consideration of uncertainties has become inevitable in state-of-the-art science and technology. Research in the field of uncertainty quantification has gained much importance in the last decades. The main focus of scientists is the identification of uncertain sources, the determination and hierarchization of uncertainties, and the investigation of their influences on system responses. Polynomial chaos expansion, among others, is suitable for this purpose, and has asserted itself as a versatile and powerful tool in various applications. In the last years, its combination with any kind of dimension reduction methods has been intensively pursued, providing support for the processing of high-dimensional input variables up to now. Indeed, this is also referred to as the *curse of dimensionality* and its abolishment would be considered as a milestone in uncertainty quantification.

At this point, the present thesis starts and investigates spline spaces, as a natural extension of polynomials, in the field of uncertainty quantification. The newly developed method 'spline chaos', aims to employ the more complex, but thereby more flexible, structure of splines to counter harder real-world applications where polynomial chaos fails.

Ordinarily, the bases of polynomial chaos expansions are orthogonal polynomials, which are replaced by B-spline basis functions in this work. Convergence of the new method is proved and emphasized by numerical examples, which are extended to an accuracy analysis with multi-dimensional input. Moreover, by solving several stochastic differential equations, it is shown that the spline chaos is a generalization of multi-element Legendre chaos and superior to it. Finally, the spline chaos accounts for solving partial differential equations and results in a stochastic Galerkin isogeometric analysis that contributes to the efficient uncertainty quantification of elliptic partial differential equations. A general framework in combination with an a priori error estimation of the expected solution is provided.

Keywords: Uncertainty Quantification, Spline Chaos, Stochastic Galerkin Isogeometric Analysis, stochastic Galerkin Method, Representation of Random Fields

Contents

Acronyms

CAD computer-aided design. 3
CAE computer-aided engineering. 3
CDF cumulative distribution function. 10, 11, 15, 63, 70

iCDF inverse cumulative distribution function. 15
IGA isogeometric analysis. 3, 4

KLE Karhunen-Lòeve expansion. 4, 5, 49, 80, 88, 109, 110, 111

MCS Monte-Carlo simulation. 2, 4, 87, 99, 101
MISC multi-index stochastic collocation. 4

NURBS non-uniform rational B-splines. 39, 40, 41, 42, 43, 98

ODE ordinary differential equation. 87, 89

PC polynomial chaos. 68, 78, 80, 88
PCE polynomial chaos expansion. 3, 4, 88, 109
PDE partial differential equation. 4, 87, 88, 103, 111, 110
PDF probability density function. 2, 11, 12
POD proper orthogonal decomposition. 4

SC spline chaos. 55
SG stochastic Galerkin method. 87
SGFEM stochastic Galerkin finite element method. 103, 105, 109
SGIGA stochastic Galerkin isogeometric analysis. 6, 103, 105, 109
SSFEM spectral stochastic finite element method. 2, 103
SSIGA spectral stochastic isogeometric analysis. 4, 5

UQ uncertainty quantification. 1, 5, 9

1 Introduction

1.1 Stochastic Modeling

Mathematical models form basis for our scientific understanding of the world. In the course of the 20th century, these models were enhanced by computer simulations, which enabled the behaviour of increasingly complex physical systems to be reproduced and predicted. In recent decades, computing and storage capacity has increased exponentially, in accordance with Moore's Law, which was in effect at least until recently Mack, 2011; Moore, 1965. This, in turn, led to computer simulations becoming an indispensable tool for engineering systems, without being limited to it, with ever-growing precision.

Despite their increasing accuracy and irreplaceable value, computational models inevitably remain approximations of real-world phenomena. Depending on the application, various reasons contribute to this:

1. So far, no closed-form solution could be determined for the model. This leads to approximated solutions which are inherently subject to numerical and discretization errors.
2. The considered model is not sufficiently sharp for the underlying problem and the associated inquiry. More sophisticated methodologies have to be deployed.
3. Model parameters cannot be specified perfectly, creating uncertainty that is transmitted through the system to the response, with potentially devastating consequences.

In other words, it is unavoidable to minimize model errors and quantify uncertainties.

In the last two decades, the latter has gained strongly in importance and uncertainty quantification (UQ) is a necessity in all branches of science and engineering. As an interdisciplinary subject between mathematics, physics, engineering and computer science, UQ objectives are to include uncertainties in model parameters of a physical system and to investigate the influence on the system response. A general framework forUQ is sketched in Fig. 1.1 Bruno Sudret, 2007:

Quantifying input uncertainty: Taking uncertainties into account involves identifying all sources of inaccuracies in terms of input parameters and describing them in an appropriate setting. A variety of modeling tools are available, e.g. random

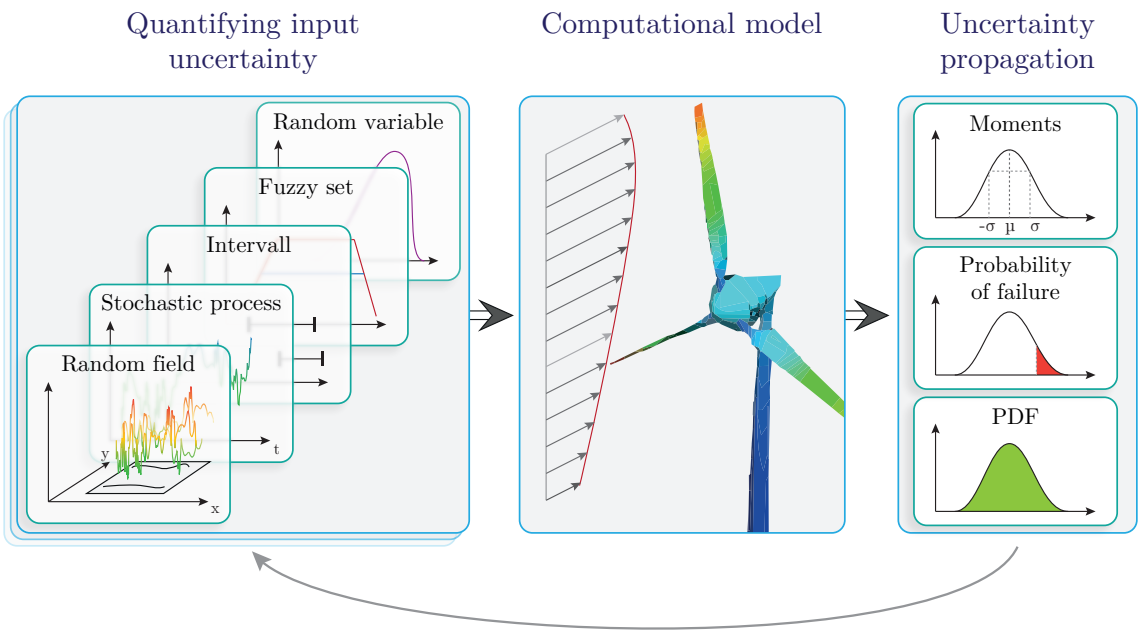

Figure 1.1: Framework for uncertainty quantification in engineering.

variables and fields, stochastic processes, intervals, fuzzy sets, and imprecise probabilities.

Computational model: An extremely diversified field, this includes everything from simple analytical equations to complex calculations that take months to complete. In general, this is not much involved in the context of an uncertainty analysis, since the computational model can be regarded as a black box and is provided by external sources. The model maps the set of input parameters to a set of outputs, often referred to as model responses or quantities of interest.

Uncertainty propagation: The uncertainty characterization of the system response propagated from the input through the system depends on the research question. A number of various techniques are available for the different levels of detail, which can be categorized as follows:

- In order to determine moments, in particular, mean and variance of the response, second moment methods are used, which include Monte-Carlo simulation (MCS), perturbation, quadrature and weighted integral methods.Bruno Sudret, 2007
- Structural reliability methods Ditlevsen and Madsen, 1996a; Lemaire, 2013 aim to measure the probability of failure, where the tail of the probability density function (PDF) needs to be investigated in more detail. Suitable methods are MCS, importance sampling, subset simulation, first- and second order reliability methods.

- Most information gain is obtained by spectral approaches describing the response as a random quantity - usually in terms of the PDF. The spectral stochastic finite element method (SSFEM) is the most famous example and was developed by R.G. Ghanem and P. Spanos (2003).

To obtain reliable results including uncertainty, it is often necessary to invest thousands, millions, or even more evaluations of the numerical model Ripley, 2009a. The computational effort required increases exponentially with the number of uncertain parameters, and random inputs in the two- or three-digit range are highly desirable Davis and Rabinowitz, 2007. Especially for advanced high-reality models, the continuous increasing computational power mentioned above is not able to tackle these problems. It is not uncommon for efficient deterministic analysis to take several hours to run for a single input set - and there are some that take months. For example, if a five-hour simulation had to be repeated one thousand times to account for uncertainties, it would take 208 days. The analysis of an offshore wind turbine could be such an example and is subject to various random phenomena. It is immensely important that such systems have a negligible probability of failure. Therefore, probabilistic approaches provide essential concepts for general engineering practice. Among other aspects, advances in the analysis or representation of random quantities are therefore particularly beneficial.

A widespread approach for representing random quantities, such as random variables and fields, is the polynomial chaos expansion (PCE). Its origins date back to the 1938s Wiener, 1938 and it is still the subject of intensive research Beck, Raul Tempone, et al., 2012; Haji-Ali et al., 2020; Lüthen et al., 2021; P. D. Spanos and Roger Ghanem, 1989; Xiu and Karniadakis, 2002. Increasingly efficient polynomial based methods try to break the *curse of dimensionality* Bellman, 1966 in stochastic modeling, making increasingly higher stochastic dimensions become tractable. Spline spaces, as a natural extension of polynomials, have only recently found their way into stochastic modeling.

1.2 Spline-based Methods in Uncertainty Quantification

The use of spline-based techniques within uncertainty quantification and their interaction with algorithms is a fairly unexplored area of research, although splines are widely used in various areas of science and engineering, e.g. computer-aided design (CAD), interpolation, and data fitting. Splines provide an alternative to Lagrangian and orthonormal polynomials for high-dimensional functional approximations and could consequently be applied in UQ methods. They also have features that could be exploited to more efficiently solve UQ problems with random domains or shape optimization Beck, Tamellini, et al., 2019. Besides, the use of splines of arbitrary order and continuity is the primary ingredient for the success of isogeometric analysis (IGA), which bridges the gap between CAD and computer-aided engineering (CAE) Hughes et al., 2005. IGA successfully has enhanced many deterministic engineering applications - see e.g. the

work done by Auricchio et al. (2012), Y. Bazilevs et al. (2008), Cottrell, J. Evans, et al. (2010), Cottrell, Reali, et al. (2006), Gómez et al. (2008), G. Sangalli et al. (2010), and Schillinger et al. (2012). In this regard, it is noteworthy that the basic idea of IGA, in particular splines, has only recently been incorporated into the stochastic framework:

- First approaches were done by T D Hien and Lam (2016) and H. Nguyen et al. (2017), who investigated a plate problem under random load, and buckling under an uncertain material field, respectively. Load and material fields were both modeled by the spectral representation method. Subsequently, the stochastic analysis was done by MCS.
- In 2018, Li and co-workers proposed a method called spectral stochastic isogeometric analysis (SSIGA) and applied it to several problems in stochastic mechanics, e.g. linear elasticity, free vibration, functionally graded plates Li, Gao, et al., 2018; Li, Wu, and Gao, 2018, 2019; Li, Wu, Gao, and Song, 2019. For representing uncertainties, they numerically solved the Karhunen-Lòeve expansion (KLE), and used an isogeometric solver for the arising spatial integrals in the underlying eigenvalue problem (Fredholm integral equation). Mika et al. (2021) increased the efficiency when solving the Fredholm integral equation by a matrix-free scheme. A multi-patch treatment with collocation is captured by Jahanbin and S. Rahman (2021).
- W. Wang et al. (2019), Ta Duy Hien and Noh (2017), and Ta Duy Hien and P. C. Nguyen (2020) combined low-order perturbation techniques within an isogeometric environment to study different plate problems, with uncertain material field modeled by KLE and integration point method, respectively.
- C. Ding, Cui, et al. (2018) solved a steady heat transfer problem by representing the geometry and deterministic solution via isogeometric basis functions. The randomness of thermal conductivity coefficients are modeled by a high-order perturbation method. The high-order perturbation method is subsequently used to solve a shell structure under geometric uncertainties by C. Ding, Tamma, Cui, et al. (2020).
- In the field of structural analysis, C. Ding, Deokar, Cui, et al. (2019) and C. Ding, Deokar, Y. Ding, et al. (2019) treated high-dimensional material, geometric and force randomness with MCS and an isogeometric solver. In order to handle the computational burden, they used proper orthogonal decomposition (POD) as model order reduction technique.
- Beck, Tamellini, et al. (2019) extended the multi-index stochastic collocation (MISC) method for forward UQ problems by an isogeometric solver for elliptic partial differential equation (PDE)s with random coefficients. MISC is a multi-grid method in spatial and stochastic space, which tries to find an optimal balance for the grids being used. It is derived from the multi-level/multi-index Monte Carlo method and obtained its superiority because highly-efficient quadrature rules can be made applicable.
- Uncertainties in shape are considered by H. Zhang and Shibutani (2019). The

randomness is handled with PCE and intrusively combined with IGA using standard Galerkin. In constrast, Dsouza et al. (2020) applied PCE non-intrusively for functionally graded plates and concludes with a sensitivity analysis using Sobol'indices.
- To process high-dimensional inputs for an UQ analysis of functionally graded plates, meta-models were employed by Z. Liu, Yang, Cheng, Wu, et al. (2020, 2021). Within the SSIGA framework, a Nyström based KLE is implemented. The meta-modeling is done by Kriging enhanced neural networks and arbitrary polynomial chaos-Kriging method, respectively.
- Z. Liu, Yang, Cheng, and Tan (2021) proposed a stochastic isogeometric analysis method based on reduced basis vectors (SRBIGA) for complex structural analysis with random material and force. Derived from SSIGA, it exhibits increased efficiency, accuracy and robustness by representing the response over reduced basis vectors, which are inspired by stochastic Krylov subspace theory.
- A reduced-order Monte Carlo stochastic isogeometric method is presented in order to treat plate and solid problems subjected to spatially uncorrelated and high-dimensional load uncertainties by C. Ding, Tamma, Lian, et al. (2021).

In summary, the trend is towards taming high-dimensional inputs, where an isogeometric description is at the basis of the deterministic model. It has been shown that a wide variety of approaches are currently being pursued, but extensive benchmarks have not yet been established.
Although all listed publications merge spline-based methods and UQ, they do not actually use splines to directly represent uncertainties. This idea was first presented on a conference by the author in 2018 and is the essential part of this dissertation. Later, the idea was taken up by Sharif Rahman (2020), where the lost orthogonality was recovered using a whitening transformation. The sequel work deals with dimension reduction to handle high dimensional inputs in linear elasticity Jahanbin and Sharif Rahman, 2020.

The listed literature as well as the increasing number of publications clearly show the scientific need for this research area, which can help to break the *curse of dimensionality*, and in this way enable the processing of high-dimensional random inputs for complex practical applications. As a natural extension of polynomials, splines are definitely worth investigating. However, they also have a more complex structure. The complexity and the use cases for extending the polynomials to spline spaces remain to be seen.

1.3 Objective and Outline

The objective of this thesis is to give a comprehensive and mathematically rigorous introduction to the theory of spline chaos, as well as to investigate associated properties,

in order to characterize uncertainties within an efficient stochastic analysis.
The manuscript aims at:

- Investigating a novel method describing uncertainties that can help to improve the accuracy and effectiveness of spectral methods in the field of stochastic analysis.
- Examining assets and challenges of the new approach on one- and multi-dimensional stochastic systems.
- Presenting a rigorous mathematical treatment including proofs of convergence.
- Providing a new Galerkin based method for solving stochastic partial differential equations including an a priori error estimation.

To this end, the work conducted during the PhD is divided into the following eight chapters including this introduction:

In chapter 2, the basic concepts of probability theory are briefly reviewed and prepared in a thorough but compact manner, which are tailored to the requirements of this thesis. At the end, proper definitions of stochastic processes and fields, which are indispensable, are derived, as well as the modes of convergence, which are necessary for proofs of convergence in the methodical chapter 5.

Chapter 3 introduces polynomial and spline spaces, as well as related useful propositions, especially about approximation quality. Thereby, diverse notations from different references are adapted and harmonized with each other. The chapter aims to give an explicit error estimation for spline spaces, which needs rigorous and adjusted definitions. In particular, the recently published estimation by Sande et al. (2019) is reprocessed in order to be applied in chapter 7.

Stochastic systems need to be prepared to make them numerically feasible, which is formulated in chapter 4. In particular, common methods characterizing uncertain inputs are discussed, which is a key feature for this purpose. In chapter 6 and 7, this adjusted and generalized system formulation is utilized.

A new method named spline chaos, which can be seen as an extension of polynomial chaos, is defined in chapter 5. Strong and weak convergence, substantiated by several numerical examples, are proposed. This is accompanied by an accuracy analysis for random variables, vectors, and stochastic processes. The method is compared with the homogeneous chaos and similarities to the Legendre chaos are revealed.

In chapter 6, the new introduced concept of spline chaos is applied to different stochastic systems. Uncertain in- and output are modeled with the new expansion and compared to exact solutions, multi-element chaos approaches and Monte-Carlo simulations.

Finally, chapter 7 deals with the holistic view of a stochastic elliptic partial differential equation. A general framework for the stochastic Galerkin isogeometric analysis (SGIGA) is presented where the concept of isogeometric approximations, using the spline chaos,

is assigned to the stochastic part of the problem. This is flanked by the proof of an a priori error estimation of the mean solution and discussed for the elliptic context.

The summary in chapter 8 concludes this thesis, where several important open issues in the development of spline chaos are addressed, too.

2 Probability Theory

In this chapter, the basic concepts of probability theory that are needed for stochastic computational modeling are briefly summarized and adapted for the purpose of this monograph. The objective is to provide a mathematically rigorous introduction describing stochastic processes and random fields and all related objects whose definitions will be used frequently throughout this work. The chapter ends with the definition of the four types of stochastic convergence which are relevant for the proofs of convergence in chapter 5. Definitions and statements in this chapter are adapted from the book by Mircea Grigoriu (2003). Details of statements and proofs can be found there, and in the pertinent literature of e.g. Feller (1968), Kiyosi Itô et al. (1984), Karatzas and Shreve (2014), and Rao and Swift (2006a).

2.1 Probability Space

The introduction of uncertainties in engineering problems, which is referred to as UQ, requires advanced mathematical tools. The engineering problem is considered as a random experiment and one is interested in the probability of a certain outcome of this experiment. All possible outcomes ω are gathered in a sample set (or space) Ω. Events are described by subsets of Ω containing outcomes $\omega \in \Omega$. The set of events in a random experiment forms a set system $\mathcal{F}$ over Ω, thus a subset of the power set 2^{Ω}. If $\mathcal{F}$ satisfies the topological requirements that $\mathcal{F}$ contains the sample space and is stable in concerns of the operations complement and countable union, $\mathcal{F}$ is called a σ-field. The aim of probability theory is to give each event of the collection $\mathcal{F}$ a numerical value between 0 and 1. This is done by a probability measure P over $\mathcal{F}$ which suffice specific axioms (requirements) motivated by the colloquial concept of probability.

Definition 1: Kolmogorov axioms

A probability space is a triple $(\Omega, \mathcal{F}, P)$ consisting of a non-empty set Ω (the sample space), a σ-field $\mathcal{F}$ over Ω, and a set function $P : \mathcal{F} \to [0,1]$ with the properties:

1. $P(\Omega) = 1$
2. $P(E) \geq 0$ for all events $E \in \mathcal{F}$
3. $P(\sum_{i=1}^{\infty} E_i) = \sum_{i=1}^{\infty} P(E_i)$ for all pairwise disjoint events $E_1, E_2, \ldots \in \mathcal{F}$

A set function with these properties is a probability measure.

The mathematical construct of a probability space offers us a secure framework for an intuitive concept of probability. For example, if we consider the failure of a bridge or truss, the topology of the σ-field and the properties of the probability measure ensure that the counter probability of the failure probability p is actually $1 - p$ and that failure or non-failure occurs with probability 1. The third property guarantees the additivity of two independent events, e.g. if the failure probability of two components p_1 and p_2 are independent of each other, then the components will fail simultaneously with the probability $p_1 + p_2$.
For further considerations we still need the concept of a measurable space, which is obtained by omitting the probability measure from a probability space. Or the other way round: The definition of a probability measure on a measurable space makes it a probability space. The measurable space $(\mathbb{R}, \mathcal{B})$ is of particular interest. The σ-field $\mathcal{B}$ generated by the half-open intervals $(a, b]$, $-\infty < a \leq b < \infty$ is called the σ-field of Borel sets of $\mathbb{R}$. Furthermore, the d-dimensional extension is denoted by $\mathcal{B}^n$.

2.2 Random Variables

In general, there is less interest in a concrete result ω, but rather in the random variable $X(\omega)$. Of special concern is the case when X is real, because a variety of random experiments can be unified by applying the description of random events to intervals of the real line.

Definition 2: Random variable

A (real-valued) random variable X on the probability space $(\Omega, \mathcal{F}, P)$ is a mapping $X : \Omega \to \mathbb{R}$ which is $(\mathcal{F}, \mathcal{B})$-measurable, i.e. $X^{-1}(B) = \{\omega \in \Omega \mid X(\omega) \in B\} \in \mathcal{F}$ for all $B \in \mathcal{B}$.

To get a better idea, it is useful to look at the set B as half open intervals $(-\infty, a]$. A mapping $X : \Omega \to \mathbb{R}$ is a random variable if and only if $X^{-1}((-\infty, a]) \in \mathcal{F}$ is satisfied for all $a \in \mathbb{R}$. Thus, each interval from the measurable space $(\mathbb{R}, \mathcal{B})$ is assigned to an event on the probability space $(\Omega, \mathcal{F}, P)$. Therefore, a random variable transfers the probability structure from Ω to $\mathbb{R}$ and makes the measurable space $(\mathbb{R}, \mathcal{B})$ a probability space $(\mathbb{R}, \mathcal{B}, P^X)$. Here, $P^X : \mathcal{B} \to [0, 1]$ is the probability measure over $(\mathbb{R}, \mathcal{B})$ induced by the random variable X with

$$B \mapsto P^X(B) := P(X \in B) \equiv P(X^{-1}(B))$$

and is named the distribution of X. As already mentioned above, it is not necessary to describe the underlying probability space $(\Omega, \mathcal{F}, P)$ of a random variable exactly. It is sufficient to know about the distribution of X and it is common practice to assume a suitable distribution for random variables, such as material parameters or wind loads. Nevertheless, it is not practical to calculate probabilities haphazardly using Borel sets. Therefore, the distribution of X is described by using cumulative distribution functions (CDFs) defined over the real line:

$$F_X : \mathbb{R} \to [0,1], \quad x \mapsto F_X(x) := P^X((-\infty, x]) \equiv P(X \leq x).$$

The distribution function $F_X(x)$ determines the probability that the random variable takes on a value less than or equal to x by searching the underlying probability space for all events projected into the interval $(-\infty, x]$ by the mapping X. In the following, the image space of a random variable is always $\mathbb{R}$, unless otherwise specified.

Random variables can be divided by their distribution into continuous and discrete. If the associated distribution function of a random variable X has jumps, i.e.

$$F_X(x) = \sum_{x_k < x} p(x_k)$$

with

$$0 \leq p(x_k) \leq 1 \quad \text{and} \quad \sum_{x_k} p(x_k) = 1,$$

then X is a discrete random variable.
In contrast, if X assumes any single value $x \in \mathbb{R}$ with probability 0, i.e.

$$P(X = x) = 0 \quad \forall x \in \mathbb{R},$$

then X is a continuous random variable. If, for a CDF of a continuous random variable, there exists a PDF $f_X(x)$ with

$$F_X(x) = \int_{-\infty}^{x} f_X(\tilde{x})\, d\tilde{x}$$

and

$$f_X(x) \geq 0 \quad \forall x\mathbb{R}, \quad \text{and} \quad \int_{-\infty}^{\infty} f_X(x)\, dx = 1,$$

then X is absolutely continuous.

Examples of important distributions

Discrete distributions

Important discrete distributions are the binomial distribution $\mathrm{Bin}(n,p)$ with $n \in \mathbb{N}_0$ and $p \in (0,1)$:

$$P(X=k) = \binom{n}{k} p^k (1-p)^{n-k} \qquad k = 0,\dots,n,$$

and the Poisson distribution $\mathrm{Poi}(\lambda)$ with $\lambda \in \mathbb{R}_+$:

$$P(X=k) = \exp(-\lambda)\frac{\lambda^k}{x!} \qquad k = 0,1,\dots\ .$$

Continuous distributions

Among others, the normal, beta, and gamma distribution are common representatives of continuous distributions and are used in many applications:
X is normal or Gaussian distributed with expectation $\mu \in \mathbb{R}$ and variance $\sigma^2 \in \mathbb{R}_+$, i.e. $X \sim \mathcal{N}(\mu,\sigma^2)$. Then, the PDF is given by

$$f_X(x) = \frac{1}{\sqrt{2\pi\sigma^2}} \exp -\frac{(x-\mu)^2}{2\sigma^2} \qquad x \in \mathbb{R}.$$

$\mathcal{N}(0,1)$ denotes the standard normal distribution.
X is a beta distributed random variable on $[a,b] \subset \mathbb{R}$, i.e. $\mathrm{Beta}(a,b,\alpha,\beta)$ with density function

$$f_X(x) = \frac{1}{\mathrm{B}(a,b,\alpha,\beta)}(x-a)^{\alpha-1}(b-x)^{\beta-1} \quad \text{with } \alpha,\beta > 0\,,$$

where $\mathrm{B}(a,b,\alpha,\beta) = \int_a^b (u-a)^{\alpha-1}(b-u)^{\beta-1}\,du$ is the beta function. For $\alpha = \beta = 1$ the beta distribution degenerates to the important uniform distribution. Then, X is uniformly distributed on $[a,b]$, i.e. $X \sim \mathrm{unif}([a,b])$, with density

$$f_X(x) = \begin{cases} \frac{1}{b-a}, & \text{for } a \le x \ge b, \\ 0, & \text{otherwise.} \end{cases}$$

Finally, assume X is a gamma distributed random variable on $[0,\infty]$, i.e. $\mathrm{Gam}(a,b)$ with PDF

$$f_X(x) = \frac{b^a}{\Gamma(a)} x^{a-1} e^{-bx} \quad a,b > 0$$

where $\Gamma(a)$ is the gamma function. In the case of $a = 1$ the gamma distribution reproduces the exponential distribution $\mathrm{Exp}(b)$.

2.2.1 Moments

Random variables can be described not only by their distribution, but also by other characteristics. In particular, the expected value, the variance and higher moments are important quantities that are used in many applications to describe a random variable. Often it is not possible or not necessary to know the complete distribution of a random variable in a system to be analyzed. Note, the following detailed and in part different notations are mentioned here because they are partly applied in the later progression and thus should avoid confusion.
If the random variable X over the probability space $(\Omega, \mathcal{F}, P)$ is P-integrable, i.e. $\int |X| dP < \infty$, then the expectation - the most likely value of X - exists and is defined by

$$\mu_X \equiv E[X] := \int X \, dP \equiv \int_\Omega X(\omega) \, dP(\omega).$$

In the scope of this work mainly absolute continuous random variables are considered, so that the expectation can be determined by

$$E[X] = \int_\Omega X(\omega) \, dP(\omega) = \int_{\mathbb{R}} x \, dF_X(x) = \int_{-\infty}^{\infty} x f_X(x) \, dx.$$

Analogously, if X is k-times P-integrable the k^{th} moment of X exists and is defined by

$$E[X^k] := \int X^k \, dP = \int_{-\infty}^{\infty} x^k f_X(x) \, dx.$$

Furthermore, there are centralized versions of the moments of which the variance is most frequently used:

$$\sigma_X^2 \equiv \mathrm{Var}[X] := E[(X - \mu)^2] = \int_{-\infty}^{\infty} (x - \mu)^2 f_X(x) \, dx.$$

The variance or more precise the standard deviation σ provides information about the degree of dispersion around the expected value.
In order to show how important the first moments of a random variable can be and that for the complete characterization of a random variable the distribution is not necessarily mandatory, we consider a normally distributed random variable $X \sim \mathcal{N}(\mu, \sigma^2)$. The

moments of X are given by

$$
\begin{aligned}
&E[X] = \mu \\
&\mathrm{Var}[X] = \sigma^2 \\
&E[(X-\mu)^{2n-1} = 0, \quad n = 1,2,\dots \\
&E[(X-\mu)^{2n} = 1 \cdot 3 \cdot 5 \dots \cdot (2n-1) \cdot \sigma^{2n}, \quad n = 1,2,\dots ,
\end{aligned}
$$

thus all moments are described by μ and σ^2 and consequently the random variable itself. For example, the distribution of wind speed can be realized very well by measuring average wind speeds and choosing a shape parameter. These examples provide an indication that there are methods for the analysis of stochastic problems which are voluntarily limited to the determination of the first moments, e.g. the moment equation approach.

2.2.2 Hilbert Spaces

Denote by $L^p(\Omega, \mathcal{F}, P)$ the collection of random variables X on $(\Omega, \mathcal{F}, P)$ with $E[|X|^p] < \infty$ for $p \geq 1$. The case $p = 2$ is of special interest for many applications, because it connects the second moment calculation and the error estimation at the later part of this work. This is partly due to the fact that $L^2(\Omega, \mathcal{F}, P)$ is a Hilbert space. In addition, useful inequalities, such as the Chebyshev's, Chauchy-Schwarz's, Minkowski's, etc., become accessible for both applications and theoretical considerations. Denote by $L^2(\Omega, \mathcal{F}, P)$ the space (of equivalence classes) of all square P-integrable (real-valued) random variables, i.e.

$$
L^2_P \equiv L^2(\Omega, \mathcal{F}, P) := \left\{ X : \Omega \to \mathbb{R} \mid E[|X|^2] < \infty \right\} (/ \sim_P) .
$$

$L^2(\Omega, \mathcal{F}, P)$ is a Hilbert space with the inner product and norm:

$$
\langle X, Y \rangle_{L^2_P} := E[XY] \qquad \text{and} \qquad \|X\|_{L^2_P} = \sqrt{\langle X, X \rangle} = \left(E[X^2] \right)^{1/2}
$$

for $X, Y \in L^2(\Omega, \mathcal{F}, P)$.

2.2.3 Random Number Generation

One of the essential tasks in the field of stochastic simulation is the generation of random numbers. The most common procedure is the generation of uniformly distributed random numbers in the interval [0,1], which are based on a deterministic algorithm.

Therefore such a sequence is also called pseudo-random numbers. The methods implemented in common software are very mature and therefore so fast and stable that they rarely need or can be improved substantially. More detailed information of random number generation can be found, in the pertinent literature of Gentle, 2006; Knuth, 1998; L'Ecuyer, 1994; Ripley, 2009b, for example.
A simple method to create realizations of a non-uniform continuous random variable is the inversion method. It is based on the essential fact that every distribution maps to the interval $(0,1)$. Now consider the inverse of a distribution and a uniformly distributed random variable Z to $(0,1)$. Then the inverse as a function of a random variable is again a random variable, which is enough for the desired distribution. More precisely:

Proposition 2.2.1. *Let F_X be the CDF of a random variable X. If $U \sim \text{unif}([0,1])$, then $F_X^{-1}(U)$ is a random variable with CDF F_X.*

In the scope of this work, we will see that this property is not only useful for the generation of random numbers, but also plays an essential role in the development of B-spline chaos.
It is obvious and well known from stochastic theory, that the inverse cumulative distribution function (iCDF) of a random variable X, given by

$$F_X^{-1}(u) := \inf\{x \ : \ F_X(x) \geq u\}$$

always exists and is unique. Besides, if the distribution function is strictly monotonic increasing and continuous, then $x = F^{-1}(u)$ is unique and well-defined for all $u \in [0,1]$. This case is the most user-friendly. Let X be an exponential distributed random with rate $b > 0$, then $f_X(x) = b\exp(-bx)$ and the inverse of F_X is $F_X^{-1} = -b^{-1}\log(1-u)$. Thus, we can generate realizations of X by the inversion method with $X = -b^{-1}\log(1-U)$ and $U \sim \text{unif}([0,1])$.
In case the inverse is not easy to determine analytically, numerical schemes can help, but induce additional inaccuracies. Let X be a standard Gaussian random variable, then $f_X(x) = \frac{1}{\sqrt{2\pi}}\exp -\frac{(x)^2}{2}$ and neither the distribution nor its inverse can be given in closed form. There are quite simple and accurate approximations of F_X^{-1}. For example:

$$F_X^{-1}(u) \approx \text{sign}(1-\frac{1}{2})\left(t - \frac{c_0 + c_1 t + c_2 t^2}{1 + d_1 t + d_2 t^2 + d_3 t^3}\right)$$

with $t = \sqrt{-\ln(\min\{u, 1-u\}^2)}$ and

i	c_i	d_i
0	2.515517	-
1	0.802853	1.432788
2		0.189269
3	-	0.001308

.

The absolute error is less than $4.5 \cdot 10^{-4}$ Hastings Jr et al., 2015. Although the absolute error of many methods is small, this is often not the case with relative errors. But just a small relative error is indispensable for many engineering applications such as structural failure probabilities or menace curves of natural hazards, because tail probabilities are needed. Recently, Luis (2015) presented a simple and accurate method that addresses this problem. It shows relative errors lower than $2.5 \cdot 10^{-3}$ over a wide range of the support of the random variable and absolute errors lower than $9.5 \cdot 10^{-4}$ for $x < 3$ and $6.4 \cdot 10^{-7}$ for $x \geq 3$. This improved accuracy is achieved by dividing the approximation into three ranges of $[0, 3)$, $[3, 8)$, and $[8, 20)$. The same analytical approximation rule is used for all intervals, whereby the coefficients are adjusted accordingly.

Besides the inversion method for generating non-uniform random numbers, the most important one is the acceptance-rejection method. Further details can be found in Devroye, 1986; Gentle, 2006; Hörmann et al., 2013.

2.3 Random Vectors

Broadly speaking, a finite collection of one-dimensional real-valued random variables is a random vector. Therefore, the basic concepts of random variables can be transferred to random vectors with certain extensions and adaptations. In the following, the definition of random vectors analogous to the definition of random variables is introduced, as well as terms and notations necessary for this work.

Definition 3: Random vector

A d-dimensional random vector $\mathbf{X} = (X_1, \ldots, X_d)$ on the probability space $(\Omega, \mathcal{F}, P)$ is a mapping $\mathbf{X} : \Omega \to \mathbb{R}^d$ which is $(\mathcal{F}, \mathcal{B}^d)$-measurable, i.e. $\mathbf{X}^{-1}(B) \in \mathcal{F}$ for all $B \in \mathcal{B}^d$, on the measurable space $(\mathbb{R}^d, \mathcal{B}^d)$.

As with random variables, a random vector or d-dimensional random variable transmits the probability structure of Ω to $\mathbb{R}^d$.
If we look at the rectangle $B = (-\infty, x_i]$ in $\mathbb{R}^d$ with $x_i \in \mathbb{R}$, $i = 1, \ldots, d$, then $B \in \mathcal{B}^d$ and $\mathbf{X}^{-1}(B) \in \mathcal{F}$, such that the joint distribution function $F_{\mathbf{X}} : \mathbb{R}^d \to [0, 1]$ of $\mathbf{X} = (X_1, \ldots, X_d)$ makes sense:

$$F_{\mathbf{X}}(\mathbf{x}) = P\left(\bigcap_{i=1}^{d} \{X_i \leq x_i\}\right) \equiv P\left(X_1 \leq x_1, \ldots, X_d \leq x_d\right),$$

for any $\mathbf{x} = (x_1, \ldots, x_d) \in \mathbb{R}^d$. If the derivative

$$f_{\mathbf{X}}(\mathbf{x}) = \frac{\partial^d F_{\mathbf{X}}(\mathbf{x})}{\partial x_1 \cdots \partial x_d}$$

exists, then $f_{\mathbf{X}}$ is the joint density function of $\mathbf{X}$ and it holds

$$F_{\mathbf{X}}(\mathbf{x}) = \int_{-\infty}^{x_1} \cdots \int_{-\infty}^{x_d} f_{\mathbf{X}}(\tilde{x}_1, \ldots, \tilde{x}_d)\, d\tilde{x}_1 \cdots d\tilde{x}_d \,.$$

The joint density function satisfies the following properties

$$f_{\mathbf{X}}(\mathbf{x}) \geq 0 \quad \forall \mathbf{x} \in \mathbb{R}^d$$

and

$$\int_{-\infty}^{+\infty} \cdots \int_{-\infty}^{+\infty} f_{\mathbf{X}}(\tilde{x}_1, \ldots, \tilde{x}_d)\, d\tilde{x}_1 \cdots d\tilde{x}_d = 1 \,.$$

Furthermore, marginal distribution and density functions can be defined, e.g. for X_i by

$$F_{X_i}(x_i) = \lim_{\substack{x_k \to +\infty \\ 1 \leq k \leq d; k \neq i}} F_{\mathbf{X}}(x_1, \ldots, x_d)$$

and

$$f_{X_i}(x_i) = \int_{-\infty}^{+\infty} \cdots \int_{-\infty}^{+\infty} f_{\mathbf{X}}(\tilde{x}_1, \ldots, \tilde{x}_d)\, d\tilde{x}_1 \cdots d\tilde{x}_{i-1} d\tilde{x}_{i+1} \cdots d\tilde{x}_d = \frac{\partial F_{\mathbf{X}}(\mathbf{x})}{\partial x_i} \,.$$

Again, the most interesting characteristics of a random vector are the first moments, i.e. the expectation vector

$$\mu_{\mathbf{X}} \equiv E[\mathbf{X}] := (E[X_1], \ldots, E[X_d]) \equiv \{\mu_i\}_{i=1,\ldots,d},$$

the correlation matrix

$$\mathrm{Cor}[\mathbf{X}] := E[\mathbf{X}\mathbf{X}^T]$$

the covariance matrix

$$\mathrm{Cov}[\mathbf{X}] := \{\mathrm{Cov}(X_i, X_j)\}_{i,j=1,\ldots,d}$$

with

$$\mathrm{Cov}(X_i, X_j) := E[(X_i - \mu_{X_i})(X_j - \mu_{X_j})] = E[X_i X_j] - \mu_{X_i}\mu_{X_j}$$

is the covariance of X_i and X_j. Note, $\mathrm{Cov}(X_i, X_i) = \sigma_i^2$ is the variance of X_i and

$$\mathrm{Var}[\mathbf{X}] := \{\sigma_i^2\}_{i=1,\ldots,d}$$

is the variance vector.
It is also common to normalize the covariances by their standard deviations in order to get the correlation coefficients

$$\rho(\mathbf{X}) := \left\{ \frac{E[(X_i - \mu_i)(X_j - \mu_j)]}{\sigma_{ii}\sigma_{jj}} \right\}_{i,j=1,\dots,d} \equiv \{\rho_{ij}\}_{i,j=1,\dots,d}$$

with

$$|\rho_{ij}| \leq -1 \, .$$

In the case $\rho_{ij} = 0$ the random variables X_i and X_j are uncorrelated and for $|\rho_{ij}| \approx 1$ for strongly correlated X_i and X_j. If X_i and X_j are independent, then they are uncorrelated. In general, the inverse is not true.

2.3.1 Independence and Conditional Expectation

Consider the random vector $\mathbf{X} = (X_1, \dots, X_d)$ with joint distribution $F_{\mathbf{X}}$ and F_{X_i} is the distribution of X_i. The random variables $X_1, \dots, X_d$ are independent if and only if

$$F_{\mathbf{X}}(\mathbf{x}) = \prod_{i=1}^{d} F_{X_i}(x_i) \quad \forall \mathbf{x} \in \mathbb{R}^d \, .$$

The same holds for the density, if it exists, i.e. the random variables $X_1, \dots, X_d$ are independent if and only if

$$f_{\mathbf{X}}(\mathbf{x}) = \prod_{i=1}^{d} f_{X_i}(x_i) \quad \forall \mathbf{x} \in \mathbb{R}^d \, .$$

Therefore, the property of independence has a direct influence when calculating moments.
Next, consider the two random vectors $\mathbf{X} = (X_1, \dots, X_{d_1})$ and $\mathbf{Y} = (Y_1, \dots, Y_{d_2})$ over the probability space $(\Omega, \mathcal{F}, P)$. Often, there is interest in determining the probability of $\mathbf{X}$ under the condition that a realization $\mathbf{y}$ of $\mathbf{Y}$ has already occurred. This can be calculated by limiting the probability space to $\mathbf{Y}$. Therefore, we introduce the conditional density

$$f_{\mathbf{X}|\mathbf{Y}=\mathbf{y}}(\mathbf{x}) := \frac{f_{\mathbf{XY}}(\mathbf{x}, \mathbf{y})}{f_{\mathbf{Y}}(\mathbf{y})}$$

of $\mathbf{X}$ given $\mathbf{Y} = \mathbf{y}$, where $f_{\mathbf{XY}}$ is the joint density of $\mathbf{X}$ and $\mathbf{Y}$, $f_{\mathbf{Y}}$ the density of $\mathbf{Y}$, and $\mathbf{y} \in \mathbb{R}^{d_2}$. With this definition it is easy to introduce the conditional expectation

$$E[\mathbf{X}|\mathbf{Y} = \mathbf{y}] := \int_{\mathbb{R}^{d_1}} \mathbf{x} f_{\mathbf{X}|\mathbf{Y}=\mathbf{y}}(\mathbf{x}) \, d\mathbf{x}$$

of $\mathbf{X}$ given the information $\mathbf{Y} = \mathbf{y}$. This notion of conditional expectations can be extended by considering more general information then $\mathbf{Y} = \mathbf{y}$. Denote by $\mathcal{G}$ a sub-σ-field of $\mathcal{F}$. Then, the conditional expectation $E[\mathbf{X}|\mathcal{G}]$ of $\mathbf{X}$ with respect to $\mathcal{G}$ is the class of $\mathcal{G}$-measurable functions satisfying

$$\int_G \mathbf{X} dP = \int_G E[\mathbf{X}|\mathcal{G}]\, dP \quad \forall G \in \mathcal{G},$$

and has the following properties

- If $\mathcal{G} = \{\emptyset, \Omega\}$, then $E[\mathbf{X}|\mathcal{G}] = E[\mathbf{X}]$
- If $\mathcal{G} = \mathcal{F}$, then $E[\mathbf{X}|\mathcal{G}] = \mathbf{X}$ a.s.
- $E[E[\mathbf{X}|\mathcal{G}]] = E[\mathbf{X}]$

which results directly from the definition. The conditional expectation $E[\mathbf{X}|\mathcal{G}]$ is the projection of $\mathbf{X}$ on $\mathcal{G}$ and can be viewed as an approximation of $\mathbf{X}$. For a better understanding, consider the random variable $X \in L^2(\Omega, \mathcal{F}, P)$ and $\hat{X} \in L^2(\Omega, \mathcal{G}, P)$ with

$$\langle X - \hat{X}, Y \rangle = 0 \quad \forall Y \in L^2(\Omega, \mathcal{G}, P),$$

i.e. the error $X - \hat{X}$ is orthogonal to $L^2(\Omega, \mathcal{G}, P)$, then

$$\|X - \hat{X}\| = \min_{Y \in L^2(\Omega, \mathcal{G}, P)} \Big\{ \|X - Y\| \Big\}.$$

Therefore, $\hat{X}$ has the smallest mean square error and is called the best mean square estimator of X. Because

$$E[(\mathbf{X} - E[\mathbf{X}|\mathcal{G}])G] = 0 \quad \forall G \in \mathcal{G},$$

$\mathbf{X} - E[\mathbf{X}|\mathcal{G}]$ is orthogonal to $\mathcal{G}$ and $E[\mathbf{X}|\mathcal{G}]$ is the best m.s. estimator of $\mathbf{X}$ with respect to the information given by $\mathcal{G}$. Therefore, conditional expectations attach much importance to many applications, where a lack of information can usually be assumed.

2.4 Stochastic Processes and Random Fields

A significant role in many applications plays the characterization of randomness which varies discretely or continuously over time or physical space. Therefore, random variables or vectors are equipped with time or space functions.

Definition 4: Stochastic process

Let $\mathbf{X} : I \times \Omega \to \mathbb{R}^d$ be a function of two arguments $\omega \in \Omega$ and $t \in I$ with $(\Omega, \mathcal{F}, P)$ is a probability space and $I \subset \mathbb{R}$ an index set. If $\mathbf{X}(t)$ is a d-dimensional random variable for each $t \in I$, i.e. $\mathbf{X}(t) \in \mathcal{F}$, then $\mathbf{X}(t)$ is a stochastic process. If $d = 1$ the process is denoted by $X(t)$.

The index set $I \subset \mathbb{R}$ can either be an interval, e.g. $I = [0, \infty)$, or a finite or countably infinite set, then the corresponding stochastic process is continuous or discrete, respectively. Often, the index set is referred to as time. For example, consider a mechanical system subjected to wind loads or other dynamic forces over a time period. Then, the randomness of these forces can be handled by a continuous time stochastic process.
On the other hand, randomness appears also over physical space and is then called a random field. A most typically example in stochastic mechanics are the varying properties of materials, e.g. the Young's modulus. Random fields are defined in the same way.

Definition 5: Random field

Let $\mathbf{X} : I \times \Omega \to \mathbb{R}^d$ be a function of two arguments $\omega \in \Omega$ and $x \in I$ with $(\Omega, \mathcal{F}, P)$ is a probability space and $I \subset \mathbb{R}^q$, $q \in \mathbb{N}_+$, an index set. If $\mathbf{X}(x)$ is a d-dimensional random variable for each $x \in I$, i.e. $\mathbf{X}(x) \in \mathcal{F}$, then $\mathbf{X}(x)$ is a random field.

Stochastic processes and random fields share many properties and in the one-dimensional case they can often be used interchangeably. However, there are remarkable differences between them, e.g. the notion of past and future is not directly applicable for random fields. Besides, the randomness can depend on both time and space and is then referred to as a space-time stochastic process, e.g. the evolution in time of the temperature in a bounded domain. Therefore, in the scope of this book, definitions and characterisations of stochastic processes holds also for random fields and vice versa unless otherwise stated, and a random function generally encompasses both terms.

Example 2.4.1. *The function* $X : I \times \Omega \to \mathbb{R}$ *defined by* $X(t, \omega) := Y(\omega)(t - \frac{t^3}{6})$ *with* $I = [-4, 4]$ *and* $Y(\omega) := \omega$ *a uniform random variable on* $([0, 1], \mathcal{B}([0, 1]), P)$ *is a stochastic process.*

The function $\mathbf{X}(\cdot, \omega)$ for a fixed $\omega \in \Omega$ is called a realization, a trajectory, or a sample path of the process $\mathbf{X}$. The other way around, $\mathbf{X}(t, \cdot)$ for a fixed time $t \in I$ is a d-dimensional random variable by definition.

The general goal in the subsequent analysis will be the determination of statistics of stochastic processes. The task is much more involved than the one for random vectors or variables, because a stochastic process with an infinite index set belongs to an infinite-dimensional space which must be approximated by finite-dimensional subspaces in

order to make them numerically accessible. The discussion is limited to one-dimensional processes for simplicity. The extension to $d > 1$ is straightforward. One way to overcome this challenge is to think of a process as a collection of random vectors. As a result, the finite-dimensional distributions of order $n \in \mathbb{N}$ of the stochastic process $\mathbf{X}(t)$ are specified by the distributions of the finite-dimensional vectors

$$(\mathbf{X}(t_1), \dots, \mathbf{X}(t_n)), \qquad t_1, \dots, t_n \in I,$$

for all possible choices of the index $t_1, \dots, t_n \in I$ and every n, i.e. for $d = 1$:

$$F_n(x_1, \dots, x_n; t_1, \dots, t_n) = P\left(X(t_1) \leq x_1, \dots, X(t_n) \leq x_n\right), \quad \forall n \in \mathbb{N}.$$

The finite dimensional densities of $X(t)$ are the derivatives of the distributions:

$$f_n(x_1, \dots, x_n; t_1, \dots, t_n) = \frac{\delta^n}{\delta x_1 \cdots \delta x_n} F_n(x_1, \dots, x_n; t_1, \dots, t_n), \quad \forall n \in \mathbb{N}.$$

Furthermore, the marginal distribution and density of $X(t)$ are $F_1(\cdot; t)$ and $f_1(\cdot; t)$, or simply $F(\cdot; t)$ and $f(\cdot; t)$, respectively. In most applications, the available information suffice to estimate at least the first and second order finite dimensional distributions of X, which are essential for the meaningful second order calculus Mircea Grigoriu, 2003. Therefore, many of the definitions and properties of moment theory for random vectors in section 2.3 are relatable for random functions as well: The expectation, correlation, covariance and variance function of $X(t)$ is given by

$$\begin{aligned}
&\mu_X(t) := E[X(t)], \\
&r_X(t,s) := E[X(t)X(s)], \\
&c_X(t,s) := E[(X(t) - \mu_X(t))(X(s) - \mu_X(s))], \\
&\sigma_X^2(t) := c_X(t,t),
\end{aligned}$$

$t, s \in I$, respectively. Obviously, these quantities are considered as deterministic functions of time, and the pair (μ_X, r_X) or (μ_X, c_X) define the second moment properties of X. The expectation function $\mu_X(t)$ is a deterministic path representing the average of all possible sample paths of $X(t)$, the variance function $\sigma_X^2(t)$ measures the deviation of the sample paths around the expectation function, and the correlation function $r_X(t,s)$ and covariance function $c_X(t,s)$ return a measure of dependence at two timestamps t and s.

2.4.1 Classes of Stochastic Processes

The finite-dimensional distributions of a stochastic process are a appropriate auxiliary to define different classes of processes frequently used in applications. Examples are

Gaussian, Markov, Poisson, stationary, parametric, and independent increment processes among many others. The interested reader is referred to the diverse and excellent books such as Gardiner et al., 1985; Mircea Grigoriu, 1995, 2003; Karatzas and Shreve, 2014; Ross, 1996.

Stationary Processes

The stochastic process $X(t)$ is called stationary in the strict sense or stationary if the finite-dimensional distributions of the process are invariant under time shifts, i.e.

$$(X(t_1), \ldots, X(t_n)) \stackrel{d}{=} (X(t_1 + \tau), \ldots, X(t_n + \tau))$$

for any $n \in \mathbb{N}$, distinct times $t_1, \ldots, t_n \in I$, and time shift τ such that $t_1 + \tau, \ldots, t_n + \tau \in I$. Hence, a stationary process depends on only the lag between timestamps rather then their values itself. Here, $\stackrel{d}{=}$ means equal in distribution - see the following section 2.5. In concern of second order properties, for a stationary stochastic process $X(t)$ it yields

$$\mu_X(t) = constant, \tag{2.1}$$
$$r_X(t,s) \text{ and } c_X(t,s) \text{ depend only on } \tau = t - s\ . \tag{2.2}$$

In practice, it is useful to define a process by the properties (2.1) and (2.2), i.e. if a stochastic process $X(t)$ has a constant expectation function $\mu_X(t)$ and the correlation function $r_X(t,s)$ or covariance function $c_X(t,s)$ depends only on the lag $\tau = t - s$, then $X(t)$ is stationary in the wide sense, second-order stationary, or weakly stationary. A stationary random function is weakly stationary but the converse is not generally true. In order to ensure that the functions in (2.1) and (2.2) exist, $X(t)$ need to be an element of $L^2(\Omega, \mathcal{F}, P)$, i.e. , $X(t)$ has finite second moments at all times. Many applications require at least weakly stationary processes in $L^2(\Omega, \mathcal{F}, P)$, because modelling and calculation are tremendous simplified.
An alternative way for specifying a weakly stationary process $X(t) \in L^2(\Omega, \mathcal{F}, P)$ is the power spectral density. If the correlation function is continuous, it has the representation (Bochner's theorem Mircea Grigoriu, 2003, section 3.7.2.1):

$$r_X(\tau) = \int_{\infty}^{\infty} e^{\sqrt{-1}\nu\tau} d\mathcal{S}(\nu)$$

where $\mathcal{S}$ is a real-valued, increasing, and bounded function, called the spectral distribution function of $X(t)$. If $\mathcal{S}$ is absolutely continuous, there exists the power spectral density function $s(\nu) = d\mathcal{S}(\nu)/d\nu$, $\nu \in \mathbb{R}$. The power spectral density and correlation

function are Fourier pairs:

$$r_X(\tau) = \int_{\infty}^{\infty} e^{\sqrt{-1}\nu\tau} s(\nu) d\nu \quad s_X(\tau) = \frac{1}{2\pi} \int_{\infty}^{\infty} e^{-\sqrt{-1}\nu\tau} r(\tau) d\tau \, .$$

Example 2.4.2. *Consider the uncorrelated random variables A_i, B_i with zero mean and unit variance, and the constants $c_i, \nu_i > 0$. Then,*

$$X(t) := \sum_{i=1}^{n} c_i \big(A_i \cos(\nu_i t) + B_i \sin(\nu_i t) \big)$$

is a weakly stationary stochastic process with mean zero and covariance function

$$c_X(t,s) = \sum_{i=1}^{n} c_i^2 \cos(\nu_i (t-s)).$$

The random function in example 2.4.2 is of particular interest for many applications, because it can be shown that any weakly stationary stochastic process can be represented by a superposition of harmonics with random amplitude and phase Mircea Grigoriu, 2003. Note, the property of stationary and second moment calculus can be transmitted directly to random fields Mircea Grigoriu, 2003. The term homogeneous random field instead of stationary is sometime used. A very useful access to random fields can be found in Adler, 2010.

Gaussian Processes

A stochastic process $X(t)$ with all its finite-dimensional distributions are Gaussian, is called a Gaussian process. For a Gaussian process, its mean and covariance function can completely characterize the distribution of the process. Consequently, a Gaussian process is stationary if and only if it is weakly stationary.

Example 2.4.3. *Consider the Gaussian vector $\mathbf{Y} = (Y_1, \ldots, Y_m) \in \mathbb{R}^m$ and the continuous function $\mathbf{f} : [0, \infty) \to \mathbb{R}^m$ of time. Then,*

$$X(t) := \sum_{i=1}^{m} f_i(t) Y_i$$

is a Gaussian process.

Let $g : [0, \infty) \times \mathbb{R}^m \to \mathbb{R}$ be a measurable function and $\mathbf{Z}$ be an m-dimensional random vector with $m \in \mathbb{N}$. Then, $X(t) := \mathbf{g}(t, \mathbf{Z})$ is a parametric stochastic process. They are

often used for approximating general stochastic processes in Monte Carlo simulation. The Gaussian process in example 2.4.3 is parametric.

Example 2.4.4. *If in example 2.4.2 A_i, B_i are Gaussian variables, then $X(t)$ is a stationary parametric Gaussian process. This kind of processes is approximated later in chapter 5.*

2.5 Modes of Convergence

For the following analysis, it is useful to briefly introduce the four main concepts of convergence in stochastic. For this purpose the random variable X and a sequence of random variables X_n on the probability space $(\Omega, \mathcal{F}, P)$ are considered with associated distribution functions F and F_n, respectively. The convergence notions are based on the different ways of measuring the distance of X and X_n.

mean square: $X_n \xrightarrow{m.s.} X$, if $\lim_{n\to\infty} E[|X_n - X|^2] = 0$

almost sure: $X_n \xrightarrow{a.s.} X$, if $\lim_{n\to\infty} X_n(\omega) = X(\omega), \forall \omega \in \Omega \setminus N$ with $P(N) = 0$

probability: $X_n \xrightarrow{P} X$, if $\lim_{n\to\infty} P(|X_n - X| > \epsilon) = 0, \forall \epsilon > 0$

distribution: $X_n \xrightarrow{d} X$, if $\lim_{n\to\infty} F_n(x) = F(x), \forall x \in \mathbb{R}$

The different types of convergence are related to each other, so that one implies the other, but not vice versa. The convergence in mean square and the almost sure convergence imply convergence in probability. Convergence in probability implies convergence in distribution. Therefore, mean square and almost sure convergence are often referred to as strong convergence and convergence in probability and distribution as weak convergence. Under certain conditions, convergence in probability can be attributed to mean square and almost sure convergence.

3 Polynomial and Spline Spaces

In this chapter, the basic aspects of orthogonal polynomials and splines, especially B-spline basis functions, are discussed in terms of their approximation quality. The focus is on the univariate case for polynomials, while for splines both, univariate and multivariate, cases are considered. Essentially, reliable mathematical literature Bazilevs et al., 2006; Sande et al., 2020; Szegö, 1939; Xiu, 2010 is prepared in such a way that it is directly accessible as appropriate tools for the ensuing analyses and examples in chapters 5, 6, and 7.

3.1 Orthogonal Polynomials

First, the basics of orthogonal polynomials are reviewed with an adjusted notation. The scope of the content is narrowed down to include the essentials for this dissertation. More detailed considerations about the properties of orthogonal polynomials can be found in the comprehensive references - e.g. Beckmann (1973), Chihara (2014), Jackson (2012), and Szegö (1939).

A system of polynomials $\{P_n(x) \mid n \in N\}$, where N is a finite or countably infinite index set of natural numbers, is called orthogonal with respect to the density w if the orthogonality condition

$$\langle P_n, P_m \rangle_{L^2_w} := \int_S P_n(x) P_m(x) w(x) dx = \gamma_n \delta_{nm}$$

is satisfied for all $n, m \in N$; where δ_{nm} is the Kronecker delta function, S the support of w, and obviously

$$\gamma_n = \|P_n\|^2_{L^2_w}$$

normalization factors. If $\gamma_n = 1$ for all $n \in N$ the system is orthonormal. Every orthogonal system can be normalized very easily.
There are several ways to describe orthogonal polynomials. The most general form, which is valid for all of them, is the three-term recurrence relation:

$$-P_{n+1}(x) = (a_n x + b_n) P_n(x) - c_n P_{n-1}(x), \quad n \geq 1, \tag{3.1}$$

where $A_n \neq 0$, $C_n \neq 0$, $C_n A_n A_{n-1} > 0$, $P_{-1}(x) = 0$, and $P_0(x) = 1$. The inverse is also true and is called Favard's Theorem - see Chihara (2014).
Another possibility is the derivation of orthogonal polynomials from the Askey scheme Askey and Wilson, 1985, which is based on the generalized hypergeometric series

$$ {}_rF_s(a_1, \ldots, a_r; b_1, \ldots, b_s; z) := \sum_{k=0}^{\infty} \frac{(a_1)_k \cdots (a_r)_k}{(b_1)_k \cdots (b_s)_k} \frac{z^k}{k!}, $$

where $b_i \neq 0, -1, -2, \ldots$, and the Pochhammer symbol

$$ (a)_n = \begin{cases} a, & n = 0 \\ a(a+1)\cdots(a+n+1), & n = 1, 2, \ldots . \end{cases} $$

The infinite series can be terminated in a natural way if one of the numerator parameters a_i is a negative integer. For example, if $a_1 = -n$, then the series is zero for $n \geq 0$, because $(a_1)_k = 0$ for $k = n+1, n+2, \ldots$, i.e.

$$ {}_rF_s(a_1, \ldots, a_r; b_1, \ldots, b_s; z) := \sum_{k=0}^{n} \frac{(a_1)_k \cdots (a_r)_k}{(b_1)_k \cdots (b_s)_k} \frac{z^k}{k!}, $$

and results in a polynomial of degree n.
The orthogonal polynomials from the Askey scheme can be well illustrated by a tree structure, which also shows their limit relations - see for example Koekoek, Lesky, et al. (2010, p.184). A selection of the orthogonal polynomials from the hypergeometric series can be found in Tab. 3.1, which are sufficient for the treatment in this work. For a detailed consideration, the reader is referred to the literature of Koekoek, Lesky, et al. (2010), Koekoek and Swarttouw (1996), and Schoutens (2012) and to Xiu (2010) and Xiu and Karniadakis (2002) within a stochastic setting. A few of the corresponding density functions of orthogonal polynomials coincide with the most important distributions for the stochastic modeling of parameters in practical applications. Therefore, they are presented below, namely Hermite, Legendre, Jacobi and Laguerre polynomials.

${}_2F_0(0)$	Hermite		
${}_1F_1(1)$	Laguerre	Charlier	
${}_2F_1(2)$	Jacobi	Legendre ($\alpha = \beta = 0$)	Chebyshev ($\alpha = \beta = -0.5$)

Table 3.1: Selection from the Askey scheme - cf. Xiu and Karniadakis (2002).

3.1.1 Examples

In the following, the polynomial bases used in this work including their construction and essential properties are briefly outlined. For further details, refer to the work of Xiu

(2010).

Hermite Polynomial and Gaussian Distribution

Hermite polynomials are defined by

$$H_n(x) := \left(\sqrt{2}x\right)^2 {}_2F_0\left(-\frac{n}{n}, -\frac{n-1}{2}; ; -\frac{2}{x^2}\right)$$

with orthogonality

$$\int_{-\infty}^{\infty} H_n(x) H_m(x) w(x) dx = n! \delta_{nm}$$

with

$$w(x) = \frac{1}{\sqrt{2\pi}} e^{-\frac{x^2}{2}},$$

which is the standard Gaussian density.
Recurrence relation:

$$H_{n+1}(x) = xH_n(x) - nH_{n-1}(x).$$

Rodriguez formula:

$$H_n(x) = e^{\frac{x^2}{2}} (-1)^n \frac{d^n}{dx^n} \left(e^{-\frac{x^2}{2}}\right).$$

The Rodriguez formula is the third way to construct orthogonal polynomials, and worked via derivatives. The Hermite polynomials are of outstanding importance in stochastic analysis, because the most common discretization methods for random functions lead to normally distributed vectors. We will discuss this aspect in more detail later. The first Hermite polynomials are depicted in Tab. 3.2 and in Fig. 3.1.

Legendre Polynomial and Uniform Distribution

Legendre polynomials are defined by

$$L_n(x) := {}_2F_1\left(-n, n+1; 1; -\frac{1-x}{2}\right)$$

with orthogonality

$$\int_{-1}^{1} L_n(x) L_m(x) w(x) dx = \frac{1}{2n+1} \delta_{nm}$$

with

$$w(x) = \frac{1}{2},$$

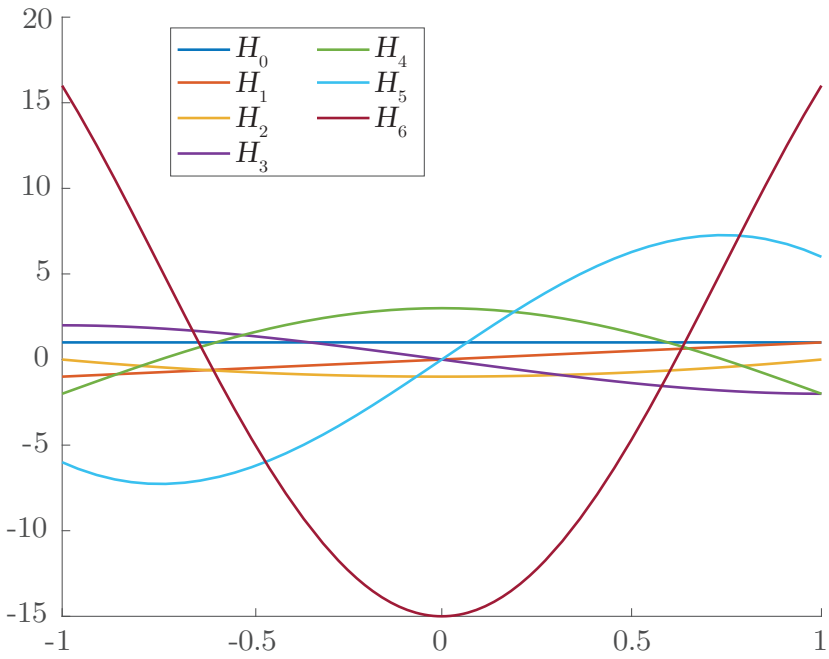

Figure 3.1: Hermite polynomials

n	$H_n(x)$	$L_n(x)$
0	1	1
1	x	x
2	$x^2 - 1$	$\frac{3}{2}x^2 - \frac{1}{2}$
3	$x^3 - 3x$	$\frac{5}{2}x^3 - \frac{3}{2}x$
4	$x^4 - 6x^2 + 3$	$\frac{35}{8}x^4 - \frac{15}{4}x^2 + \frac{3}{8}$
5	$x^5 - 10x^3 + 15x$	$\frac{63}{8}x^5 - \frac{35}{4}x^3 + \frac{15}{8}x$

Table 3.2: First six orthogonal polynomials.

which is the uniform density on the interval $[-1, 1]$.
Recurrence relation:

$$L_{n+1}(x) = \frac{2n+1}{n+1} x L_n(x) - \frac{n}{n+1} L_{n-1}(x).$$

Rodriguez formula:

$$L_n(x) = \frac{(-1)^n}{2^n n!} \frac{d^n}{dx^n} \Big((x^2 - 1)^n \Big).$$

The first Legendre polynomials are depicted in Tab. 3.2 and in Fig. 3.2.

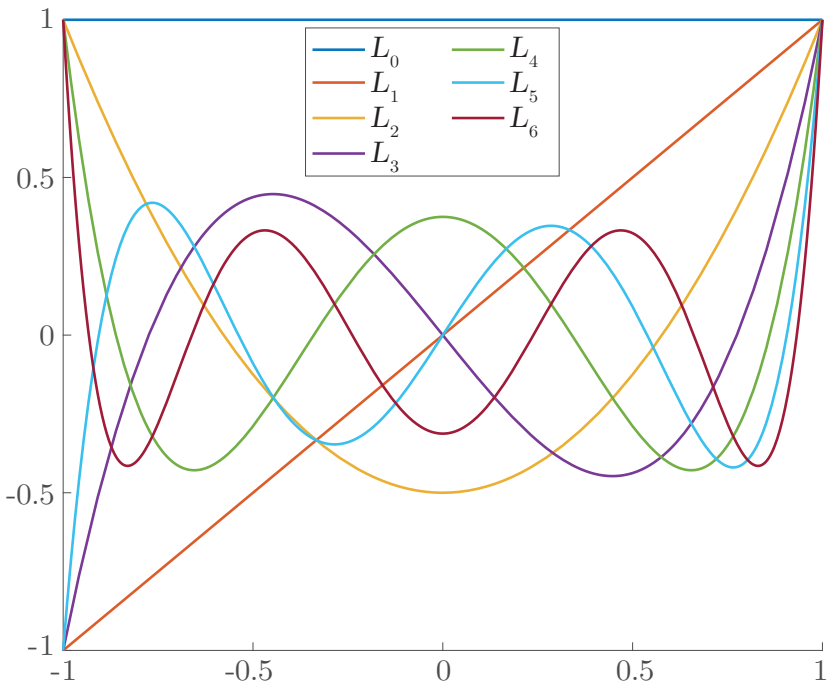

Figure 3.2: Legendre polynomials.

Laguerre Polynomial and Gamma Distribution

Laguerre polynomials are defined by

$$P_{n;\alpha}^{LG}(x) := \frac{(\alpha+1)_n}{n!} {}_1F_1\Big(-n, \alpha+1; 1; x\Big), \qquad \alpha > -1,$$

with orthogonality

$$\int_0^\infty P_{n;\alpha}^{LG}(x) P_{m;\alpha}^{LG}(x) w(x) dx = \frac{(\alpha+1)_n}{n!} \delta_{nm}$$

with

$$w(x) = \frac{e^{-x} x^\alpha}{\Gamma(\alpha+1)}.$$

which is the gamma density with scale parameter equal one. Recurrence relation:

$$(n+1) P_{n+1;\alpha}^{LG}(x) = (-x + 2n + \alpha + 1) P_{n;\alpha}^{LG}(x) - (n+\alpha) P_{n-1;\alpha}^{LG}(x) = 0.$$

Rodriguez formula:

$$e^{-x}x^{\alpha}P^{LG}_{n;\alpha}(x) = \frac{1}{n!}\frac{d^n}{dx^n}\Big((e^{-x}x^{n+\alpha})\Big).$$

Jacobi Polynomial and Beta Distribution

Jacobi polynomials are defined by

$$P^{J}_{n;\alpha\beta}(x) := \frac{(\alpha+1)_n}{n!}{}_2F_1\Big(-n, n+\alpha+\beta+1; \alpha+1; \frac{1-x}{2}\Big), \qquad \alpha,\beta > -1,$$

with orthogonality

$$\int_{-1}^{1} P^{J}_{n;\alpha\beta}(x)P^{J}_{m;\alpha\beta}(x)w(x)dx = \frac{(\alpha+1_n)(\beta+1_n)}{n!(2n+\alpha+\beta+1)(\alpha+\beta+2)_{n-1}}\delta_{nm}$$

with

$$w(x) = \frac{\Gamma(\alpha+\beta+2)}{2^{\alpha+\beta+1}\Gamma(\alpha+1)\Gamma(\beta+1)}(1-x)^{\alpha}(1+x)^{\beta}.$$

Recurrence relation:

$$\begin{aligned}\frac{(2n+1)(n+\alpha+\beta+1)}{(2n+\alpha+\beta+1)(2n+\alpha+\beta+2)}P^{J}_{n+1;\alpha\beta}(x) = \\ (x - \frac{\alpha^2+\beta^2}{(2n+\alpha+\beta)(2n+\alpha+\beta+2)})P^{J}_{n;\alpha\beta}(x) \\ - \frac{2(n+\alpha)(n+\beta)}{(2n+\alpha+\beta)(2n+\alpha+\beta+1)}P^{J}_{n-1;\alpha\beta}(x).\end{aligned}$$

Rodriguez formula:

$$(1-x)^{\alpha}(1+x)^{\beta}P^{J}_{n;\alpha\beta}(x) = \frac{(-1)^n}{2^n n!}\frac{d^n}{dx^n}\Big((1-x)^{\alpha+n}(1+x)^{\beta+n}\Big).$$

Bernstein Polynomial and Uniform Distribution

The main goal of this thesis is the study of Bernstein polynomials and especially their spline generalization in a stochastic framework. Therefore, standard and orthogonal Bernstein polynomials and their relationship with Legendre polynomials are introduced in the following. The relationship of both polynomials will be solidified later in the analysis.
The univariate Legendre polynomials are traditionally defined on the interval $[-1,1]$. In order to related them to Bernstein polynomials, which are defined on $[0,1]$, they are

considered on the interval $[0,1]$ which can be done with a simple linear mapping. Then, the univariate Legendre polynomials of order p on the interval $[0,1]$ can be expressed by Farouki, 2000:

$$L^p(x) = \sum_{n=0}^{p} (-1)^{p+n} \binom{p}{n} B_n^p(x), \tag{3.2}$$

where

$$P_{n;p}^B(x) = \binom{p}{n} x^n (1-x)^{p-n} \quad \text{for} \quad n = 0, \ldots, p$$

are the standard Bernstein polynomials of order p on the interval $[0,1]$ - see Fig. 3.3. The relation (3.2) suggests that the orthogonal Bernstein polynomials also correspond to the uniform distribution. This conjecture is also strengthened by the fact that orthogonal Bernstein polynomials can be constructed over simple Bernstein polynomials. Orthogonal Bernstein polynomials are defined by Bellucci, 2014:

$$P_{n;p}^{OB}(x) := \sqrt{2(p-n)+1} \sum_{i=0}^{n} (-1)^i \frac{\binom{2p+1-i}{n-i}\binom{n}{i}}{\binom{p-n}{i-n}} P_{n-i;p-i}^B(x) \quad \text{for} \quad n = 0, \ldots, p$$

and it holds

$$\int_{-1}^{1} P_{n;p}^{OB}(x) P_{m;p}^{OB}(x) \frac{1}{2}\, dx = 0 \quad \text{for} \quad n \neq m,$$

with $n, m = 0, \ldots, p$. Fig. 3.4 visualizes orthogonal Bernstein polynomials for $p = 6$. As is readily seen, the orthogonal splines lose important properties that make their relatives valuable for deterministic analysis, i.e. variation diminishing and convex hull

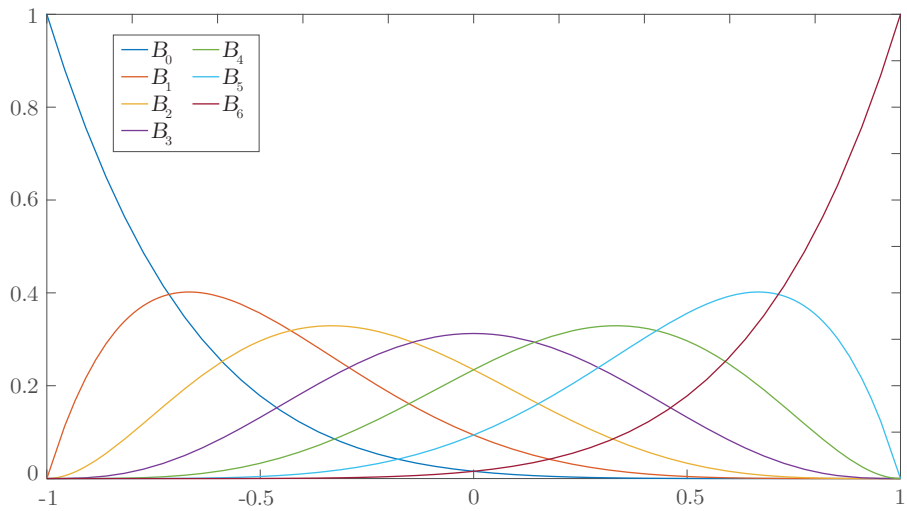

Figure 3.3: Bernstein polynomials.

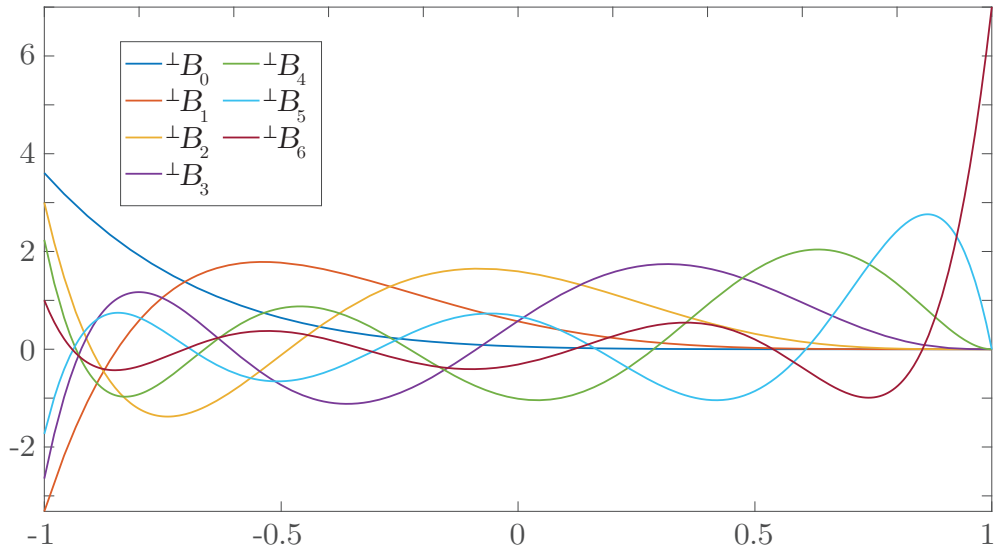

Figure 3.4: Orthogonal Bernstein polynomials.

(non-negative values). Note, in contrast to the Hermite and Legendre polynomials the orthogonal Bernstein polynomials $P_{n;p}^{OB}$ have to be regenerated for each order p, which is suggested by the additional index p. For instance, that means for $p = 6$, the orthogonal Bernstein basis consists of seven polynomials of order six, where as the Hermite and Legendre polynomials consists of seven polynomials with order $0, 1, \ldots, 6$, respectively. This fact can easily be seen by comparing in Fig. 3.1, Fig. 3.2, and Fig. 3.4.

3.1.2 Polynomial Approximation

This section is devoted to the approximation theory of polynomials and briefly summarizes the necessary statements for the definition of orthogonal projections. The orthogonal projections are an essential step to determine the coefficients for the methods presented in chapter 5. Furthermore, the terms spectral convergence and quadrature formulas are clarified. This is an adapted selection from the book of Xiu (2010, chapter 3), where is referred to for further details and to the literature therein.

Denote by

$$\mathcal{P}_p := \left\{ P(x) \mid P(x) = \sum_{i=0}^{p} a_i x^i \text{ with } a_i, x \in \mathbb{R} \right\} \tag{3.3}$$

the space of polynomials with maximal degree p Schumaker, 2007. First, the very important and fundamental Weierstrass theorem from the approximation theory of polynomials is presented. It states that for every continuous function in a closed interval there exists a polynomial which can approximate this function arbitrarily exactly.

Theorem 3.1.1 (Weierstrass). *Let I be a bounded interval and $f \in \mathcal{C}^0(I)$. For $\epsilon > 0$ there exists $p \in \mathbb{N}$ and a polynomial $P \in \mathcal{P}_p$, such that*

$$\|f(x) - P(x)\|_\infty < \epsilon, \quad \forall x \in I.$$

Proof. The proof can be found in various books on approximation theory, for example Atkinson and Han (2009, p.114) or Cheney (1966), Timan (1963), and Todd (1963) □

Many important results have arisen from this strong theorem, and it seems natural to ask the question: What is the best approximation for a given degree p, or in other words:

$$\text{Find the polynomial } P_f \in \mathcal{P}_p \text{ such that}$$

$$\left\|f(x) - P_f(x)\right\|_\infty = \inf_{g \in \mathcal{P}_p} \|f(x) - g(x)\|_\infty .$$

Of course, the solution and quality depends largely on the norm or, in other words, on the space in which the function is sought and measured. In the following, this is studied for orthogonal polynomials in the weighted space of square integrable functions L^2_w.

Orthogonal Projection

Consider a fixed degree $p \in \mathbb{N}_0$ and $\{P_n(x)\}_{n=0}^p \subset \mathcal{P}_p$ a system of orthogonal polynomials of degree at most p with respect to the density or weight $w(x)$. The projection operator $\Pi_{\mathcal{P}_p} : L^2_w(I) \to \mathcal{P}_p$ is defined by Xiu, 2010:

$$f \mapsto \Pi_{\mathcal{P}_p} f := \sum_{n=0}^{p} \hat{f}_n P_n(x) \qquad \text{with} \qquad \hat{f}_n := \frac{1}{\|P_n\|^2_{L^2_w}} \langle f, P_n \rangle_{L^2_w} .$$

$\Pi_{\mathcal{P}_p}$ is called the orthogonal projection of f onto $\mathcal{P}_p$ with respect to the inner product $\langle \cdot, \cdot \rangle_{L^2_w}$ and it holds

$$\Pi_{\mathcal{P}_p} f = f \qquad \forall f \in \mathcal{P}_p ,$$

ant the error is orthogonal to the polynomial space, i.e.,

$$\left\langle f - \Pi_{\mathcal{P}_p} f, P \right\rangle = 0 \qquad \forall P \in \mathcal{P}_p .$$

Furthermore, $\Pi_{\mathcal{P}_p} f$ is the best approximation in the weighted L^2-space:

Theorem 3.1.2. *Let $f \in L^2_w(I)$ and $p \in \mathbb{N}_0$, then*

$$\left\| f - \Pi_{\mathcal{P}_p} f \right\|_{L^2_w} = \inf_{g \in \mathcal{P}_p} \| f(x) - g(x) \|_{L^2_w} .$$

Proof. For the proof and details see, for example, Atkinson and Han (2009, p.153). □

After it is clear that $\Pi_{\mathcal{P}_p}$ provides the best approximation, the question arises whether the approximation gains in quality with increasing degree and, if this is the case, what is the performance or rate of convergence.

Theorem 3.1.3. *Let $f \in L^2_w(I)$, then*

$$\lim_{p \to \infty} \left\| f - \Pi_{\mathcal{P}_p} f \right\|_{L^2_w} = 0 .$$

Proof. See Funaro (2008) for a bounded interval and Courant and Hilbert (2008) for the unbounded case. □

With increasing degree of the orthogonal polynomials the approximation becomes sufficiently exact. The rate of convergence depends on the regularity and also on the type of the orthogonal polynomials. A wide literature has accumulated over the years dealing with convergence rates for different approximations Xiu, 2010. As an example, the case for Legendre polynomials is demonstrated here. The measurability of the regularity can be refined by the introduction of Sobolev spaces, where also the derivatives must be square integrable. As in the case of L^2-spaces, the weighted variant is used here, i.e.,

$$H^k_w(I) := \left\{ v \in L^2_w \mid \frac{d^i v}{dx^i} \in L^2_w \text{ for } 0 \leq i \leq k \right\}$$

equipped with the inner product

$$\langle u, v \rangle_{H^k_w} := \sum_{i=0}^{k} \left\langle \frac{d^i u}{dx^i}, \frac{d^i v}{dx^i} \right\rangle_{L^2_w} ,$$

and standard norm. Consider the set of orthogonal Legendre polynomials $\{L_n\}$ on the interval $[-1, 1]$.

Theorem 3.1.4 (Spectral convergence)**.** *Let $k \in \mathbb{N}_0$. For $f \in H^k_w([-1,1])$ there exists a polynomial $\Pi_{\mathcal{P}_p} f \in L_n$, such that*

$$\left\| f - \Pi_{\mathcal{P}_p} f \right\|_{L^2_w([-1,1])} \leq C p^{-k} \| f \|_{H^k_w([-1,1])}$$

with C constant and independent of p.

Proof. See Xiu (2010, p.33) □

The convergence rate depends on the smoothness of the function f and relies not on the degree of the polynomial. If the regularity k increases, the approximation error becomes smaller. Compared to finite element approximation this kind of convergence is not common. It is also called spectral convergence. As a limit result, for an infinitely smooth function, the convergence rate is faster than any algebraic order, and spectral convergence becomes exponential convergence, i.e.,

$$\left\| f - \Pi_{\mathcal{P}_p} f \right\|_{L^2_w} \sim C e^{-\alpha p} \left\| f \right\|_{L^2_w} ,$$

where C and α are generic positive constants. Xiu, 2010

As a last important property of orthogonal polynomials in this work, attention should be drawn to the zeros and their application in quadrature formulas. Consider a set of orthogonal polynomials $\{P_n\} \subset \mathcal{P}_p$ and their real zeros $\{z_k^{(p)}\}_{k=1}^{p}$, as well as $l_k^{(p)}$ the p-th-degree Lagrange polynomial through the nodes $z_k^{(p)}$. Then

$$\int_I f(x) w(x) dx \approx \sum_{k=1}^{p} f(z_k^{(p)}) w_k^{(p)}$$

with

$$w_k^{(p)} := \int_I l_k^{(p)} w(x) dx, \qquad 1 \leq k \leq p \, .$$

These integration formulas are highly accurate, because it is exact if $f \in \mathcal{P}_{2p-1}$. In the stochastic part of this work it will be shown that not only the polynomials used but also the quadrature formulas employed for the emerging integrals are crucial for the accuracy. Moreover, it is very easy to construct this kind of integration formulas. Xiu, 2010

3.2 Spline Spaces

In this section the B-spline functions in focus will be defined and the recently refined a priori error estimates will be presented. At the end of this chapter there will be statements about the convergence rate as already shown in the previous section about polynomials. As presented before, in the stochastic applications mainly spectral convergences are considered, that means that the refinement for approximation improvement is done by the degree. Orthogonal polynomials do not have any further degrees of

freedom to increase the approximation quality. This is different for spline spaces. Besides increasing the degree p, the element size h can be refined and the regularity k can be varied over element boundaries. Obviously, this h-p-k refinement complicates the convergence analysis considerably and continues to be the subject of current research, especially with respect to explicit constants Da Veiga, Buffa, Rivas, et al., 2011; Sande et al., 2019, 2020; S. Takacs and T. Takacs, 2016. In addition, the element knots need not be distributed equidistantly, but also arbitrarily, which is also exceedingly challenging, but increasing the flexibility of these spaces as well. Despite all this, Sande et al. (2020) have found explicit bounds of the form (simplified)

$$\|f - \Pi f\| \leq \left(\frac{eh}{4(p-k)}\right)^r \|\delta^r f\|$$

for any $f \in H^k$, all $p > r-1$, and with e the Euler's number. Overall, the authors provide a priori error estimates with explicit constants for the approximation by spline spaces of arbitrary smoothness defined on arbitrary sequences of knots. They improve the estimates of Da Veiga, Buffa, Rivas, et al. (2011), Sande et al. (2019), and S. Takacs and T. Takacs (2016) and in addition they solve the problem of dealing with smoothness in the estimates. These significant results are achieved by representing the considered Sobolev spaces and the approximating spline spaces in terms of integral operators described by appropriate kernels Pinkus, 2012. Using these kernels, an abstract framework is provided that converts explicit constants in the polynomial approximation to explicit constants in the spline approximation. Both univariate and multivariate spline spaces are considered, and mapped geometries as well. Following the literature of Da Veiga, Buffa, Giancarlo Sangalli, et al. (2014) and Da Veiga, Cho, et al. (2012), for mapped geometries suitable curved Sobolev spaces must be introduced to account for a less smooth setting for the geometry.

3.2.1 Definitions

Let

$$\mathfrak{P} := \{\zeta_i\}_{i=1}^{k} \quad \text{with } 0 = \zeta_0 < \zeta_1 < \ldots < \zeta_k < \zeta_{k+1} = 1 \tag{3.4}$$

be a partition of the interval $[0,1]$ into $k+1$ subintervals

$$\begin{aligned} I_i &:= [\zeta_i, \zeta_{i+1}) \quad \text{for } i = 0, 1, \ldots, k-1 \\ I_k &:= [\zeta_k, \zeta_{k+1}], \end{aligned} \tag{3.5}$$

$p \in \mathbb{N}$ be a positive integer, and let $\mathfrak{M} := (m_1, \ldots, m_k) \in \mathbb{N}^k$ be a vector of positive integers with $m_i \leq p+1$, $i = 1, \ldots, k$.

Definition 6: Polynomial splines

The space

$$\begin{aligned}\mathcal{S}_p\left(\mathfrak{P};\mathfrak{M}\right) := \big\{ S(\zeta) \mid \exists\, P_0,\dots,P_k \in \mathcal{P}_p \text{ such that} \\ S(\zeta) = P_i(\zeta) \text{ for } \zeta \in I_i, \text{ and} \\ \nabla^j P_{i-1}(\zeta_i) = \nabla^j P_i(\zeta_i) \\ \text{for } \; i = 1,\dots,k,\; j = 0,1,\dots,p-m_i \big\}\end{aligned} \tag{3.6}$$

is called the space of polynomial splines of degree p with knots $\zeta_i \in \mathfrak{P}$ and multiplicity vector $\mathfrak{M}$. Schumaker, 2007

The multiplicity vector $\mathfrak{M}$ controls the smoothness of the splines at the knots. For $\mathfrak{M} = (1,\dots,1)$ maximal smoothness is achieved and the space of splines is a subset of $\mathcal{C}^{p-1}[0,1]$. If $\mathfrak{M} = (p,\dots,p)$, all splines are $\mathcal{C}^0$-continuous across knots, and if $m_i = p+1$, the spline can be discontinuous at the knot ζ_i. Furthermore, $\mathcal{S}_p\left(\mathfrak{P};\mathfrak{M}\right)$ is a linear space of dimension

$$n = p + 1 + \sum_{i=1}^{k} m_i. \tag{3.7}$$

In IGA and CAD, commonly an open knot vector Ξ is defined which characterizes B-spline bases. Ξ is an extended partition which can be uniquely determined by degree p, partition $\mathfrak{P}$, and multiplicity vector $\mathfrak{M}$ as follows:

$$\Xi := [\xi_1,\dots,\xi_{n+p+1}] = [\underbrace{0,\dots,0}_{p+1},\underbrace{\zeta_1,\dots,\zeta_1}_{m_1},\dots,\underbrace{\zeta_k,\dots,\zeta_k}_{m_k},\underbrace{1,\dots,1}_{p+1}]. \tag{3.8}$$

The B-spline basis functions with open knot vector Ξ can then be constructed by the CoxCOX, 1972-de BoorBoor, 1972 recursion formula:

$$B_i^0(\xi) := \begin{cases} 1 & \text{for } \xi_i \le \xi < \xi_{i+1} \\ 0 & \text{otherwise} \end{cases} \qquad \text{for } i = 1,\dots,n+p, \tag{3.9}$$

and

$$B_i^k(\xi) := \frac{\xi - \xi_i}{\xi_{i+k} - \xi_i} B_i^{k-1}(\xi) + \frac{\xi_{i+k+1} - \xi}{\xi_{i+k+1} - \xi_{i+1}} B_{i+1}^{k-1}(\xi) \tag{3.10}$$

for $k = 1,\dots,p$, $i = 1,\dots,n+p-k$. Furthermore, the spline space can be spanned by the B-spline basis functions Schumaker, 2007:

$$\mathcal{S}_p \equiv \mathcal{S}_p(\mathfrak{P};\mathfrak{M}) \equiv \mathcal{S}_p(\Xi) := \operatorname{span}\{B_i^p\}_{i=1}^n. \tag{3.11}$$

Example of $\mathcal{C}^{p-1}$ B-spline basis

Consider the space $\mathcal{S}_4(\mathfrak{P};\mathfrak{M})$ with partition $\mathfrak{P} = \{0.25, 0.5, 0.75\}$, and multiplicity vector $\mathfrak{M} = (1,1,1)$. This leads to an extended partition or open knot vector

$$\Xi = [0,0,0,0,0,\tfrac{1}{4},\tfrac{1}{2},\tfrac{3}{4},1,1,1,1,1]. \tag{3.12}$$

Single inner knots reveal the maximal $\mathcal{C}^{p-1}$-continuity. The B-spline basis spanning the space $\mathcal{S}_4(\mathfrak{P};\mathfrak{M})$ with dimension

$$n = p + 1 + \sum_{i=1}^{k} m_i = 4 + 1 + \sum_{i=1}^{3} 1 = 8 \tag{3.13}$$

can be seen in Fig. 3.5.

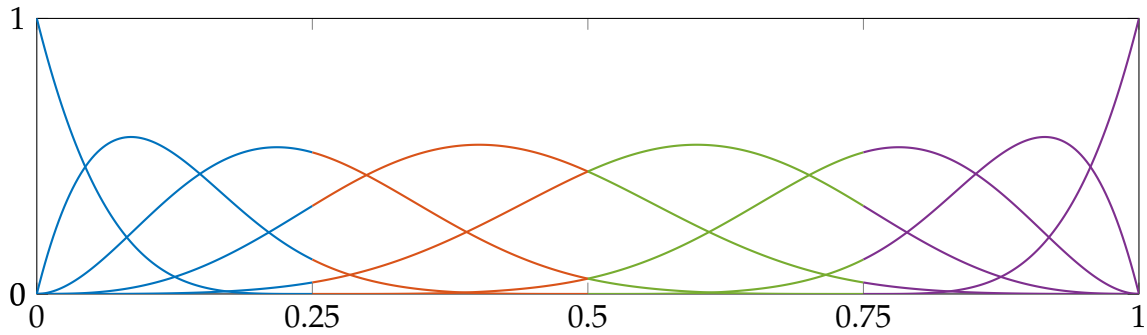

Figure 3.5: B-spline basis of order $p = 4$, $\mathfrak{P} = \{0.25, 0.5, 0.75\}$ and dimension $n = 8$.

Example of $\mathcal{C}^0$ B-spline basis

Consider the space $\mathcal{S}_4(\mathfrak{P};\mathfrak{M})$ with partition $\mathfrak{P} = \{0.25, 0.5, 0.75\}$, and multiplicity vector $\mathfrak{M} = (4,4,4)$. This leads to the open knot vector

$$\Xi = [0,0,0,0,0,\tfrac{1}{4},\tfrac{1}{4},\tfrac{1}{4},\tfrac{1}{4},\tfrac{1}{2},\tfrac{1}{2},\tfrac{1}{2},\tfrac{1}{2},\tfrac{3}{4},\tfrac{3}{4},\tfrac{3}{4},\tfrac{3}{4},1,1,1,1,1]. \tag{3.14}$$

Repeating the inner knots $p-1$-times results in the lowest $\mathcal{C}^0$-continuity. The B-spline basis spanning the space $\mathcal{S}_4(\mathfrak{P};\mathfrak{M})$ with dimension

$$n = p + 1 + \sum_{i=1}^{k} m_i = 4 + 1 + \sum_{i=1}^{3} 4 = 17. \tag{3.15}$$

can be seen in Fig. 3.6. A prescribed continuity affects profoundly the number of basis functions. Important to note is, that the spaces in both examples have the same order

and partition, but the dimension significantly differs, which is indeed is the main reason for the effectiveness of the subsequently presented methodology.

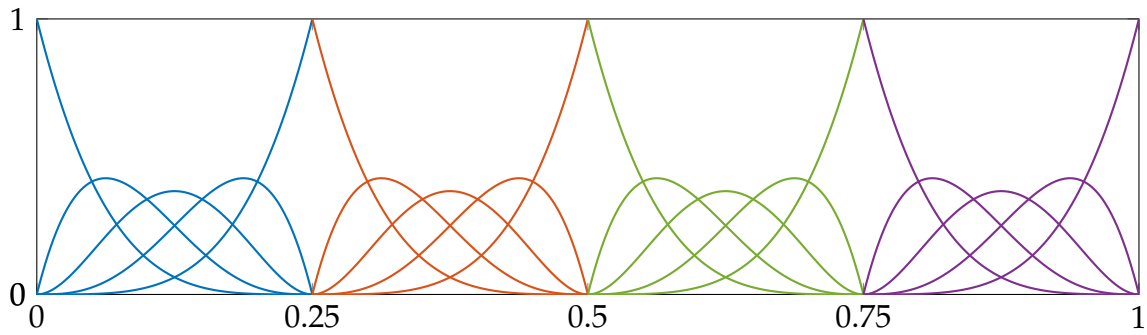

Figure 3.6: B-spline basis of order $p = 4$, $\mathfrak{P} = \{0.25, 0.5, 0.75\}$ and dimension $n = 17$.

The tensor product B-spline basis functions are defined by Bazilevs et al., 2006:

$$B_{i_1 \dots i_d} := B_{i_1,1} \otimes \dots \otimes B_{i_d,d}, \tag{3.16}$$

over the mesh

$$\begin{aligned} \mathcal{Q} \equiv \mathcal{Q}(\mathfrak{P}) \equiv \mathcal{Q}(\Xi) &:= \{Q = \otimes_{\alpha=1}^{d} (\zeta_{i_\alpha,\alpha}, \zeta_{i_{\alpha+1},\alpha}) \mid i_\alpha = 0, 1, \dots, k_\alpha\} \\ &= \{Q = \otimes_{\alpha=1}^{d} (\xi_{i_\alpha,\alpha}, \xi_{i_{\alpha+1},\alpha}) \mid i_\alpha = 1, \dots, n_\alpha + p_\alpha \wedge Q \neq \emptyset\}, \end{aligned} \tag{3.17}$$

which is a partition of the d-dimensional hyper cube into d-dimensional open knot spans, or elements. For each $Q \in \mathcal{Q}$ associate the support extension $\tilde{Q} \subset (0,1)^d$ defined by Bazilevs et al., 2006:

$$\tilde{Q}(Q) := \otimes_{\alpha=1}^{d} (\xi_{i_\alpha - p_\alpha,\alpha}, \xi_{i_\alpha + p_\alpha + 1,\alpha}) \tag{3.18}$$

which is the union of supports of basis functions whose support intersects Q.

Definition 7: Tensor product spline space

The space

$$\mathcal{S}_{\mathbf{p}} \equiv \mathcal{S}_{\mathbf{p}}(\mathfrak{P}; \mathfrak{M}) := \bigotimes_{\alpha=1}^{d} \mathcal{S}_{p_\alpha}(\mathfrak{P}_\alpha; \mathfrak{M}_\alpha) = \operatorname{span}\{B_{i_1 \dots i_d}\}_{i_1=1,\dots,i_d=1}^{n_1,\dots,n_d}. \tag{3.19}$$

is called the tensor product space of splines of degree $\mathbf{p} = (p_1, \dots, p_d)$ with partition $\mathfrak{P} = (\mathfrak{P}_1, \dots, \mathfrak{P}_d)$ and multiplicity vector $\mathfrak{M} = (\mathfrak{M}_1, \dots, \mathfrak{M}_d)$. Schumaker, 2007

Next, non-uniform rational B-splines (NURBS) space on $[0,1]^d$ and on an arbitrary

physical domain D are defined. Therefore, a strictly positive weighting function

$$W := \sum_{i_1=1}^{n_1} \dots \sum_{i_d=1}^{n_d} w_{i_1 \dots i_d} B_{i_1 \dots i_d} \tag{3.20}$$

with $w_{i_1 \dots i_d} \in \mathbb{R}$ is introduced. The NURBS basis functions on the patch $[0,1]^d$ are defined by the projectionFarin, 1995:

$$N_{i_1 \dots i_d} := \frac{w_{i_1 \dots i_d} B_{i_1 \dots i_d}}{W}, \tag{3.21}$$

and, accordingly, the one-dimensional space of NURBS is given by

$$\mathcal{N}_p \equiv \mathcal{N}_p(\mathfrak{P}; \mathfrak{M}; W) \equiv \mathcal{N}_p(\Xi; W) := \operatorname{span}\{N_i\}_{i=1}^{n}. \tag{3.22}$$

Definition 8: Tensor product NURBS space

The space

$$\begin{aligned} \mathcal{N}_{\mathbf{p}} &\equiv \mathcal{N}_{\mathbf{p}}(\boldsymbol{\mathfrak{P}}; \boldsymbol{\mathfrak{M}}; \mathbf{W}) \\ &:= \bigotimes_{\alpha=1}^{d} \mathcal{N}_{p_\alpha}(\mathfrak{P}_\alpha; \mathfrak{M}_\alpha; W_\alpha) = \operatorname{span}\{N_{i_1 \dots i_d}\}_{i_1=1,\dots,i_d=1}^{n_1,\dots,n_d} \end{aligned} \tag{3.23}$$

is called the tensor product NURBS space of degree $\mathbf{p} = (p_1, \dots, p_d)$ with partition $\boldsymbol{\mathfrak{P}} = (\mathfrak{P}_1, \dots, \mathfrak{P}_d)$, multiplicity vector $\boldsymbol{\mathfrak{M}} = (\mathfrak{M}_1, \dots, \mathfrak{M}_d)$, and weighting function $\mathbf{W} = (W_1, \dots, W_d)$.

Further, for parameterizing a physical domain $D \subset \mathbb{R}^d$ the NURBS geometrical mapHughes et al., 2005:

$$F : [0,1]^d \to D, \qquad \xi \mapsto F(\xi) = \sum_{i_1=1}^{n_1} \dots \sum_{i_d=1}^{n_d} C_{i_1 \dots i_d} R_{i_1 \dots i_d}(\xi) \tag{3.24}$$

is introduced and it is assumed that F is invertible, with smooth inverse, on each element $Q \in \mathcal{Q}$. Besides, $\mathcal{Q}$ induces a mesh in the physical domain:

$$\mathcal{K} := \{K = F(Q) \mid Q \in \mathcal{Q}\}. \tag{3.25}$$

Analogously, the support extension $\tilde{Q}$ of $Q \in \mathcal{Q}$ is mapped in the same fashion, i.e.

$$\tilde{K} := F(\tilde{Q}). \tag{3.26}$$

Finally, the space of tensor product NURBS on the physical domain D can be defined, which is the push-forward of $\mathcal{N}_{\mathbf{p}}$ on $[0,1]^d$.

Definition 9: Tensor product NURBS space on the physical domain

The space

$$\begin{aligned}\mathcal{V}_{\mathbf{p}} &\equiv \mathcal{V}_{\mathbf{p}}(\mathfrak{P};\mathfrak{M};\mathbf{W}) \\ &\equiv \bigotimes_{\alpha=1}^{d} \mathcal{V}_{p_\alpha}(\mathfrak{P}_\alpha;\mathfrak{M}_\alpha;W_\alpha) := \operatorname{span}\{N_{i_1\dots i_d}\circ F^{-1}\}_{i_1=1,\dots,i_d=1}^{n_1,\dots,n_d}\end{aligned} \tag{3.27}$$

is called the tensor product NURBS space on the physical domain of degree $\mathbf{p} = (p_1,\dots,p_d)$ with partition $\mathfrak{P} = (\mathfrak{P}_1,\dots,\mathfrak{P}_d)$, multiplicity vector $\mathfrak{M} = (\mathfrak{M}_1,\dots,\mathfrak{M}_d)$, and weighting function $\mathbf{W} = (W_1,\dots,W_d)$.

3.2.2 Bent Sobolev Spaces

In the following, proper function spaces are defined in order to derive error estimations for splines in terms of norms on bent Sobolev spaces Bazilevs et al., 2006. Denote by $L^p(D)$ and $H^k(D)$, $1 \le p \le \infty$, $1 \le k < \infty$, the standard Lebesgue and Sobolev spaces defined on a domain $D \subset \mathbb{R}^d$, respectively, endowed with the usual norms $\|\cdot\|$ and seminorms $|\cdot|$. For $Q_1, Q_2 \in \mathcal{Q}$ adjacent elements, denote by k_{Q_1,Q_2} the number of continuous derivatives across their common edge $\partial Q_1 \cap \partial Q_2$.

Definition 10: Bent Sobolev space

The space

$$\begin{aligned}\mathcal{H}^k := \{&v \in L^2((0,1)^d) \mid v_{|Q} \in H^k(Q)\ \forall Q \in \mathcal{Q}, \text{ and} \\ &\nabla^j v_{|Q_1} = \nabla^j v_{|Q_2} \text{ on } \partial Q_1 \cap \partial Q_2 \\ &\text{for } 0 \le j \le \min\{k_{Q_1,Q_2}, k-1\},\ \forall \text{ disjoint } Q_1, Q_2 \in \mathcal{Q}\}\end{aligned} \tag{3.28}$$

is called the bent Sobolev space of order $k \in \mathbb{N}$.

A bent Sobolev space is a well-defined Hilbert space Bazilevs et al., 2006 with norm

$$\|v\|_{\mathcal{H}^k}^2 := \sum_{i=0}^{k} |v|_{\mathcal{H}^i}^2 \tag{3.29}$$

and seminorms

$$|v|^2_{\mathcal{H}^i} := \sum_{Q \in \mathcal{Q}} |v|^2_{H^i(Q)}, \quad 0 \leq i \leq k. \tag{3.30}$$

Analogously, define the Hilbert space $\mathcal{H}^k(\tilde{Q}) := \{v_{|\tilde{Q}} \mid v \in \mathcal{H}^k\}$ on the restriction $\tilde{Q}$ endowed with norm

$$\|v\|^2_{\mathcal{H}^k(\tilde{Q})} := \sum_{i=0}^{k} |v|^2_{\mathcal{H}^i(\tilde{Q})} \tag{3.31}$$

and seminorms

$$|v|^2_{\mathcal{H}^i(\tilde{Q})} := \sum_{Q' \subset \tilde{Q}} |v|^2_{H^i(Q')}, \quad 0 \leq i \leq k. \tag{3.32}$$

As it can be seen in Eq. (3.30) and Eq. (3.32) the norms and seminorms over bent Sobolev spaces are defined by sums over d-dimensional hyper-cubes (elements) of their respective standard Sobolev spaces. This connection is also evident in definition 10. Functions in a bent Sobolev space, are element by element in a standard Sobolev space. The elements are connected to each other up to $k-1$-continuity, but can also be discontinuous if desired. Therefore, bent Sobolev spaces are between standard and brokenI. Babuška et al., 1999 Sobolev spaces in concern of continuity. Bazilevs et al., 2006

3.2.3 Local Approximation

The goal of this section is to provide estimations of quasi-interpolants including the geometric mapping of NURBS structures, which is necessary to estimate the deterministic error later in the chapter. The results of Bazilevs et al. (2006, chapter 3) necessary for this purpose are reproduced in a simplified adapted manner.

The following analysis is based on families of meshes and spaces starting from $\{\mathcal{Q}_h\}_h$ on $(0,1)^d$ with

$$h = \max\{h_Q \mid Q \in \mathcal{Q}_h\} \tag{3.33}$$

and h_Q is the diameter of Q. Assume that the family $\{\mathcal{Q}_h\}_h$ is shape regular. Upon these meshes meshes on the physical domain $\{\mathcal{K}_h\}_h$ are induced and further the families of spaces $\{\mathcal{S}_h\}_h$, $\{\mathcal{N}_h\}_h$, $\{\mathcal{V}_h\}_h$, and $\{\mathcal{H}_h\}_h$ endowed with their respective norms. Furthermore, it is assumed that there is a coarsest mesh $\mathcal{Q}_{h_0}$ of which all other meshes are refined by simultaneously preserving the geometry, i.e. F and $\mathbf{W}$ are fixed for all h. The next lemma gives a local approximation property for spline spaces in bent Sobolev spaces.

Lemma 3.2.1 (local approximation). *Let* $p := \min_{1 \leq \alpha \leq d} \{p_\alpha\}$ *and* $0 \leq k \leq p+1$. *For* $Q \in \mathcal{Q}_h$

and $v \in \mathcal{H}_h^k(\tilde{Q})$*, there exists an* $s \in \mathcal{S}_h$ *such that*

$$\|v - s\|_{L_h^2(\tilde{Q})} \leq C h_Q^k \, |v|_{\mathcal{H}_h^k(\tilde{Q})} \,. \tag{3.34}$$

Proof. See Bazilevs et al. (2006). □

Next, define the quasi-interpolant $\Pi_{\mathcal{S}_h}$ on the spline space $\mathcal{S}_h$ by - see Schumaker (2007, Theorem 12.6):

$$\Pi_{\mathcal{S}_h} v := \sum_{i_1=1}^{n_1} \dots \sum_{i_d=1}^{n_d} \lambda_{i_1 \dots i_d}(v) B_{i_1 \dots i_d}, \qquad \forall v \in L^1((0,1)^d), \tag{3.35}$$

which is a bounded linear operator mapping $L^1((0,1)^d)$ onto $\mathcal{S}_h$ with

$$\Pi_{\mathcal{S}_h} s = s, \qquad \forall s \in \mathcal{S}_h. \tag{3.36}$$

In Eq. (3.35), the $\lambda_{i_1 \dots i_d}$ are dual basis functionals using local integrals Schumaker (2007, Theorem 4.41). Further, define quasi-interpolants on the parametric and physical NURBS spaces, respectively, by:

$$\begin{aligned} &\Pi_{\mathcal{N}_h} : L^2((0,1)^d) \to \mathcal{N}_h, \qquad v \mapsto \Pi_{\mathcal{N}_h} v := \frac{\Pi_{\mathcal{S}_h}(v\mathbf{W})}{\mathbf{W}}; \\ &\Pi_{\mathcal{V}_h} : L^2(D) \to \mathcal{V}_h, \qquad v \mapsto \Pi_{\mathcal{V}_h} v := (\Pi_{\mathcal{N}_h}(v \circ F)) \circ F^{-1}. \end{aligned} \tag{3.37}$$

Using, among others, Lemma 3.2.1 the following estimations for quasi-interpolants are at hand.

Lemma 3.2.2. *Let* $p := \min_{1 \leq \alpha \leq d} \{p_\alpha\}$ *and* $0 \leq k \leq p+1$*. For all* $Q \in \mathcal{Q}_h$ *it holds:*

$$\left\|v - \Pi_{\mathcal{S}_h} v\right\|_{L^2(Q)} \leq C_1 \, h_Q^k \, |v|_{\mathcal{H}_h^k(\tilde{Q})} \qquad \forall v \in \mathcal{H}_h^k(\tilde{Q}) \cap L^2((0,1)^d) \tag{3.38}$$

$$\left\|v - \Pi_{\mathcal{N}_h} v\right\|_{L^2(Q)} \leq C_2(\mathbf{W}) \, h_Q^k \, \|v\|_{\mathcal{H}_h^k(\tilde{Q})} \qquad \forall v \in \mathcal{H}_h^k(\tilde{Q}) \cap L^2((0,1)^d) \tag{3.39}$$

$$\left\|v - \Pi_{\mathcal{V}_h} v\right\|_{L^2(K)} \leq C_3(F, \mathbf{W}) \, h_K^k \, \|v\|_{H^k(\tilde{K})} \qquad \forall v \in H^k(\tilde{K}) \cap L^2(D) \tag{3.40}$$

with $h_K = \|\nabla F\|_{L^\infty(Q)} \, h_Q$*; and* C_1*,* $C_2(\mathbf{W})$*, and* $C_3(F, \mathbf{W})$ *positive, dimensionless constants independent of* h *and* v*.*

Proof. See Bazilevs et al. (2006). □

Lemma 3.2.1 and 3.2.2 provide optimal rate of convergence for the spline spaces $\Pi_{\mathcal{S}_h}$, $\Pi_{\mathcal{N}_h}$, and $\Pi_{\mathcal{V}_h}$ of degree p. Furthermore, $\Pi_{\mathcal{S}_h}$ is characterized by the k-th order seminorm

only, whereas $\Pi_{\mathcal{N}_h}$ and $\Pi_{\mathcal{V}_h}$ need the full k-th order norm of v due to the additional weighting function $\mathbf{W}$ and geometrical map F.

3.2.4 Explicit Error Estimation

In the sequel, main results for univariate and multivariate spline spaces from Sande et al. (2019, 2020) are summarized and prepared for multi-dimensional deployment. The first result is the actuelly best known explicit error estimation for sufficient smooth functions. The numerical evidence found in the literature on the superior approximation per degree of freedom of smoother spline spaces is not proven with Theorem 3.2.3, but it is a step towards a complete theoretical understanding Sande et al., 2020. For fixed spline degree, smoother spline spaces exhibit better approximation properties per degree of freedom - see, e.g. J. A. Evans et al., 2009. This is true even when the smoothness of the functions to be approximated is low. Bressan and Sande (2019) show a more detailed theoretical consideration of the approximation performance of spline spaces per degree of freedom in the extreme cases $k = 0, -1, p-1$. For uniform sequences of knots, it has been formally shown that $\mathcal{C}^{p-1}$ spline spaces perform better than $\mathcal{C}^{-1}$ and $\mathcal{C}^0$ spline spaces in nearly all situations of practical concern; at least for deterministic problems. In this section, set

$$I := [0,1], \quad h := \max_{i=0,\dots,k}\{I_i\} \quad \text{and} \quad k := \max\{p - \mathfrak{M}\},$$

the spline smoothness.

Theorem 3.2.3. *Let $f \in H^r(I)$. Then,*

$$\left\| f - \Pi_{\mathcal{S}_p} f \right\|_{L^2(I)} \leq C_{h,p,k,r} \left\| f \right\|_{H^r(I)}$$

for all $p \geq r-1$ with

$$C_{h,p,k,r} := \min\left\{ c_{p,k,r} h^r ; \left(\frac{1}{2}\right)^r \sqrt{\frac{(p+1-r)!}{(p+1+r)!}} \right\} \tag{3.41}$$

and

$$c_{p,k,r} := \left(\frac{1}{2}\right)^r \begin{cases} \left(\frac{1}{\sqrt{(p-k)(p-k+1)}}\right)^r, & k \geq r-2 \\ \left(\frac{1}{\sqrt{(p-k)(p-k+1)}}\right)^{k+1} \sqrt{\frac{(p+1-r)!}{(p-1+r-2k)!}}, & k < r-2 \end{cases} \tag{3.42}$$

$$\leq \left(\frac{e}{4(p-k)}\right)^r \tag{3.43}$$

Proof. See Sande et al. (2020, Corollary 1 & 3). □

Note, the second argument in Eq .(3.41) is an error estimate for global polynomial approximation deduced from Christoph Schwab, Ch Schwab, et al. (1998, Theorem 3.11), which coincides with $c_{p,k,r}$ for $k = -1$, the discontinuous case. Therefore, the first argument in Eq. (3.41) is better for any p, r, and $h < 1$. On the other hand, for the exciting case of maximally smooth splines, i.e., k=p-1, and large values for p compared to 1/h, the second argument can become smaller, making the error estimate for the splines consistent with the global polynomial approximation Sande et al., 2020. For this case, the sharper estimate

$$C_{h,p,p-1,r} = \min\left\{ \left(\frac{h}{\pi}\right)^r ; \left(\frac{1}{2}\right)^r \sqrt{\frac{(p+1-r)!}{(p+1+r)!}} \right\} \tag{3.44}$$

$$\leq \left(\frac{2eh}{e\pi + 4h(p+1)}\right)^r \tag{3.45}$$

can be found Sande et al., 2020. Even if Eq. (3.42) and (3.44) seem to be much more unwieldy, they are much more informative than the simplified formulas (3.43) and (3.45). However, for some problems they are useful and sufficient as will be shown later in chapter 7. Moreover, all variants show the most useful $h - p - k$-refinement, i.e. convergence for $h \to 0$ and/or $p \to \infty$ against infinity under the condition $k = p - 1$ or k arbitrary Sande et al., 2020.

The last step is to extend the error estimates to the case of tensor product spline spaces. From the univariate error estimates, the following result can be derived using a standard argument of the triangle inequality.

Theorem 3.2.4. *Let $f \in H^r(I^d)$. Then,*

$$\left\| f - \Pi_{\mathcal{S}_p} f \right\|_{L^2(I^d)} \leq \sum_{i=1}^{d} C_{h_i,p_i,k_i,r} \left\| \partial_i^r f \right\|_{L^2(I^d)}$$

for all $p_i > r - 1$.

Proof. See, e.g., Bazilevs et al., 2006; Da Veiga, Buffa, Giancarlo Sangalli, et al., 2014; Da Veiga, Cho, et al., 2012; Sande et al., 2019. □

4 Formulation of Stochastic Systems

In this chapter, the general aspects for formulating stochastic systems necessary for numerical approaches within this thesis are presented, and a general framework for the needs of subsequent uncertainty quantification is prepared. In general, it has to be investigated how, for an elaborated deterministic model of an engineering system, a suitable stochastic concept that characterizes the uncertainty effects of the system input can be established. Therefore, before numerical simulation is possible, the mostly infinite-dimensional probability spaces must be reduced or discretized so that the random inputs are described by elements from finite-dimensional probability spaces - e.g. Ivo Babuška and Chatzipantelidis, 2002; R.G. Ghanem and P. Spanos, 2003; Mircea Grigoriu, 2003. This is accomplished by parameterization, which leads to representation by a finite number of random variables or simply a finite-dimensional random vector. When introducing uncertainty into a system by means of random vectors, it is above all important that the respective random variables have a certain independence structure or at least uncorrelatedness Xiu, 2010. The independence condition is a prerequisite for most practical numerical methods and less a strict theoretical condition Mircea Grigoriu, 2003; Xiu, 2010. This widely adopted requirement is also adopted in this work. However, there are also efforts to study dependent variables, e.g. Jakeman et al. (2019) and Sharif Rahman (2018). In summary, this means that in order to set up a suitable stochastic problem, a probability space must be specified, which is defined by a set of finite random variables, mutually independent in the best case. In general, this first step already induces an approximation error except for very trivial cases Xiu, 2010.

4.1 Input Parameterization

For the simple case that the random inputs are the system parameters themselves, the parameterization process is straightforward. Merely the independence has to be ensured. This can be stated as follows Ivo Babuška and Chatzipantelidis, 2002:

> For the system parameters $A = (A_1, \ldots, A_m)$ in an appropriate probability space $(\Omega, \mathcal{F}, P)$, find a set of mutually independent random variables $Y = (Y_1, \ldots, Y_{d_s})$ with $1 \leq d_s \leq m$, such that $A = T(Y)$ for a suitable transformation function T.

Depending on the type of information available for the description of the input parameters, it is not always easy to find such a mapping, especially in the high-dimensional case. Usually, distribution functions can be given in different ways, also empirically. The task is then to transform the parameters into independent random parameters with the help of their distributions Xiu, 2010.
For Gaussian distributed parameters, T is just a linear transformation, since it is invariant and the distribution is fully characterized by the first two moments. For a more general theorem of this fact see, e.g. Anderson, 1958. As can be seen, it is particularly easy to obtain a suitable parameterization for Gaussian distribution parameters in order to apply numerical methods and therefore this type is also very common R.G. Ghanem and P. Spanos, 2003; Sudret and Der Kiureghian, 2000.
For non-Gaussian distributed parameters, the problem is more difficult, although there is theoretically a remarkably simple way to transform an arbitrarily distributed random vector to an independently and equally distributed vector through the Rosenblatt transformation Rosenblatt, 1952.

If, instead, the random inputs are stochastic processes or random fields the task is more challenging. The need for this representation is very obvious and desirable. For example, in elasticity theory, time-dependent external forces on a body are naturally represented via stochastic processes, e.g. wind loads, likewise material properties such as elastic modulus inherently vary in reality in the object under consideration over space. The parameterization task for random functions can be stated as follows Xiu, 2010:

> For the stochastic process $Y(t)$ with $t \in I$ an index set in an appropriate probability space $(\Omega, \mathcal{F}, P)$, find a set of mutually independent random variables $Y = (Y_1, \ldots, Y_{d_s})$ with $d_s \geq 1$, such that $Y(t) \approx T(Y)$ for a suitable transformation function T.

As described in the previous chapter, the index set can describe time or space and is usually infinite-dimensional. For numerical tangibility, d_s must be finite and therefore the transformation here will always induce an approximation error; the accuracy is problem-dependent Xiu, 2010. A direct approach is to consider the stochastic process over its finite-dimensional distributions Mircea Grigoriu, 2003. For this, the index set is discretized and the process becomes a d_s-dimensional vector

$$(Y(t_1), \ldots, Y(t_{d_s})), \qquad t_1, \ldots, t_{d_s} \in I.$$

The random vector can now be treated with the techniques of parameterization for random parameters, for example using the Rosenblatt transformation.
The discretization of the stochastic process $Y(t)$ into a vector Y is obviously an approximation that improves with finer discretization. However, this also entails an increase in the stochastic dimension d_s, which in turn can lead to an enormous computational burden. It remains an open and active research topic to improve the approximation accuracy while simultaneously keep the dimension as low as possible Lüthen et al.,

2021; Stefanou, 2009; Tao et al., 2021.

4.1.1 Karhunen-Loève Expansion

One of the most widely spread techniques for dimension reduction in representing random functions is the KLE - see e.g. Karhunen, 1947; Loève, 1948, 1977. A stochastic process with finite second moments, and this applies to most physical processes Mircea Grigoriu, 2003, can be represented by a linear combination of a countable number of deterministic functions with random coefficients by the KLE and it is a generalization of example 2.4.2 which also holds for random fields Adler, 2010, section 3.3. Given the expectation $\mu(t)$ and covariance function $C(t,s)$ of the input process $Y(t)$, then the KLE of $Y(t) \in L^2(\Omega, \mathcal{F}, P)$ is Mircea Grigoriu, 2003:

$$Y(t) = \mu(t) + \sum_{i=1}^{\infty} \sqrt{\lambda_i}\varphi(t)Y_i(\omega) \ , \tag{4.1}$$

where $\varphi_i(t)$ the orthogonal eigenfunctions and λ_i the corresponding eigenvalues of the eigenvalue problem

$$\int_I C(t,s)\varphi_i(s)ds = \lambda_i\varphi_i(t), \quad t \in I. \tag{4.2}$$

The set of random variables $\{Y_i(\omega)\}$ is mutually uncorrelated and satisfies:

$$\mathbf{E}(Y_i) = 0, \quad \mathbf{E}(Y_iY_j) = \delta_{ij},$$

and is defined by

$$Y_i(\omega) := \frac{1}{\sqrt{\lambda_i}} \int_I (Y(t) - \mu(t))\varphi_i(t)dt, \quad \forall i.$$

The expansion in Eq. (4.1) in its infinite form is not suitable for a numerical treatment. Therefore, the series is truncated, i.e.

$$Y(t) = \mu(t) + \sum_{i=1}^{d_s} \sqrt{\lambda_i}\varphi(t)Y_i(\omega) \ . \tag{4.3}$$

One of the most important properties of the KL is that its approximation (4.3) is optimal in the sense of the mean-square error. The approximation determines the stochastic dimension d_s for the considered problem. The accuracy depends significantly on the decreasing eigenvalues. The faster they decrease, the lower is the stochastic dimension. The general procedure for using the KLE is to choose an appropriate covariance function. One frequently used is the exponential covariance function R.G. Ghanem and P. Spanos, 2003:

$$C(t,s) = \exp\Big(-\frac{|t-s|}{c}\Big)$$

with c the correlation length. The eigenvalue problem (4.2) can be solved analytically, see Van Trees, 2004. The eigenvalue decay rate is larger when the correlation length is longer. The decay rate helps to determine the number of terms used in the finite KL series. Depending on the problem, the term is determined above which the influence of the eigenvalue is negligible. A strongly correlated process has a long correlation length, so that fewer terms are needed. The KL is therefore less suitable for weakly correlated processes. For further properties, the reader is referred to the reference of, e.g. Christoph Schwab and Todor (2006).
There are other covariance functions in use whose analytical solutions can be given. For more general cases, the eigenvalue problem (4.2) must be solved numerically, for example using a finite element method, see e.g. R.G. Ghanem and P. Spanos, 2003. In the context of isogeometric analysis, a new research area for the solution of this Fredholm equation has recently emerged. The focus is on random fields on curved domains, which can preferably be solved using B-splines or their extension NURBS Li, Gao, et al., 2018; Li, Wu, and Gao, 2018, 2019; Li, Wu, Gao, and Song, 2019; Mika et al., 2021.

4.1.2 Wiener-Hermite Expansion

Impractical is the KL, if the covariance function is not known. This is the case for the response representation of the answer, but it is also possible for the input. An alternative is the Wiener-Hermite expansion, which was originally set up in integral form by Wiener (1938) and also became known as homogeneous chaos. In the expansion, multidimensional Hermite polynomials are used with Gaussian random variables as arguments. Cameron and Martin (1947) proved that this expansion converges for random variables in the L^2-sense. For a stochastic process $Y(t)$ in $L^2(\Omega, \mathcal{F}, P)$ and fixed t, the expansion is given by:

$$
\begin{aligned}
Y(t) = a_0(t)H_0 & \\
&+ \sum_{i_1=0}^{\infty} a_{i_1}(t)H_1(Y_{i_1}(\omega)) \\
&+ \sum_{i_1=0}^{\infty}\sum_{i_2=0}^{i_1} a_{i_1 i_2}(t)H_2(Y_{i_1}(\omega), Y_{i_2}(\omega)) \\
&+ \sum_{i_1=0}^{\infty}\sum_{i_2=0}^{i_1}\sum_{i_3=0}^{i_2} a_{i_1 i_2 i_3}(t)H_3(Y_{i_1}(\omega), Y_{i_2}(\omega), Y_{i_3}(\omega)) \\
&+ \dots ,
\end{aligned}
$$

The Wiener-Hermite expansion is the original polynomial chaos. Hereafter, it will be termed Hermite chaos, to refer to the polynomial type being used. For more details

on the mathematical foundation see Engel, 1982; K. Itô, 1951; Wiener, 1938 and for applications to practical problems see R.G. Ghanem and P. Spanos, 2003; Roger Ghanem, 1999.

4.1.3 Non-Gaussian Processes

The KLE and the Wiener-Hermite expansion are well suited for the Gaussian case and therefore a popular choice. This is partly due to the fact that for normally distributed random variables uncorrelatedness implies independence, and that they are invariant under linear combination. Thus, especially for KLE, the parameterization of a Gaussian process can be constructed in a natural way by Gaussian random variables, which are subsequently optimal for numerical methods. For a non-Gaussian input, the reduction and parameterization turns out to be much more difficult. The main problem in general is that the uncorrelatedness of the random variables in Eq. (4.1) does not lead to independence, which would be desirable. Although not mathematically clean, practical procedures apply the KLE and then assume that the random variables described are independent Xiu, 2010. It is still a challenging task to specify an efficient and reduced parameterization for general processes and therefore this topic remains an open and active research area Xiu, 2010.

4.2 System Formulation

In this section, the formulation of setting up a stochastic system in the context of incorporating random inputs into a well-established deterministic system is presented.

Let $(\Omega, \mathcal{F}, P)$ be a complete probability space, where Ω is a sample space, $\mathcal{F}$ is appropriate σ-field on Ω, and P a probability measure. Further, consider a d_d-dimensional bounded domain $D \subset \mathbb{R}^{d_d}$ ($d_d \in \{1,2,3\}$) with boundary ∂D sufficiently smooth, such that the following problem is well-posed: find a random function $u : \bar{D} \times \Omega \to \mathbb{R}^{d_u}$ such that P-almost everywhere in Ω the following equation holds:

$$\begin{aligned} \mathcal{L}(x,\omega;u(x,\omega)) &= f(x,\omega) \quad \text{in } D \times \Omega \\ u(x,\omega) &= 0 \quad \text{on } \partial D \times \Omega\,. \end{aligned} \tag{4.4}$$

The random inputs of Eq. (4.4) can be random variables, vectors, processes or fields which has to be discretized properly. Therefore, the following assumption is necessary:

Assumption 1 (finite-dimensional noise). The random input of Eq. (4.4) can be represented by a finite-dimensional probability space, i.e. by a set of independent random variables

$$Y(\omega) = (Y_1(\omega), \ldots, Y_{d_s}(\omega)) \in \mathbb{R}^{d_s} \tag{4.5}$$

with $d_s \in \mathbb{N}$ and joint density function f_Y. In general, this discretization can be done for all technical applications e.g. by the Karhunen-Loève expansion.

Eq. (4.4) can then be reformulated to

$$\begin{aligned} &\mathcal{L}(x, Y(\omega); u(x, Y(\omega))) = f(x, Y(\omega)) \quad \text{on } D \times \mathbb{R}^{d_s} \\ &u(x, Y(\omega)) = 0 \quad \text{on } \partial D \times \mathbb{R}^{d_s} \end{aligned} \tag{4.6}$$

with $u : \bar{D} \times \mathbb{R}^{d_s} \to \mathbb{R}^{d_u}$ by the use of the Doob-Dynkin lemma, e.g. Rao and Swift, 2006b, p.7, and $Y_1, \ldots, Y_{d_s}$ are independent and identically distributed.

Assumption 2. Eq. (4.4) is well-posed P-a.s. in Ω, i.e. for each realization of $Y(\omega)$ Eq. (4.6) is well-posed in its deterministic sense.

4.3 Response Representation

The stochastic input parameters induce randomness to the system response. The classical techniques of probabilistic engineering mechanics can be roughly divided into three categories, depending on the response type of information desired or needed:
First, the moments of the stochastic response can be determined. Response variability methods such as the perturbation method Wing Kam Liu et al., 1986; W. Liu et al., 1986 and the weighted integral method Deodatis, 1991; Deodatis and Shinozuka, 1991; Takada, 1990 allow the calculation of the mean and variance of the mechanical response of the system. This gives a sense of the central part of the response probability density function.
For structural reliability methods, usually only the tail of the distribution is calculated by computing the probability of exceeding a given threshold Ditlevsen and Madsen, 1996b. In both academia and industry, established methods include first and second order reliability method (FORM/SORM), directional simulation, and importance sampling among others.
Finally, there is the complete description of the response density function. The main representatives are stochastic finite element methods, named after the pioneer work of R. Ghanem and P. Spanos (1993). Here, the solution is expanded by an appropriate basis of the probability space, which is called the polynomial chaos. PC-based methods are now a widely used approach in dealing with uncertainties and their optimization with respect to higher dimensions, and propagation into different application environments continue to be the state of current research - see e.g. Kaintura et al., 2018; Pavlack et al., 2021; Sun et al., 2021; Z. Wang and Roger Ghanem, 2021; J. Zhang et al., 2021. A major advantage of this approach is that the distribution of the response can be fully characterized by the expansion coefficients, although mean and standard deviation of the response are easily obtained, too. Naturally, problems belonging to the first two

classes can be considered in a post-processing setting. However, other more recent methods such as the Wiener path integral approach Petromichelakis et al., 2018 should also be mentioned here.

Lastly, it should be noted that for central part, tail or full distributions, Monte Carlo simulation is a versatile tool that usually requires a much higher computational effort than the above methods. Therefore, it is mainly a vehicle to produce a reference solution in certain cases.

5 Spline Chaos

This chapter is mainly devoted to the basics of spline chaos (SC) and thus provides a comprehensible generalization of polynomial chaos expansions. In order to recognize this generalization, the spline chaos is derived upon the general polynomial chaos in both the multi-dimensional as well as in the one-dimensional case for the sake of better clarity. Essential, besides the derivation of the theory, are the proofs of strong and weak convergence as reported by Cameron and Martin Cameron and Martin, 1947 and Xiu (2010) for the case of homogeneous and generalized polynomial chaos, respectively. The theoretical consideration is followed by simple numerical examples, which stimulate the notion of how spline chaos works and can be applied in comparison to polynomial chaos. Subsequently, B-spline based chaos is contrasted with classical homogeneous chaos, which, on the one hand, shows how to increase the accuracy throughout the flexibility of the spline spaces, and, on the other hand, consolidates the direct relationship to Legendre chaos. The chapter concludes with the examination of a stationary stochastic process.

5.1 Wiener-Askey chaos

As seen in section 4.1.2 the homogeneous chaos expansion used for input parameterization is an effective tool for the representation of stochastic processes, which, according to the theorem of Cameron and Martin Cameron and Martin, 1947, converges in the L^2-sense. It has been demonstrated by many authors that the homogeneous or Hermite chaos is effective in solving stochastic differential equations with Gaussian inputs as well as certain types of non-Gaussian inputs R.G. Ghanem and P. Spanos, 2003; Roger Ghanem and P D Spanos, 1990; Stefanou, 2009; Xiu, 2010. Nevertheless, the optimal exponential convergence rate is not achieved for general non-Gaussian random inputs or the convergence severely deteriorates Field and M. Grigoriu, 2004; Xiu and Karniadakis, 2002. A more general concept was proposed by Xiu and Karniadakis (2002) - the Wiener-Askey or generalized polynomial chaos. Thus, a general stochastic process $X(\omega) \in L^2(\Omega, \mathcal{F}, P)$, viewed as a function of ω as the random event, can be represented

by:

$$\begin{aligned} X(\omega) = a_0\Psi_0 \\ &+ \sum_{i_1=0}^{\infty} a_{i_1}\Psi_1(Y_{i_1}(\omega)) \\ &+ \sum_{i_1=0}^{\infty}\sum_{i_2=0}^{i_1} a_{i_1 i_2}\Psi_2(Y_{i_1}(\omega), Y_{i_2}(\omega)) \\ &+ \sum_{i_1=0}^{\infty}\sum_{i_2=0}^{i_1}\sum_{i_3=0}^{i_2} a_{i_1 i_2 i_3}\Psi_3(Y_{i_1}(\omega), Y_{i_2}(\omega), Y_{i_3}(\omega)) \\ &+ \dots , \end{aligned} \tag{5.1}$$

where $\Psi_p(Y_{i_1}(\omega), \dots, Y_{i_p}(\omega))$ is the Wiener-Askey or generalized polynomial chaos of order p in the variables $\mathbf{Y} = (Y_{i_1}(\omega), \dots, Y_{i_p}(\omega))$. The polynomials $\{\Psi_p\}$ are not restricted to be Hermite polynomials, but can by any orthogonal polynomial from the Askey scheme - see, e.g., Xiu and Karniadakis (2002, 2003) for a detailed description, or for a selection of Askey-polynomials section 3.1 or Tab. 5.1. These orthogonal d-variate polynomials of degree less than or equal p, span the linear space of all polynomials of degree at most p in d variables, i.e.

$$\mathcal{P}_p^d(\mathbf{Y}) = \left\{ P(\mathbf{Y}) \mid P(\mathbf{Y}) = \sum_{|\mathbf{i}|\le p} a_{\mathbf{i}} P_{\mathbf{i}}(\mathbf{Y}) \right\}, \tag{5.2}$$

where $\mathbf{i} = (i_1, \dots, i_d) \in \mathbb{N}_0^d$ is a multi-index with $|\mathbf{i}| = i_1 + \dots + i_d$, and

$$P_{\mathbf{i}}(\mathbf{Y}) = P_{i_1}(Y_{i_1}) \cdots P_{i_d}(Y_{i_d}), \qquad 0 \le |\mathbf{i}| \le p \tag{5.3}$$

are the products of the univariate orthogonal polynomials from section 3.1, whose dimension is

$$\dim(\mathcal{P}_p^d) = \binom{p+d}{p}$$

To simplify notation, Eq. (5.1) can be rewritten as

$$X(\omega) = \sum_{|\mathbf{i}|\le p}^{\infty} a_{\mathbf{i}}\Psi_{\mathbf{i}}(\mathbf{Y}(\omega)) \,, \tag{5.4}$$

with $\Psi_{\mathbf{i}}(\mathbf{Y}) \in \mathcal{P}_p^p(\mathbf{Y})$. Xiu and Karniadakis (2002) deduced, since each type of polynomial from the Askey scheme forms a complete basis in the Hilbert space, it can be expected that each generalized polynomial chaos expansion converges to any L^2-functional in the L^2-sense in the corresponding Hilbert function space as a generalized result of the Cameron-Martin theorem Cameron and Martin, 1947; Ogura, 1972.
In the following, a typical usecase of gPC in one-dimension is examined in order to

recognize later differences in comparison to the spline chaos more easily, and to prepare a framework for numerical results.

5.1.1 One-dimensional case

Consider the random variable X as a function of an arbitrary random variable Z, i.e.

$$X = g(Z), \tag{5.5}$$

where g is a deterministic, measurable mapping. In general, Eq. (5.5) describes the random output X of a stochastic system in the presents of random inputs parameterized by Z. Note, if g is the identity and Z has a specific distribution, e.g. normal or uniform, then, the gPC approximates this specific distribution. This simple case is investigated for first numerical results in order to get an intuitive notion of the correspondence between distribution and polynomial type, the capability of polynomials to represent random variables, and the quality of non-corresponding distribution and polynomial type. Next, the standard introductory description and simple calculation of a gPC approximation in one-dimension is explained.

Xiu and Karniadakis (2002) proposed the Wiener-Askey or gPC expansion which allows to represent Eq. (5.5) in terms of the series

$$X = \sum_{p=0}^{\infty} a_p \Psi_p(Z), \tag{5.6}$$

where Z is a random variable, $\Psi_p(Z)$ are orthogonal polynomials in Z of order p and a_p are deterministic coefficients to be determined. Truncating the series in Eq. (5.6) after the $P+1$ term leads to the polynomial chaos approximation of order P:

$$\tilde{X}_P = \sum_{p=0}^{P} a_p \Psi_p(Z), \tag{5.7}$$

which converges in $L^2(\Omega, \mathcal{F}, \mathcal{P})$ Mircea Grigoriu, 2003, i.e.

$$\tilde{X}_P \xrightarrow{L^2} X \quad \text{for} \quad P \to \infty. \tag{5.8}$$

Due to the orthogonality of the functions Ψ_p, the coefficients in (5.7) can simply determined by the orthogonal L^2-projection Mircea Grigoriu, 2003:

$$\mathbf{E}[g(Z)\Psi_p(Z)] = a_p \, \mathbf{E}[\Psi_p(Z)^2] \tag{5.9}$$

for every p, which make these polynomials very efficient for computational issues. The orthogonality of the space depends on the measure $\mathcal{P}$ of the underlying Hilbert space $L^2(\Omega, \mathcal{F}, \mathcal{P})$ and is in correspondence with the orthogonal polynomials from section 3.1, where the most relevant examples from the Askey scheme were introduced. The gPC identifies this correspondence between the distribution of the random input $Z \in L^2(\Omega, \mathcal{F}, \mathcal{P})$ and the type of orthogonal polynomials, leading to optimal convergence rates, i.e. exponential Xiu and Karniadakis, 2002. Some elected correspondences are shown in Tab. 5.1.

	Distribution of Z	Polynomial Basis Ψ	Support
Continuous	Gaussian	Hermite	$(-\infty, \infty)$
	Gamma	Laguerre	$[0, \infty)$
	Beta	Jacobi	$[a, b] \subset \mathbb{R}$
	Uniform	Legendre	$[a, b] \subset \mathbb{R}$
Discrete	Binomial	Krawtchouk	$\{0, 1, 2, \ldots, N\} \subset \mathbb{N}$
	Poisson	Charlier	$\{0, 1, 2, \ldots\} \subset \mathbb{N}$
	Negative binomial	Meixner	$\{0, 1, 2, \ldots\} \subset \mathbb{N}$
	Hypergeometric	Hahn	$\{0, 1, 2, \ldots, N\} \subset \mathbb{N}$

Table 5.1: Correspondence between distribution and polynomial basis - cf. Xiu and Karniadakis, 2002.

5.2 Spline chaos

As an extension of section 5.1, a spline version of the polynomial chaos expansion is used now to represent effectively stochastic processes. The space of polynomials $\mathcal{P}_p^d$ is extended to the space of splines $\mathcal{S}_{\mathbf{p}}$, which were rigorously introduced in section 3.2. The multi-dimensional representation of a stochastic process $X(\omega)$ by the spline chaos approach leads, through its richness of facets, to the expression:

$$X(\omega) = \lim_{d \to \infty} \sum_{i_1=1}^{\infty} \cdots \sum_{i_d=1}^{\infty} a_{i_1 \ldots i_d} B_{i_1 \ldots i_d}(U_{i_1}(\omega), \ldots, U_{i_d}(\omega)) \tag{5.10}$$

where $B_{i_1 \ldots i_d}(U_{i_1}(\omega), \ldots, U_{i_d}(\omega)) \in \mathcal{S}_{\mathbf{p}}(\mathfrak{P}, \mathfrak{M})$ is the d-variate B-spline chaos of order $\mathbf{p}$ in the independent and identically distributed uniform random variables $U_{i_1}(\omega), \ldots, U_{i_d}(\omega)$ with partition $\mathfrak{P} = (\mathfrak{P}_1, \ldots, \mathfrak{P}_d)$ and multiplicity vector $\mathfrak{M} = (\mathfrak{M}_1, \ldots, \mathfrak{M}_d)$.
Although the classical expansion is manufactured by orthogonal polynomials, it should be noted that, from a mathematical point of view, convergence only requires a complete basis in the underlying Hilbert space, and orthogonality is only an efficiency enhancing property. Therefore, the following theorem states the strong convergence of spline chaos by simply replacing the polynomial space.

Theorem 5.2.1. *Let $X(\omega) \in L^2(\Omega, \mathcal{F}, P)$ a stochastic process. Then, the spline chaos in Eq. (5.10) converges in mean square.*

Proof. If $X(\omega) \in L^2(\Omega, \mathcal{F}, P)$, then construct a spline chaos as in Eq. (5.10) with i.i.d. random variables $U_{i_1}(\omega), \ldots, U_{i_d}(\omega)$ and support $I_{\mathbf{U}}$. First case, the partition $\mathfrak{P} = I_{\mathbf{U}}$ has no subintervals. Then, the spline space degenerates to a polynomial space and $B_{i_1 \cdots i_p}(U_{i_1}(\omega), \ldots, U_{i_p}(\omega))$ are d-variate Bernstein polynomials. Second case, the partition $\mathfrak{P} = I_{\mathbf{U}}$ has subintervals. Then, with loss of generality, construct by knot insertion a $\mathcal{C}^0$ spline basis, which leads to d-variate basis functions $B_{i_1 \cdots i_p}(U_{i_1}(\omega), \ldots, U_{i_p}(\omega))$, which are a complete set of Bernstein basis functions on each subinterval. For both cases, Eq. (3.2) delivers an analytical one-to-one relationship between the Legendre and Bernstein polynomials in one-dimension which comes applicable with Eq. (5.3) and (3.16). Because the Legendre chaos is convergent, it follows, that the spline chaos also converges in mean square. □

Theorem 5.2.1 provides the theoretical framework for using spline chaos. This general multi-dimensional representation shows that, just like the PC, it is in principle possible to approximate an arbitrary stochastic process with finite second moment, which is usually given for all applications, over a spline space. An easy to handle basis for these spline spaces are B-splines. Although this is not the only way Schumaker, 2007, it is certainly the most intuitive and simplest one if a spline space with given properties is to be constructed. The terms spline chaos and B-spline chaos are therefore used synonymously and it should be clear that in the context of this thesis statements about B-splines can be transferred to spline spaces unless this is explicitly restricted.

Following the structure of Section 5.1.1, the one-dimensional case is considered in detail next. From this point, it will also be intuitively clear how higher dimensional representations must be addressed.

5.2.1 One-dimensional case

In this section, the generalized PC approximation in Eq. (5.7) is adapted in order to make the method accessible for B-spline basis functions instead of orthogonal polynomials. Consider the basis $\{B_{i,p}\}$ of the spline space $\mathcal{S}_p$ of order p and dimension N. The spline chaos approximation of Eq. (5.10) in one-dimension is given by

$$\tilde{X}_N = \sum_{i=1}^{N} x_i B_{i,p}(u(Z)), \tag{5.11}$$

where $\tilde{X}_N$ is the approximation of the random variable X in Eq. (5.5). B-splines can not be used for the approximation of random variables in the same manner then orthogonal polynomials, like Hermite polynomials, because of the lack of orthogonality.

Nevertheless, it suffices that the functions in use form a basis of the underlying Hilbert space $L^2(\Omega, \mathcal{F}, \mathcal{P})$ R.G. Ghanem and P. Spanos, 2003; Xiu, 2010. Thus, the coefficients in (5.11) can be determined by solving a linear algebraic system resulting from the L^2-projection:

$$\mathbf{A}\mathbf{x} = \mathbf{b} \tag{5.12}$$

with

$$\mathbf{A}_{i,j} := \mathbf{E}\left[B_{i,p}(u(Z))B_{j,p}(u(Z))\right] \tag{5.13}$$

$$\mathbf{b}_j := \mathbf{E}\left[g(Z)B_{j,p}(u(Z))\right] \tag{5.14}$$

$i, j = 1, \ldots, N$. Next, the integrals in Eq. (5.12) must be calculated. Specifically, this necessitates the introduction of a new space for the parameter u of the B-spline basis functions $B_{i,p}(u(Z))$, which explicitly depend on the random variable Z. The question next arises as to how an arbitrary random variable Z can be uniquely mapped on the parameter space $[0, 1]$ in a proper way. A convenient choice is the inverse cumulative distribution function or quantile function of a random variable Z, given by

$$F_Z^{-1}(u) := \inf\{z \ : \ F_Z(z) \geq u\} \in [0, 1], \tag{5.15}$$

where F_Z is the CDF of Z. Clearly, the inverse always exists and is unique. This allows one to connect the parameter u and the random variable Z such that u become a uniformly distributed random variable $U = F_Z(Z)$ on the interval $[0, 1]$, i.e.

$$\begin{aligned} F_U(u) &= P(U \leq u) = P(F_Z(Z) \leq u) \\ &= P(Z \leq F_Z^{-1}(u)) = F_Z(F_Z^{-1}(u)) = u \\ \implies U &\sim \text{unif}([0, 1]). \end{aligned} \tag{5.16}$$

If the distribution of Z is explicitly known, Eq. (5.12) can be expressed in terms of U by

$$u = F_Z(z) \quad \implies \quad \frac{du}{dz} = \frac{dF_Z(z)}{dz} = f_Z(z), \tag{5.17}$$

where f_Z is the probability density function of Z. Hence, a proper mapping between Ω and $[0, 1]$ by F_Z is established. So, the expressions in (5.13) and (5.14) can be expressed as

$$\begin{aligned} &\mathbf{E}_Z\left[B_{i,p}(F_Z(Z))B_{j,p}(F_Z(Z))\right] \\ &\quad = \int_\Omega B_{i,p}(F_Z(z))B_{j,p}(F_Z(z))f_Z(z)\, dz \\ &\quad = \int_{[0,1]} B_{i,p}(u)B_{j,p}(u)\, du \\ &\quad = \mathbf{E}_U\left[B_{i,p}(U)B_{j,p}(U)\right], \end{aligned} \tag{5.18}$$

and

$$\begin{aligned}
&\mathbf{E}_Z\left[g(Z)B_{j,p}(F_Z(Z))\right] \\
&\quad= \int_\Omega g(z)B_{j,p}(F_Z(z))f_Z(z)\,dz \\
&\quad= \int_{[0,1]} g(F_Z^{-1}(u))B_{j,p}(u)\,du \\
&\quad= \mathbf{E}_U\left[g(F_Z^{-1}(U))B_{j,p}(U)\right]. \qquad (5.19)
\end{aligned}$$

Thus, the matrix $\mathbf{A}$ depends only on the configuration of the B-spline basis functions, and can be stored before the analysis. Further, $\mathbf{A}$ is a band matrix, if the knot vector Ξ has inner knots, i.e.

$$\mathbf{A}_{i,j} = 0 \quad \text{for} \quad |i-j| > p+1. \qquad (5.20)$$

Examining the integrals in (5.18) and (5.19) it turns out that only the inverse cumulative distribution function of the describing random variable Z and the mapping g must be known. Thus, this procedure is not strongly limited and simultaneously paves the way for using this method with discrete random variables Xiu and Karniadakis, 2002. Besides, under the assumption that Z is a uniformly distributed random variable F_Z is the identity, and optimal convergence is expected in correspondence with the uniform distribution, which is shown in the ensuing sections.

5.2.2 Weak Convergence

The proposed method is closely related to the gPC Xiu and Karniadakis, 2002 where the same mapping property between a uniform and arbitrary distribution is utilized. It can be shown, see e.g. Xiu, 2010, that the gPC approximation converges weakly, if the random variable to be approximated is square integrable and the moments in the chaos expansion exists. This can be adopted here and $\tilde{X}_N$ converges in probability and in distribution, i.e.

$$\tilde{X}_N \xrightarrow{\mathcal{P}} X \text{ and } \tilde{X}_N \xrightarrow{\mathcal{D}} X \quad \text{for} \quad N \to \infty. \qquad (5.21)$$

To be precise, this can be stated as follows:

Definition 11: Weak chaos approximation

Let X be a random variable with CDF $F_X(x) = \mathcal{P}(X \leq x)$ and let Z be an arbitrary random variable in a set of basis functions $\Psi_i(Z)$, $i = 1, \ldots, N$. If

$$\tilde{X}_N = \sum_{i=1}^{N} a_i \Psi_i(Z) \quad \text{with } a_i \in \mathbb{R} \qquad (5.22)$$

converges to X in a weak sense, i.e.

$$\tilde{X}_N \xrightarrow{\mathcal{P}} X \text{ or } \tilde{X}_N \xrightarrow{\mathcal{D}} X \quad \text{for} \quad N \to \infty, \tag{5.23}$$

then $\tilde{X}_N$ is a weak chaos approximation of X.

Theorem 5.2.2. *Let X be a random variable with CDF $F_X(x) = \mathcal{P}(X \leq x)$ and finite second moment. Let U be a uniformly distributed random variable in $[0,1]$ such that the moments $\mathbf{E}_U(B_{i,p}(U)B_{j,p}(U))$ exists for all B-spline basis functions of order $p \in \mathbb{N}$ with $i,j \in \{1,\dots,N\}$. Let*

$$\tilde{X}_N = \sum_{i=1}^{N} x_i B_{i,p}(U) \tag{5.24}$$

the weak B-spline chaos approximation of X, where $\mathbf{x} = (x_1,\dots,x_N)$ results from the L^2-projection $\mathbf{Ax} = \mathbf{b}$ with

$$\mathbf{A}_{i,j} := \mathbf{E}_U\left(B_{i,p}(U)B_{j,p}(U)\right) \quad \textit{and} \tag{5.25}$$

$$\mathbf{b}_j := \mathbf{E}_U(F_X^{-1}(U)B_{j,p}(U)). \tag{5.26}$$

Then $\tilde{X}_N$ converges to X in probability, i.e.

$$\tilde{X}_N \xrightarrow{\mathcal{P}} X \quad \textit{for} \quad N \to \infty. \tag{5.27}$$

Proof. Let

$$\bar{X} := F_X^{-1}(U) = F_X^{-1}(F_U(U)), \tag{5.28}$$

which implies that $\bar{X}$ has the same probability distribution as X, i.e. $F_{\bar{X}} = F_X$. Thus, it holds $\bar{X} \overset{\mathcal{P}}{=} X$ and $\mathbf{E}(\bar{X}^2) < \infty$, which leads to

$$\begin{aligned} \infty > \mathbf{E}\left[\bar{X}^2\right] &= \int_{\Omega_X} x^2 \, dF_X(x) \\ &= \int_{[0,1]} \left(F_X^{-1}(u)\right)^2 \, du \\ &= \int_{[0,1]} \left(F_X^{-1}(F_U(u))\right)^2 \, dF_U(u). \end{aligned} \tag{5.29}$$

$$\begin{aligned} \implies \quad \bar{X} &\in L_2([0,1],\sigma([0,1]),dF_U) \\ &:= \left\{ f : [0,1] \to \mathbb{R} \mid \mathbf{E}_U\left[f^2\right] < \infty \right\}. \end{aligned} \tag{5.30}$$

Since (5.24) is the L^2-projection of $\bar{X}$ by $\tilde{X}_N$, $\tilde{X}_N$ converges in mean square to $\bar{X}$, which implies

$$\tilde{X}_N \xrightarrow{\mathcal{P}} \bar{X} \qquad \text{for} \quad N \to \infty. \tag{5.31}$$

This completes the proof, because $\bar{X} \overset{\mathcal{P}}{=} X$. □

Note, convergence in probability implies convergence in distribution. So, it also holds $\tilde{X}_N \xrightarrow{\mathcal{D}} X$ for $N \to \infty$. Further, if $g(Z)$ in Eq. (5.5) is explicitly known in terms of Z, L^2-convergence can be achieved as shown in theorem 5.2.1. However, in most practical numerical analyses only the probability density function of $g(Z)$ or even less information is available. But in this case, strong convergence can not established because of the lack of information concerning g and Z. Nevertheless, the above theorem ensures weak convergence.
The next sections show the versatility of the aforementioned methodology, and the theoretical convergence results are further substantiated by numerical examples.

5.3 Approximation of random variables

In the following, several random variables are approximated by different expansions and are juxtaposed with each other. To be more precise, uniform, beta, normal, and exponential distributed random variables are approximated by Hermite, Legendre and B-spline chaos, respectively, or starting from Eq. (5.5), function g is replaced by the approximating CDF. The resulting density functions are estimated by a normal kernel smoothing function available in all common statistical toolboxes[1]. The advantage of the proposed technique lies in the flexibility of adapting the order, number of elements and continuity over element boundaries, which can be quite powerful, if the underlying distribution is unknown.

5.3.1 Uniform distribution

Fig. 5.1 shows approximations of a uniform density function by Hermite, Legendre, and B-spline chaos for different orders p. Legendre and B-spline expansions remain stable and unchanged from the first order on. Neither order elevation nor knot insertion changes the accuracy. The changing values of the expansion coefficients are the main difference. While only the first two basis functions influence the representation for the Legendre chaos, because all coefficients are zero for $i > 2$, the coefficients are changing for every configuration for the B-splines - see Fig. 5.2. However, in this case only a straight line has to be approximated. Therefore, linear B-splines are sufficient. This leads to the conclusion that a correspondence between the uniform distribution and B-splines can be identified. However, for the Hermite chaos more terms are necessary to reach

[1] For the presented examples the ksdensity MATLAB-function with bandwidth 0.06 and 1.000.000 samples were used.

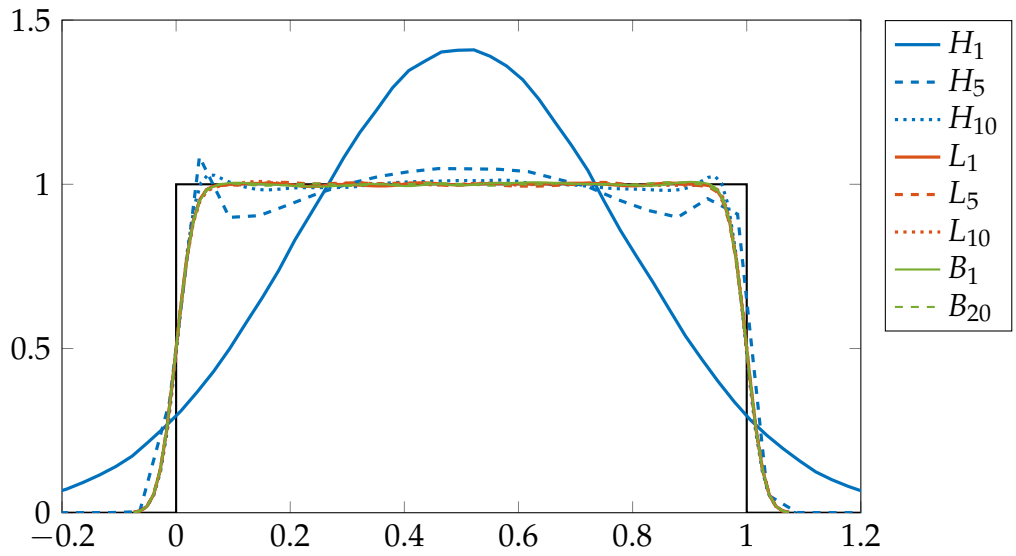

Figure 5.1: Approximations of a uniform distribution by Hermite polynomials (H_p), Legendre polynomials (L_p), and B-splines (B_p).

the same accuracy, and oscillations are observed at the corners. This is also known as the stochastic Gibbs phenomenon Xiu, 2010.

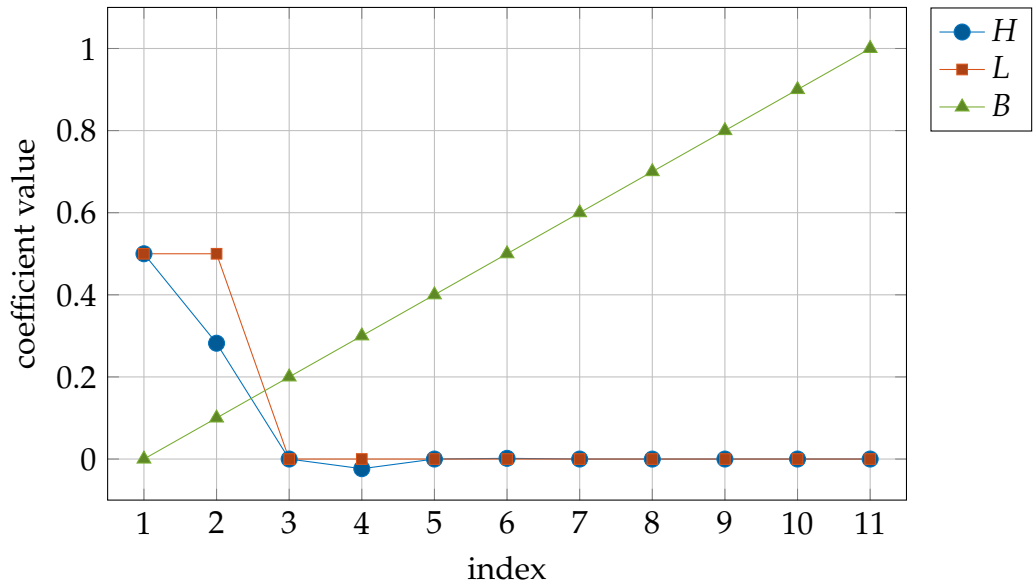

Figure 5.2: Coefficient values of Hermite, Legendre, and B-spline chaos for approximating a uniformly distributed random variable.

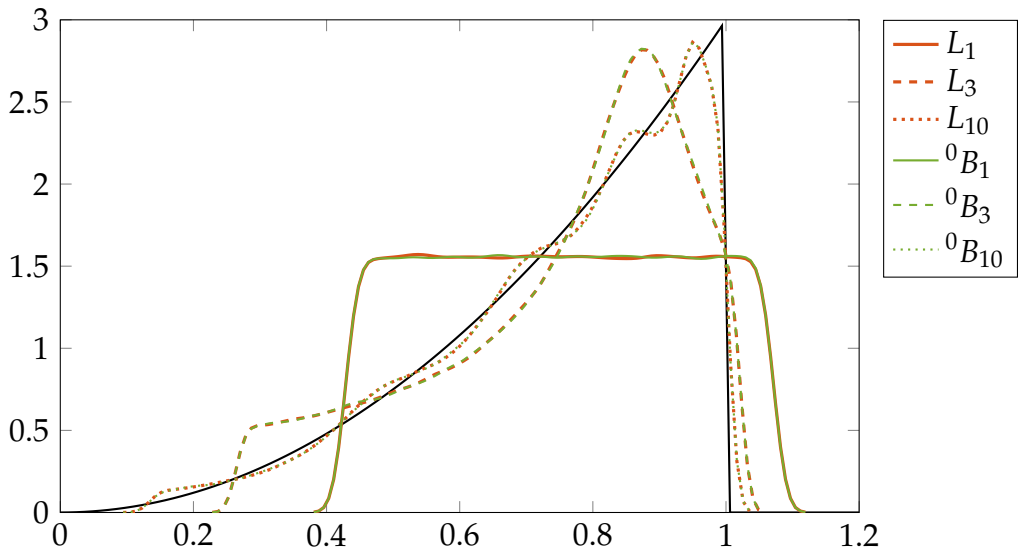

Figure 5.3: Approximations of a beta distribution with $\alpha = 3$ and $\beta = 1$ by Legendre polynomials (L_p) and $\mathcal{C}^0$ B-splines (${}^0B_p$).

5.3.2 Beta distribution

Let X be a beta distributed random variable on $[0,1]$ with density function

$$f_X(x) = \frac{1}{\mathrm{B}(\alpha,\beta)} x^{\alpha-1}(1-x)^{\beta-1} \quad \text{with } \alpha,\beta > 0\,, \tag{5.32}$$

where $\mathrm{B}(\alpha,\beta)$ is the beta function. Results of for a beta distributed random variable X with $\alpha = 3$ and $\beta = 1$ are shown in Fig. 5.3. Legendre and Bernstein ($\mathcal{C}^0$ B-spline) approximations are compared, for which an explicit one-to-one transformation exists Farouki, 2000. A further indication for the connection of Legendre and Bernstein polynomials is the indistinguishability of the illustrated results. However, the approximations could be substantially improved by adding inner knots. Then, the Bernstein polynomials become B-splines basis functions.

5.3.3 Normal distribution

Let $X \sim \mathcal{N}(\mu,\sigma^2)$ be a normal distributed random variable with density function

$$f_X(x) = \frac{1}{\sqrt{2\pi\,\sigma^2}} \exp\left(-\frac{(x-\mu)^2}{\sigma^2}\right) \tag{5.33}$$

with expectation $\mu \in \mathbb{R}$ and variance $\sigma^2 > 0$. Hermite polynomials correspond to the Gaussian measure. Thus, the Hermite chaos is exact from the first order on - see

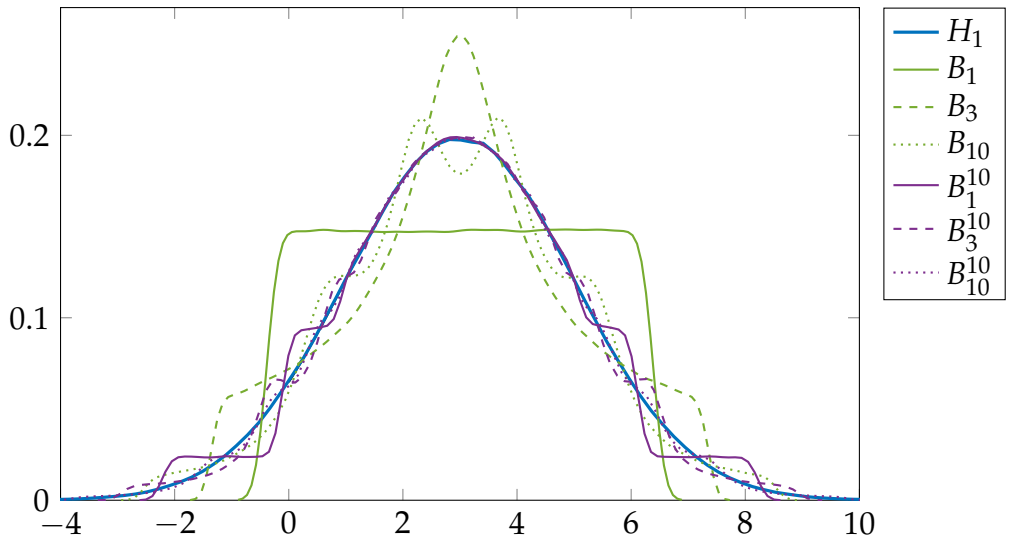

Figure 5.4: Approximations of a normal distribution with $\mu = 3$ and $\sigma = 2$ by Hermite polynomials (H_p) and B-splines with ten stochastic elements (B_p^{10}).

Fig. 5.4. Further, a Gaussian kernel is used here. Thus, the approximation fits perfectly. In contrast, a Gaussian input is not optimal for the B-spline or Legendre chaos, which can clearly be recognized. Nevertheless, inserting nine inner knots, which leads to ten stochastic elements, improves the performance distinctly, although moderate oscillations remain at the tails. The fluctuations can be attributed to the different supports. The L^2-projection must determine a proper mapping from $[0, 1]$ to $(-\infty, \infty)$.

5.3.4 Exponential distribution

Assume that X is a exponential distributed random variable on $[0, \infty]$ with density function

$$f_X(x) = \lambda \exp(-\lambda) \quad \text{with } \lambda > 0 \tag{5.34}$$

and consider the specific case of $\lambda = 1$. The Hermite chaos behaves quite well for higher orders and is smooth, although the peak decreases for $P = 10$ - see Fig. 5.5. As seen before, nine inner knots are utilized in order to diminish the oscillations for the B-splines, but the deviation remains fairly large on the right end. Now, another useful property of B-spline basis functions can be exploited to solve this issue. Inserting the same knot again reduces the continuity over element boundaries by one. This can be repeated until the B-splines become decomposed, i.e. $\mathcal{C}^0$-continuity over element boundaries. In Fig. 5.5, ${}^0B_{10}^{10}$ specifies the case for ten $\mathcal{C}^0$-elements of order ten, which leads to a much smoother approximation and can compete against the Hermite chaos. Solely, the tail is slightly fluctuating which may be caused by the support mismatch. Further, the employed normal kernel smoothing function is non-optimal for the B-splines representation.

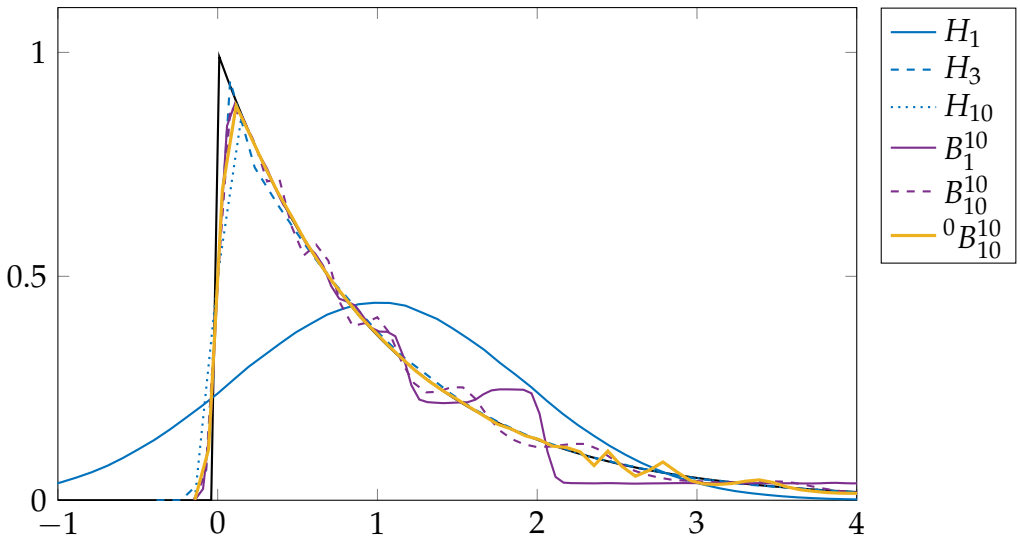

Figure 5.5: Approximations of a exponential distribution with $\lambda = 1$ by Hermite polynomials (H_p), B-splines with ten elements (B_p^{10}), and $\mathcal{C}^0$ B-splines with ten elements (${}^0B_p^{10}$)

5.4 Accuracy of Hermite and B-Spline Chaos

In this part, the accuracy of spline chaos is intensively studied and benchmarked with Hermite chaos. A detailed investigation for Hermite chaos was already done by Field and M. Grigoriu (2004) trying to identify peculiarities and limitations. Based on this study the previous described spline chaos are compared with results of Hermite polynomials. Furthermore, it should be noted that the input distribution used is Gaussian based and thus optimized for Hermite polynomials. Nevertheless, target-oriented configuration of splines spaces are able to compete.

Consider Eq. (5.5) in one dimension for

$$\begin{aligned} X^1 &= g^1(Z) := \alpha^1 + \exp(\beta^1 Z), \\ X^2 &= g^2(Z) := F_{X^2}^{-1} \circ \Phi(Z) \text{ and} \\ X^3 &= g^3(Z) := |Z| \end{aligned}$$

with

$$F_{X^2}^{-1}(x) = \begin{cases} 0 & \text{for } x < \alpha^2 \\ \frac{x-\alpha^2}{\beta^2-\alpha^2} & \text{for } \alpha^2 \leq x < \beta^2 \\ 1 & \text{for } x \geq \beta^2 \end{cases},$$

respectively. In the sequel analysis, the parameters are chosen as follows: $\alpha^1 = 0$, $\beta^1 = 1$, $\alpha^2 = -1$ and $\beta^2 = 1$. The mappings $X^i = g^i(Z)$, $i = 1, 2, 3$, are explicitly known and Eq. (5.9) and (5.12) can be solved in closed-form. In general, the mapping g of the

approximating random variable is not known in applications, which leads to additional errors, which is neglected in this academic example. Therefore, only the truncating error has influence on the accuracy of the considered approximation. Note, X^1 is simply the approximation of a log-normal random variable, because Z is normal.

Error Types

In order to get a deeper insight, Field and M. Grigoriu (2004) analyzed the approximations using seven different error types:

1. $\frac{X-\tilde{X}}{X}$
2. $MSE_{rel} = \frac{E((X-\tilde{X})^2)}{EX^2}$
3. $P(\{\omega \in \Omega \ : \ |X(\omega) - \tilde{X}(\omega)| > \epsilon\})$ for a given $\epsilon > 0$
4. $P(\{\tilde{X} \leq \inf_{\omega\in\Omega} X\} \cup \{\tilde{X} \geq \sup_{\omega\in\Omega} X\})$
5. $P(\tilde{X} > F_X^{-1}(0.99))$
6. $\frac{\mathrm{Var}(\tilde{X}(Z))}{\mathrm{Var}(X(Z))}$
7. $\frac{\mathrm{Kurt}(\tilde{X}(Z))}{\mathrm{Kurt}(X(Z))}$

A detailed description can be found in Field and M. Grigoriu, 2004. All error types were computed for $1 \leq p \leq 20$, which is much more then usually calculated. This detailed consideration led to redundant trends, so a characteristic selection is considered below. The relative means square error (MSE_{rel}), the normalized first four central moments, and convergence in probability is considered.

5.4.1 Hermite Chaos

Field and M. Grigoriu (2004) studied intensively the behavior of Hermite Polynomial Chaos approximation in one dimension of X^1, X^2 and X^3. From a geometrical perspective, the random variable X^2 is lying between X^1 and X^3, which can be confirmed by the error trends. Selected results from Field and M. Grigoriu, 2004 are shown in Fig. 5.6 for $\tilde{X}^1$ and $\tilde{X}^3$. Fig. 5.6a depicts the approximations of the random variables $X^1 = \exp(Z)$ and $X^3 = |Z|$ for orders $p = 0, \ldots, 15$, respectively, whereas Fig. 5.6b indicates the corresponding error trends.

In general, the convergence result Eq. (5.8) is confirmed, so that increasing the order p leads to an improvement of accuracy. For X^1 good results are achieved at $Z = 0$ even for $p = 3$, but for a more satisfactory approximation for $Z \in [-4, 4]$ an order $p > 5$ is necessary. For $p > 0$, it is hard to distinguish between X^1 and the approximation $\tilde{X}^1$. For X^3 a higher order is needed to be satisfactory in $Z \in [-4, 4]$. In addition, there are notable oscillation in the area of $Z = \pm 4$ and approaches zero slowly at $Z = 0$. Note, X^2 lying between X^1 and X^3. There are oscillations for $Z = \pm 4$ and for $Z = 0$ the

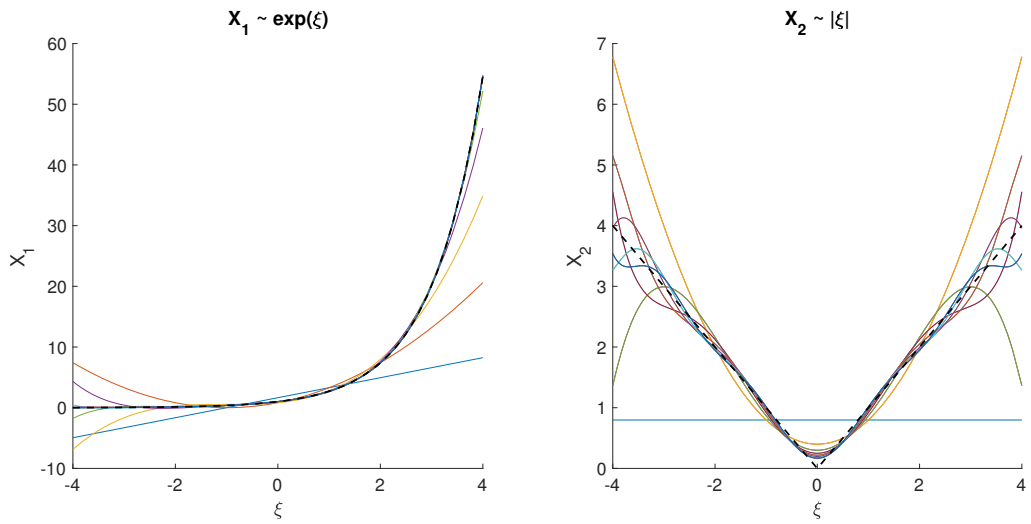

(a) Approximations for $p = 0, \ldots, 15$ and exact mappings - c.f. Field and M. Grigoriu, 2004.

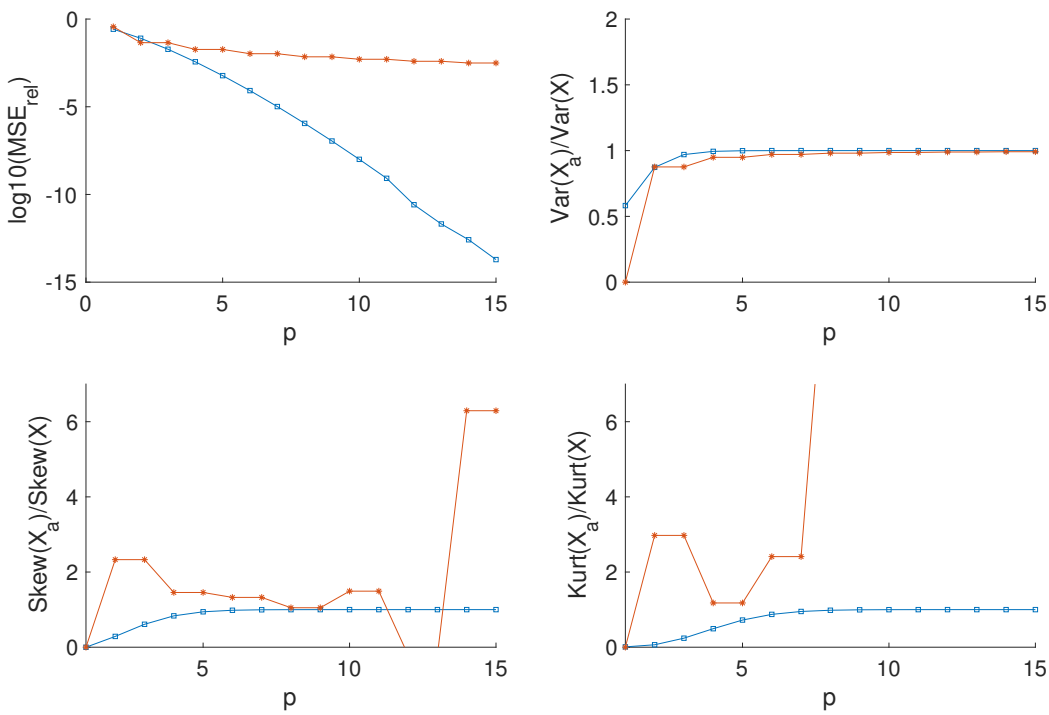

(b) Different errors types for $p = 0, \ldots, 15$ of X^1(blue) and X^3 (red) - c.f. Field and M. Grigoriu, 2004.

Figure 5.6: Homogeneous polynomial chaos approximation of X^1 and X^3.

performance is quite well.
As one of the main results of Field and M. Grigoriu (2004), which confirms the selection presented here, it turns out that despite an initially optimal input, the convergence

for certain errors, depending on g, are strongly slowed down or even deteriorated for shown orders: The relative mean square error is a function of p and decays rapidly for X^1 and slowly for X^3. The normalized variance is nearly one for $p = 5$ and $p = 15$ for X^1 and X^3, respectively. The normalized skewness and kurtosis are closed to one for $p = 5$ and converge for X^1. But, for X^3 both the normalized skewness and kurtosis deteriorates. Summarizing the results of Field and M. Grigoriu (2004), the accuracy of the Hermite polynomial chaos (PC) improves for some error types as additional terms in (5.7) were appended, but this behavior can not be exhibit for all errors. Stefanou (2009) concluded from the work of Field and M. Grigoriu (2004) and Mircea Grigoriu (2006) that the divergence usually occurs for problems involving sharp non-linearities and abrupt slope changes or bifurcations.

5.4.2 B-Spline Chaos

Next, the performance of B-Spline chaos is surveyed for X^1, X^2,X^3 and, for a better understanding and interpretation, the random input Z itself. The results are shown in Fig. 5.7, 5.8 and 5.9. In addition to the errors in 5.4.1, convergence in probability and the normalized mean ($\frac{E(\tilde{X})}{E(X)}$) is considered. Note, if no inner knots are used within the knot vector the term Bézier is applied to emphasize that no element refinement in the stochastic space is applied.
Here again, in general, the higher the order p, or number of basis functions N, the better the accuracy of the approximation.
For X^2 (red line in Fig. 5.7) the approximation is exact even for $p = 1$. The expectation, variance, skewness and kurtosis are exact - see red line in 5.7. The reason for that is the structure of the mapping $g^2(Z) = F_{Y^2}^{-1} \circ \Phi(Z)$. $F_{Y^2}^{-1}(y)$ is a linear function and $\Phi(Z)$ neutralizes the transformation from the parameter u to random variable Z, i.e. $F_Z^{-1}(u) = Z$, which occurs in the integral of Eq. (5.19):

$$g^2(F_Z^{-1}(u)) = F_{Y^2}^{-1} \circ \Phi(F_Z^{-1}(u)) = F_{Y^2}^{-1}(F_Z(F_Z^{-1}(u))) = F_{Y^2}^{-1}(u).$$

This implies every mapping g, which can be expressed as a composition of the CDF of the describing random variable, is as good as the approximation when the composition is neglected and the describing random variable is uniformly distributed. This phenomenon is very well illustrated by Fig. 5.9b. On the left side the curve is drawn in the space $\Omega_U \times g^2(\Omega_Z) = [0,1] \times [\alpha^2, \beta^2]$ and on the right in the space $\Omega_Z \times g^2(\Omega_Z) = (-\infty, \infty) \times [\alpha^2, \beta^2]$. Moreover, this emphasizes the correspondence between B-spline chaos and uniform distribution, which was already evident in section 5.3

The results for the other approximations are close to each other. They can be ordered from $\tilde{Z}$ over $\tilde{X}^3$ to $\tilde{X}^1$. Fig. 5.8 depicts the exact mapping, i.e. $Z(u) = F_Z^{-1}(u) =$

$\operatorname{erf}^{-1}(2u-1)\sqrt{2}$, and the approximation $\tilde{Z}(u)$, which fits quite good in the interior of $[0,1]$. Due to the fact, that the spline chaos is naturally defined on a closed interval, the L^2-projection must cope with transforming the open interval $(-\infty,\infty)$ to a closed one, i.e.

$$\lim_{u \searrow 1} F_Z^{-1}(u) = -\infty \qquad \text{and} \qquad \lim_{u \nearrow 1} F_Z^{-1}(u) = \infty,$$

respectively. Tab. 5.2 listed the results of the L^2-projection of the interval $[0,1]$ for increasing order. It is evident that the values are strongly varying and over all increasing if p increases. For $p < 7$ the values are quite small, which means that e.g. for $p = 5$

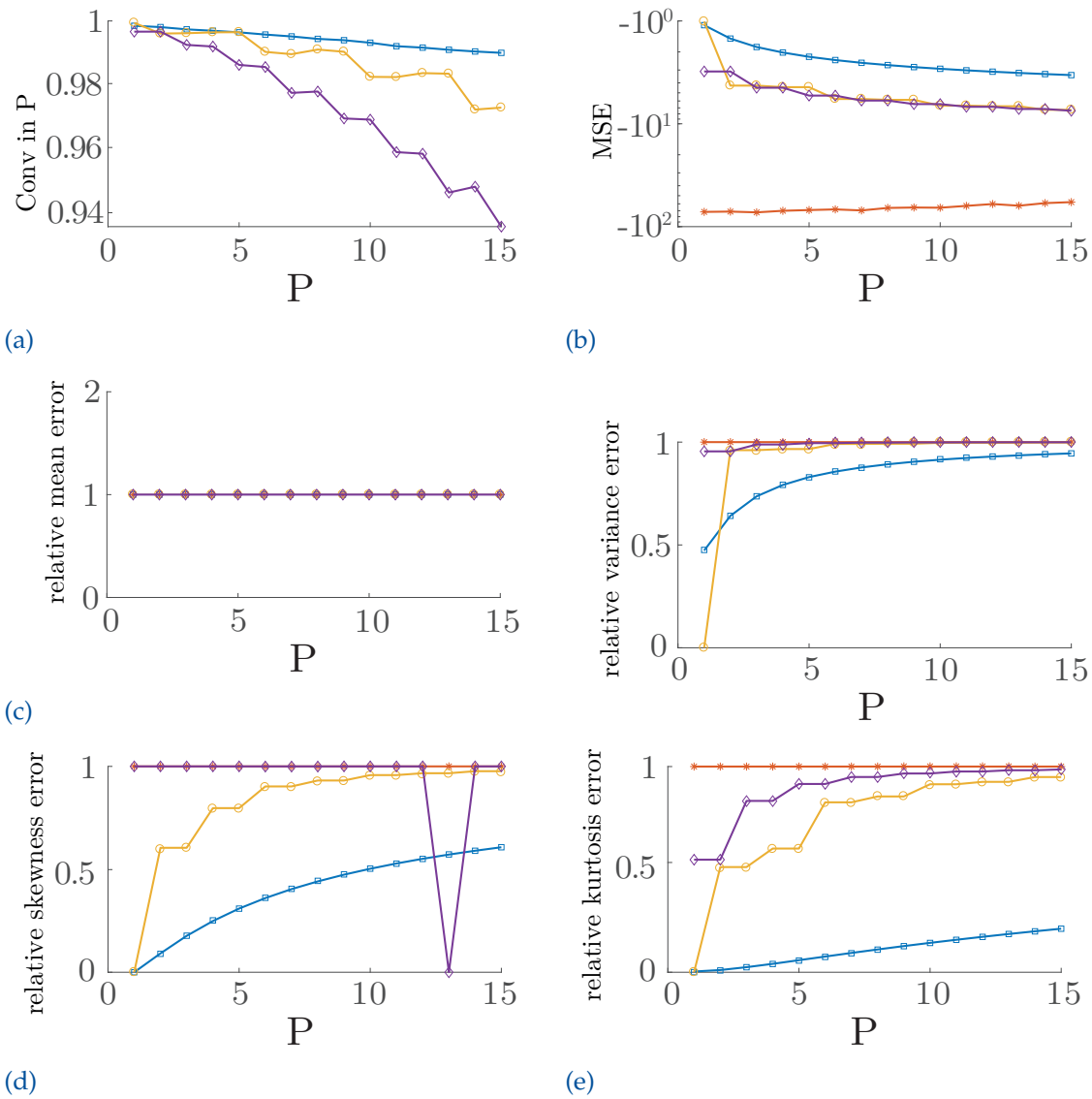

Figure 5.7: Errors of Bézier approximation of Z (purple), X^1 (blue), X^2 (red) and X^3 (yellow) with $Z \sim N(0,1)$ for $p = 1,\ldots,15$.

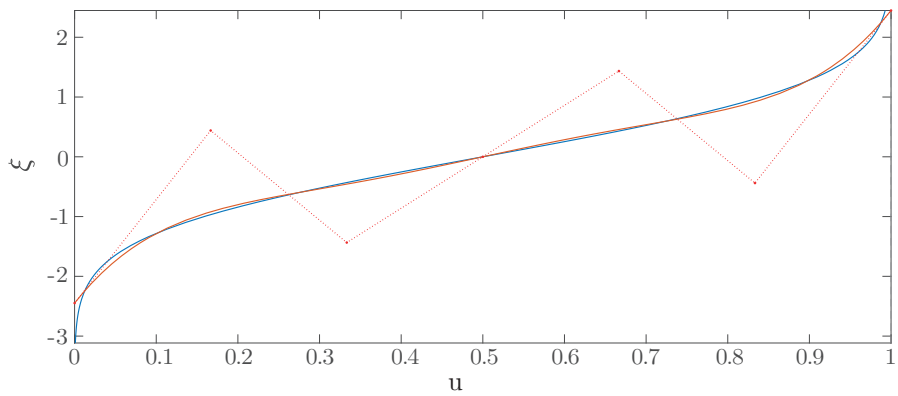

Figure 5.8: Bézier approximation of $\tilde{Z}$ for $p = 6$ and exact mapping.

p	$\tilde{\Omega}$	p	$\tilde{\Omega}$
1	[-1.6926 , 1.6926	9	[-16.6799 , 16.6799]
2	[-1.6926 , 1.6926]	10	[-6.0771 , 6.0771]
3	[-2.1768 , 2.1768]	11	[-48.7380, 48.7380]
4	[-2.1768 , 2.1768]	12	[-18.0581 , 18.0581]
5	[-2.6608 , 2.6608]	13	[-151.3264 , 151.3264]
6	[-2.4477 , 2.4477]	14	[-49.9681 , 49.9681]
7	[-5.8550 , 5.8550]	15	[-484.8692 , 484.8692]
8	[-3.2556 , 3.2556]		

Table 5.2: Results of the L^2-projection of the interval $[0,1]$ onto $\tilde{\Omega}$ for $Z \sim N(0,1)$.

$1 - 2 \cdot \Phi(-2.6608) = 99.22\%$ of the realization area is covered. Of course, it is problem dependent if this coverage is sufficient. For a tail analysis, for example, the marginal area is the most important; acceptable results can be obtained for $7 \leq p \leq 10$, capping at least 99.89% to $(100 - 1.8353e^{-60})\%$ of the area. If p goes higher then 10, the curve endpoints extremely detached from the center of the curve, i.e. $u = 0.5$ or $Z = 0$. However, the approximation in $(0,1)$ remains stable and the error curves in Fig. 5.7 converges (purple lines). The expectation and skewness is exact form the beginning, and the variance and kurtosis admits 1 sufficiently good for $p = 5$ and $p = 10$, respectively. This fluctuation limitation despite drifting endpoints, is explained by the property of variation diminishing of B-spline objects. It is not clear yet, how the intervals $\tilde{\Omega}$ are determined, but it is comprehensible that they increase when p increases.
Drawing the attention to X^1 (blue line in Fig. 5.7)and X^3 (yellow line in Fig. 5.7), apparently, better approximation results are obtained for X^3. The left-hand side figures in 5.9 represent the random variable to be approximated over the parameter space u, i.e., after transforming the input to a uniformly distributed variable. Instead, the right-hand

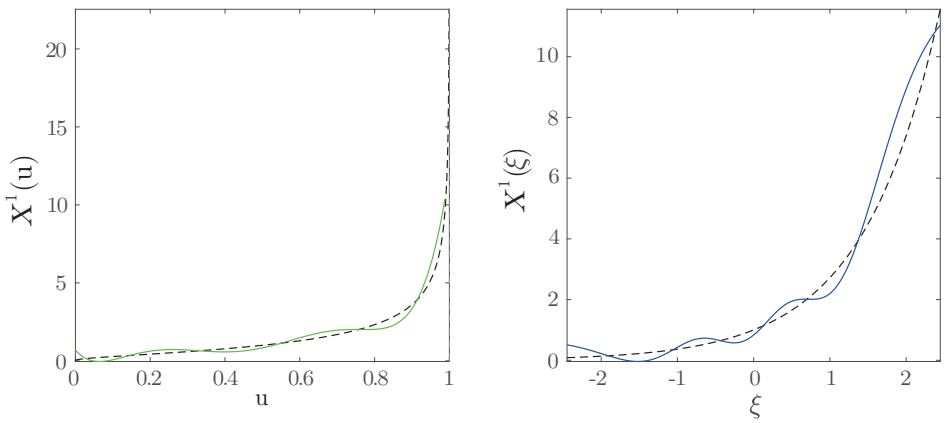

(a) Approximations of $\tilde{X}^1$ for $p = 6$ and exact mappings.

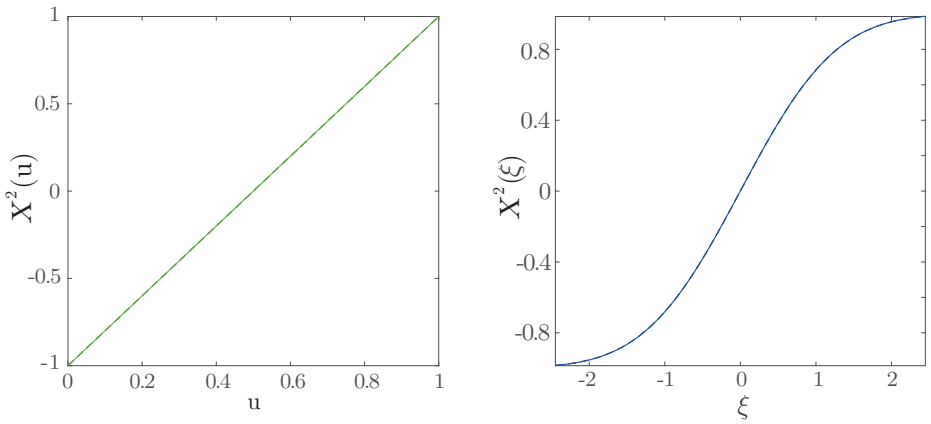

(b) Approximations of $\tilde{X}^2$ for $p = 6$ and exact mappings.

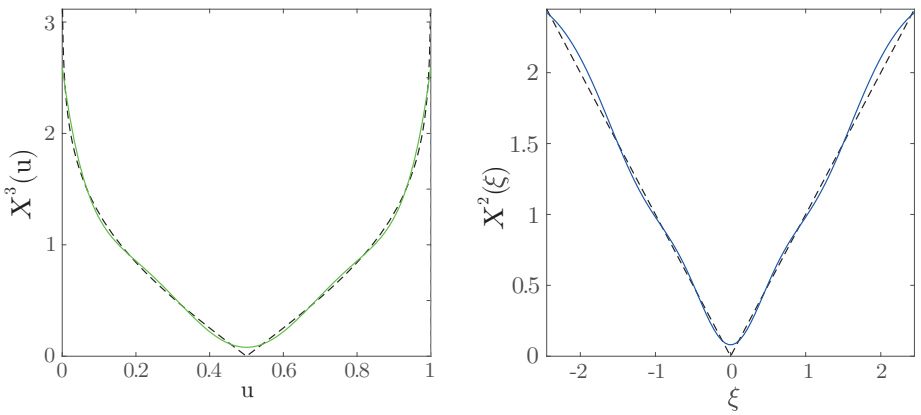

(c) Approximations of $\tilde{X}^3$ for $p = 6$ and exact mappings.

Figure 5.9: Bézier approximation of $\tilde{X}^i$ with $Z \sim N(0,1)$ in parameter space (left) and random space (right).

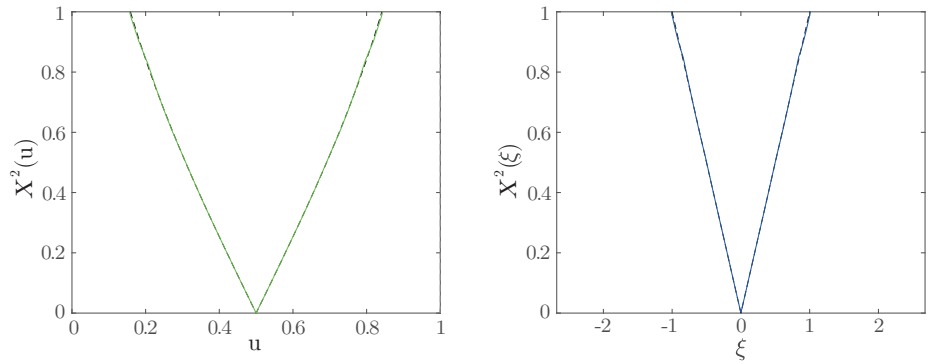

(a) $\tilde{X}^3$ for $p = 2$ and 1 inner knot with C^0-continuity and exact mappings.

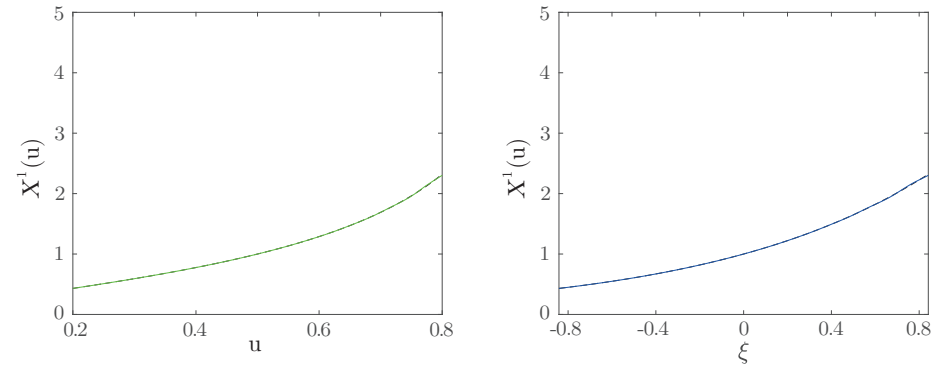

(b) $\tilde{X}^1$ for $p = 3$ and 32 inner knot with C^2-continuity and exact mappings.

Figure 5.10: B-Spline chaos of $\tilde{X}^1$ and $\tilde{X}^3$ with $Z \sim N(0,1)$ in parameter space (left) and random space (right) with varying inner knots and continuity.

side figures show the variables over the original Gaussian variable Z. The plots over u are smoother, small oscillations can be located over the entire domain, which are more distinctive for X^1. If the mapping g is contractive, the oscillations diminish, whereas the oscillations magnify, if g is not contractive. Concerning the error plot, this awareness is confirmed. The approximations converges in the order described above. Furthermore, very good results for the moments are achieved for $\tilde{Z}$ and $\tilde{X}^3$. The outcome of $\tilde{X}^1$ is worse, but can significantly be improved for $\beta^1 < 1$.
The main advantage of using splines instead of ordinary polynomials is that, besides the order p, the number of elements in the stochastic space can be taken into account and, especially for B-spline basis functions, the desired continuity over these stochastic element boundaries can be adjusted, too. Therefore, the previous results are improved by varying the degree, the number of stochastic elements (or inner knots) and the continuity over element boundaries (or knots spans). This means, on the one hand, for $\tilde{X}^3$ that a C^0-B-spline basis - see e.g. Fig. 3.6 - is utilized for describing the mapping g^3. Consequently, the analysis is considerable improved at the kink at $u = 0.5$ or $Z = 0$ - see Fig. 5.10a.

5.4.3 Comparing Results

Summarizing the numerical results of the last two sections, the accuracy of the B-spline chaos improves for all error types as the order p, or the number of basis functions

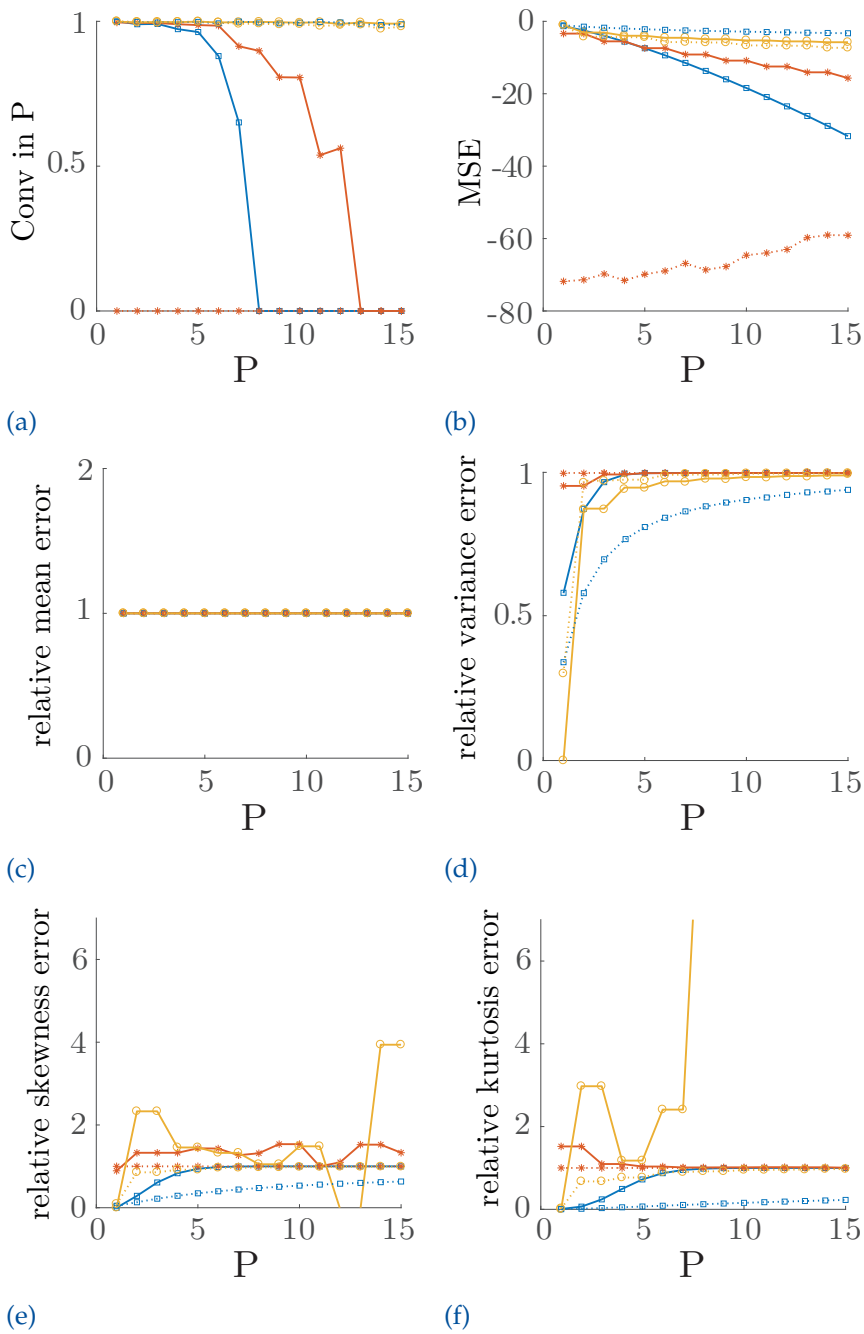

Figure 5.11: Errors of Hermite (solid line) and Bézier chaos (dotted line) of g^1 (blue), g^2 (red) and g^3 (yellow) with $Z \sim N(0,1)$ for $p = 1, \ldots, 15$.

N, is increased. This was not the case with the Hermite chaos - see for instance the kurtosis in Fig. 5.12 and 5.11. But, especially for $\tilde{X}^1$, the B-Spline chaos is liable to the Hermite chaos. And for $\tilde{X}^2$, it is the opposite. In simplified terms, the B-spline chaos performs well, were the Hermite chaos performs bad and vise versa. Nevertheless, due to the flexibility of the B-Spline concerning stochastic elements and continuity between

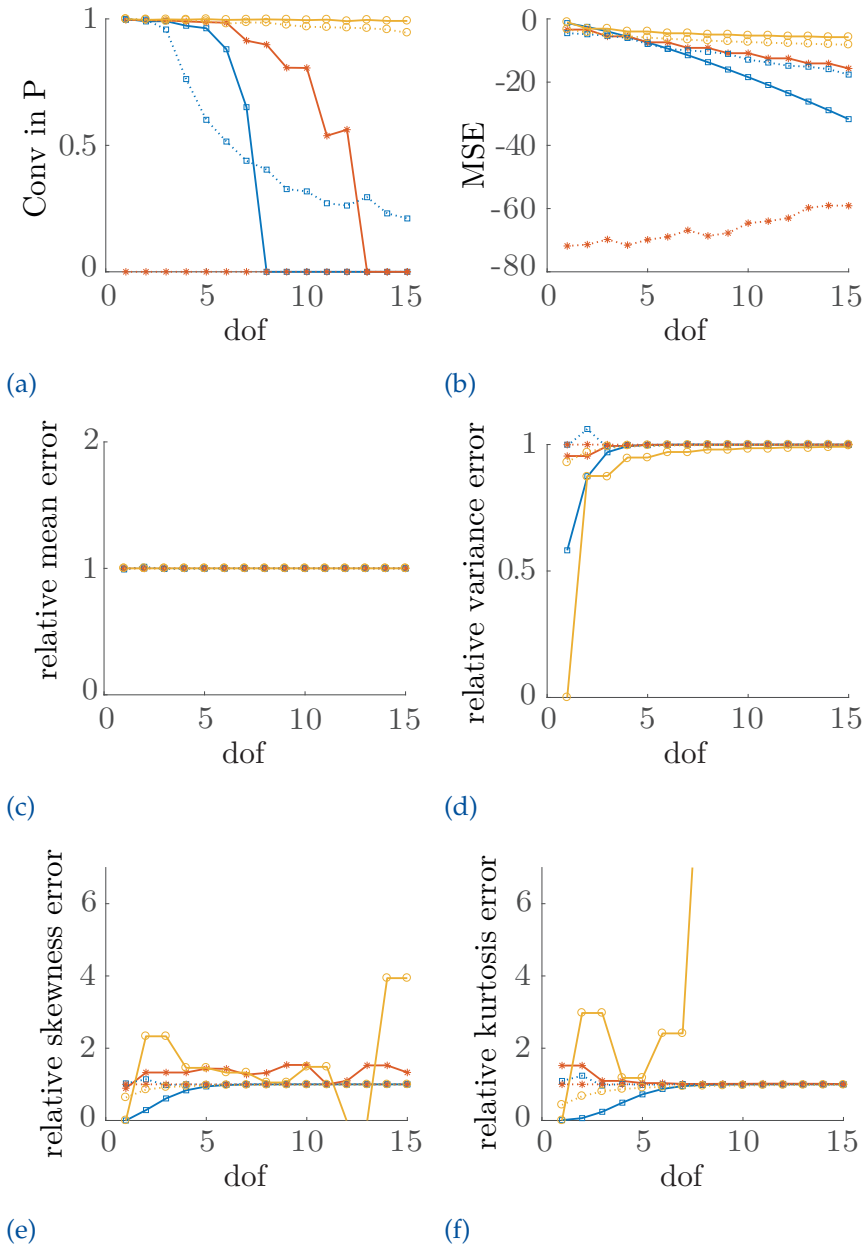

Figure 5.12: Errors of Hermite (solid line) and B-spline chaos (dotted line) of g^1 (blue), g^2 (red) and g^3 (yellow) with $Z \sim N(0,1)$ for $p = 1, \ldots, 15$. Improved configuration for g^1 and g^3 with inner knots and continuity changed.

these elements, the results can be individually improved. Fig. 5.12 and 5.11 compares both chaos techniques using the presented error types. In the upper one, results for the orders $p = 1, \ldots, 15$ for the Hermite (solid line) and B-spline chaos (dotted line) - or more precisely Bézier approximation, because no inner knots were used - are illustrated. The approximations of g^2 (red lines) and g^3 (yellow lines) of the Bézier approximations outperforms the Hermite approximation especially for the normalized moments. Certainly, the approximation of g^1 (blue lines) is worse. As stated above, the approximations can be individually improved. Fig. 5.12 depicts the improved results, when adding more inner knots or varying the continuity over knot spans. Hermite chaos is still the best choice for approximating the log-normal random variable (g^1), although the results for the spline chaos can be improved, i.e. the elements were increased from 1 to 15 with an order of $p = 9$ while retaining a C^1-continuity over element boundaries. The error values for g^3 are enhanced while using one inner knot with C^0-continuity (yellow dotted line). A better convergence rate for all error types is achieved this way. Especially for g^2, but also for the other functions, an increased stability for the calculation of the higher moments can be observed. This can be clearly seen when comparing the yellow lines for the error of the normalized skewness and kurtosis in Fig. 5.12 and 5.11. An improved configuration of the B-spline chaos for the approximation of g^2 are not necessary. This again emphasizes the link between uniformly distributed random variables and the B-spline chaos already demonstrated in section 5.3.

5.4.4 Random Vectors

In this example, the accuracy of spline chaos is demonstrated by an example of a multi-dimensional input of Eq. (5.5)

$$X = g(Z_1, Z_2) = |Z_1| + |Z_2| \quad \text{with } Z_1, Z_2 \sim N(0,1)$$

If the Z_i's are independent, the B-Spline based PC of higher dimensions can be extended by multivariate B-Splines in a straight forward manner. Thus, the two-dimensional

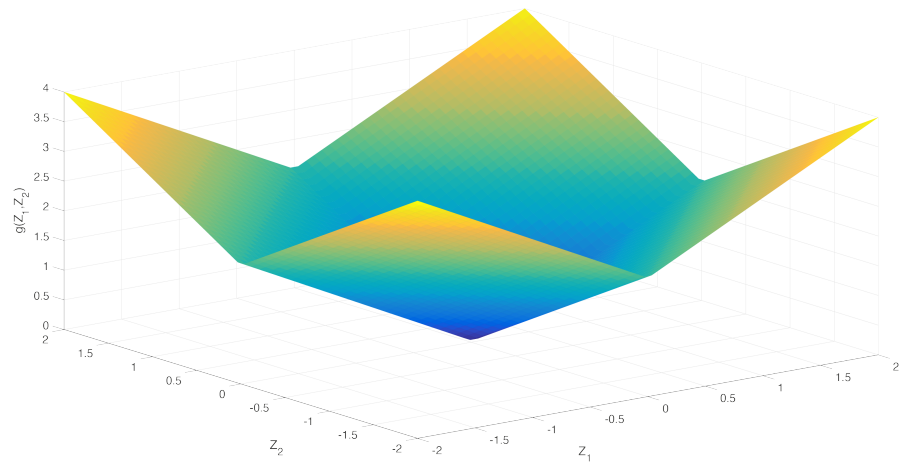

(a) Reference: $g(Z_1, Z_2) = |Z_1| + |Z_2|$.

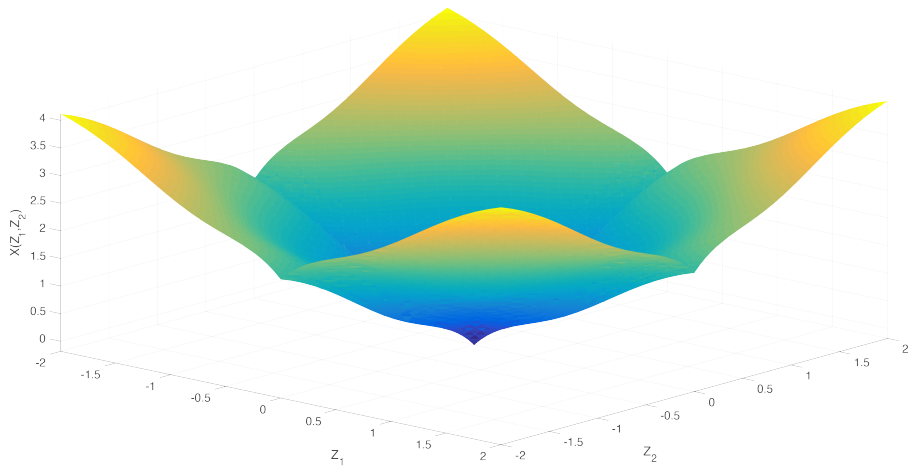

(b) Approximation: $\tilde{X}(Z_1, Z_2)$

Figure 5.13: Two-dimensional B-Spline chaos of third order with equal knot vectors [0 0 0 0 0.5 0.5 0.5 1 1 1] ($\mathcal{C}^0$-continuity along the axes) with $Z_1, Z_2 \sim N(0,1)$ iid.

B-spline chaos of order $\mathbf{p} = (p_1, p_2)$ is given by

$$\tilde{X} = \sum_{i_1=1}^{N_1} \sum_{i_2=1}^{N_2} a_{i_1 i_2} B_{i_1 i_2}(U_{i_1}(\omega), U_{i_1}(\omega)), \tag{5.35}$$

with $B_{i_1 i_2} \in \mathcal{S}_{\mathbf{p}}(\mathfrak{P}, \mathfrak{M})$ and partition $\mathfrak{P} = (\mathfrak{P}_1, \mathfrak{P}_2)$ and multiplicity vector $\mathfrak{M} = (\mathfrak{M}_1, \mathfrak{M}_2)$. The main difference between polynomial and spline chaos is the tensor product structure, which leads to

$$N_1 \cdot \ldots \cdot N_d$$

basis functions, where n_i is the number of one-dimensional basis functions in the i-th dimension. If the number of basis functions in each direction remains unchanged, the number of basis functions is determined by

$$n^d \,. \tag{5.36}$$

Ivo Babuška, Raúl Tempone, et al. (2004) used basis functions of the same dimension especially for convergence analysis, which will be explored in more detail at the end of the next chapter. In contrast, the number of basis functions of the d-dimensional Hermite chaos of order p is

$$\binom{P+d}{P}.$$

However, the focus of section 5.4 lies on the accuracy of polynomial and spline chaos. Fig. 5.13 shows the B-spline approximation of $g(Z_1, Z_2) = |Z_1| + |Z_2|$ for third order, two elements in each direction, and $\mathcal{C}^0$-continuity over element boundaries. This example can be seen as the two dimensional counterpart of $g^3(Z) = |Z|$. As it was in the one-dimensional case, due to the flexibility of elements and continuity, all error metrics converges for the B-Spline chaos, while the Hermite chaos did not exhibit this behavior in all metrics considered here. The error plots are shown in Fig. 5.14. The approximation was done by the two-dimensional Hermite chaos for order $p = 0, \ldots, 20$ (green line), which results in 231 basis functions for $p = 20$. This is compared with first to fourth order B-Splines each with two to eight elements in each direction and $\mathcal{C}^0$-continuity along the axes. For example the fourth order B-Spline has 81 basis functions with two elements and 225 basis functions with eight elements (purple line). The observations from the one-dimensional examples can be confirmed for the multi-dimensional case. It is remarkable that overall a better error behavior can be observed for the spline chaos compared to the Hermite chaos, although the latter is optimized for normal random variables.

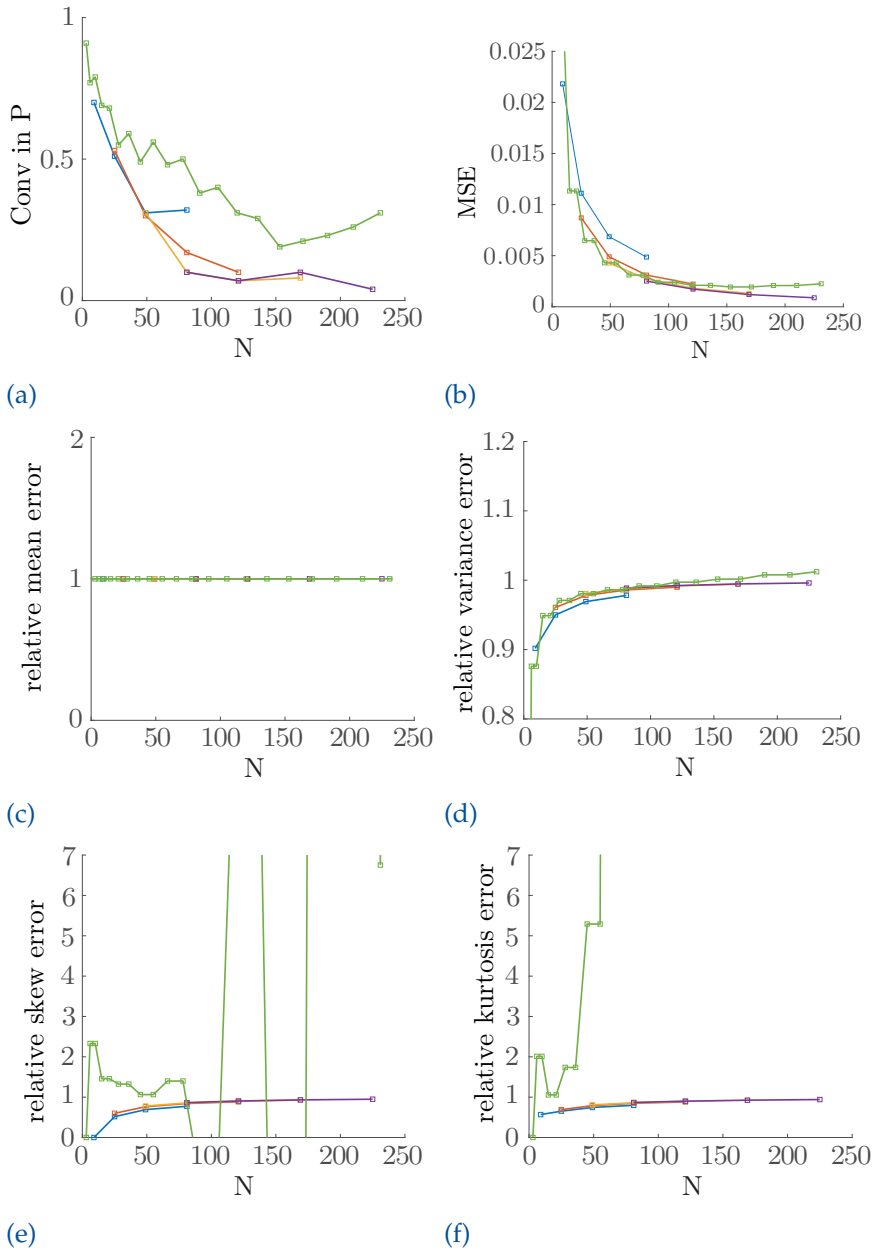

Figure 5.14: Error plots for Hermite and B-Spline chaos of $g(Z_1, Z_2) = |Z_1| + |Z_2|$: First Order B-Spline (blue), Second Order B-Spline (red), Third Order B-Spline (yellow), Fourth Order B-Spline (purple) and Hermite chaos (green) with $p = 0, \ldots, 20$.

5.4.5 Random Processes

Moreover, the proposed method can be applied to stationary processes. Then, the coefficients in Eq. (5.12) become time dependent, but for a fixed time the problem remains the same. Thus, the time-dependent coefficients are defined by collecting like

powers of Z_i Sakamoto and Roger Ghanem, 2002. This means for instance, any process which can be cast in the framework of the KLE is accessible for the presented spline chaos, too.
The efficiency for numerical models of representing stochastic processes like the KLE is of very importance Field and M. Grigoriu, 2004; P. D. Spanos and Roger Ghanem, 1989. Pol D. Spanos et al. (2007) improved the aforementioned problem for the exponential covariance kernel which is dominating in mechanical applications. They dispense the lack of non-differentiability which resulted in a significant reduction of the number of basis functions while preserving its beneficial properties. With regard to Eq. (5.36), the B-Spline based PC could become even more pertinent combined with the relatively small number of random variables corresponding to differentiable autocorrelation functions.

To investigate the accuracy of B-spline chaos for random processes, consider the stationary log-normal random process

$$Y(t) = \exp\big(X(t)\big) \tag{5.37}$$

where $X(t)$ is a parameterized, zero mean, stationary Gaussian random process with unit variance defined as

$$X(t) = \frac{\sqrt{2}}{2}\big[\cos(\pi t)Z_1 + \sin(\pi t)Z_2 + \cos(2\pi t)Z_3 + \sin(2\pi t)Z_4\big] \tag{5.38}$$

Since the process in Eq. (5.38) is already parameterized, i.e. the relationship of $X(t)$ and the random variables $\mathbf{Z} = Z_1, \ldots, Z_4$ is explicitly known, the spline chaos in four dimension is directly applicable. According to Mircea Grigoriu (1995) the stationary random function $Y(t)$ has mean

$$\mu_Y(t) = e^{0.5} \tag{5.39}$$

and covariance

$$c_Y(\tau) = e^{(1+\frac{cos(\pi\tau)}{2}+\frac{cos(2\pi\tau)}{2})} - e \tag{5.40}$$

Since $Y(t)$ is a stationary random process, the covariance function Eq. (5.40) can be written in terms of τ as the statistical properties are time independent.
Higher stochastic dimensions lead to multi-dimensional integrals in the calculation of the expansion coefficients - see for example Eq. (5.24). The dimension of parameterized field $X(t)$ according to Eq. (5.36) is $d = 4$. As a consequence, first a multivariate basis must be generated from the univariate B-spline basis functions via a tensor product and second each entry of the matrix $\mathbf{A}$ and the vector $\mathbf{b}$ must be computed via a four-dimensional integration. To determine the multivariate basis, the tensor product is applied to the univariate basis functions of each stochastic dimension generated by the knot vector U - cf. section 3.2.1. Thus, the dimension of the d-variate B-spline chaos depending on the structure of the knot vector, e.g. $U = [0\ 0\ 0\ 0\ 1\ 1\ 1\ 1]$, for the

approximation of the random field in Eq. (5.38) is then given by:

$$N = (m - p - 1)^d = (8 - 3 - 1)^4 = 256$$

Due to the exponential dependence of the multivariate basis on the stochastic dimension of the underlying random field, the number of basis functions required increases rapidly. Thus, similar to the PCE the B-spline chaos is also governed by the curse of stochastic dimensionality. Another challenge is the multi-dimensional integration, because primitive functions rarely exist considering multi-dimensional integration or can only be obtained with very high computational effort. For this reason the introduction of quadrature rules is appropriate, e.g. Gauss quadrature - see section 3.1.2. Advantageous in the study of the random field $X(t)$ given in Eq. (5.38) is the sum structure, which allows successive integration according to each dimension. The number of Gaussian points needed for integration depends on both the order p of the multivariate B-spline basis function, and the function in Eq. (5.37). For the determination of the number of Gauss points the error rate of the approximating integrals was evaluated. Thereby, the asymptotic behavior at five Gauss points shows a sufficiently exact error rate of $6,649 \cdot 10^{-8}$. Based on these theoretical observations, the stochastic process $Y(t)$ introduced by Field and M. Grigoriu (2004) is investigated using both the spline and Hermite chaos, and the results are compared.

First, the comparison of is done without any additional stochastic elements and B-Spline basis functions represent Bernstein polynomials. According to Field and M. Grigoriu, 2004, the Hermite chaos achieves an sufficient accurate approximation of the covariance function given in (5.40) for a total number of basis function $q = 210$ expansion terms. Fig. 5.15a shows the approximated covariance function of degree $p = 2,\ 4,\ 6$, resulting in $q = 15,\ 70,\ 210$ expansion terms, respectively. It can be observed that the approximation error diminishes as the number of terms is increased. In contrast, for a similar accuracy of the approximation using B-spline chaos, significantly more basis functions are needed. Fig. 5.15b shows the approximations of the covariance function for $q = 81,\ 625,\ 2401$ terms. Increasing the expansion terms leads to more accurate approximations. Nevertheless, the convergence rate of the B-spline chaos expansion is significantly slower. Fig. 5.16 shows the relative variance of $Y(t)$ given by

$$\frac{\mathrm{Var}[\tilde{Y}(t)]}{\mathrm{Var}[Y(t)]} \tag{5.41}$$

By increasing the expansion terms, the relative variance error for both approximations approaches the expected value of one. It can be seen from Fig. 5.16a that the Hermite chaos retains the stationary property of the original random process $Y(t)$. B-spline chaos approximations are initially non-stationary and keep a small deviation even when using $q = 2401$ terms - see Fig. 5.16b. Since the oscillations of the normalized variance error become smaller by increasing the expansion terms, it is expected that the B-spline chaos will be stationary in the limit case, too. In the following, the influence of multiple

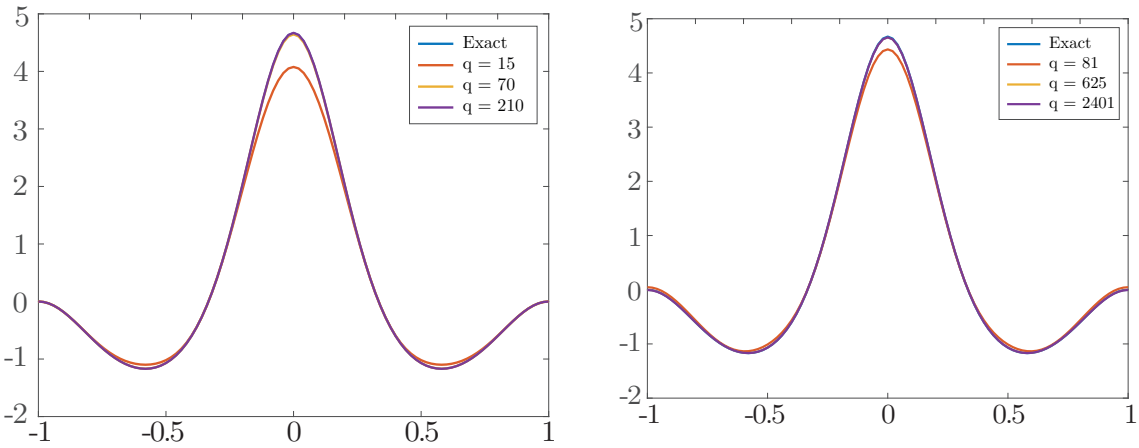

(a) **Hermite chaos** : Approximated covariance of $Y(t)$, $\tau \in [-1\ 1]$

(b) **B-Spline chaos** : Approximated covariance of $Y(t)$, $\tau \in [-1\ 1]$

Figure 5.15: Approximations of the covariance function of $Y(t)$.

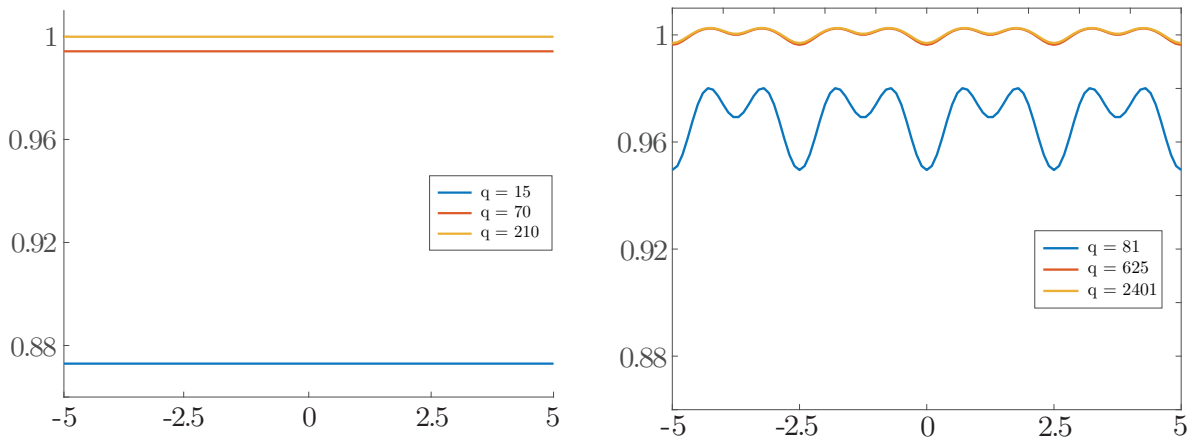

(a) **Hermite chaos** : relative Variance of $Y(t)$ depending on number of expansion terms

(b) **B-Spline chaos** : relative Variance of $Y(t)$ depending on number of expansion terms

Figure 5.16: Relative variance of $Y(t)$.

stochastic elements is investigated, which can be generated by adding inner knots in the B-spline characterizing knot vectors. In order to study the properties of B-spline basis functions to approximate a random field using several stochastic elements, investigations are carried out for the choice of $q = 625$ expansion terms and various knot vectors. The results for maximum covariance error , and minimum and maximum relative variance error according to Eq. (5.41) of the approximations are given in Tab. 5.3. Best results for the maximum covariance error with $q = 625$ terms are obtained by increasing the degree p of the B-splines basis functions. The introduction of one additional stochastic element on the domain with C^{p-1} continuity and $p = 3$ yields almost similar results

#	p	**knot vector** U	ε_{Cov}	**min.**σ_{rel}	**max.**σ_{rel}
1	2	[0 0 0 0.1 0.9 1 1 1]	0.2239	0.9521	0.9811
2	2	[0 0 0 0.2 0.8 1 1 1]	0.1587	0.9660	0.9871
3	2	[0 0 0 0.3 0.7 1 1 1]	0.1046	0.9776	0.9925
4	2	[0 0 0 0.4 0.6 1 1 1]	0.0181	0.9961	1.0023
5	2	[0 0 0 0.5 0.5 1 1 1]	0.0366	0.9922	1.0007
6	3	[0 0 0 0 0.5 1 1 1 1]	0.0173	0.9963	1.0024
7	4	[0 0 0 0 0 1 1 1 1 1]	0.0173	0.9963	1.0024

Table 5.3: Comparison of statistical values of $Y(t)$ for the choice of different knot vectors with 625 expansion terms of B-spline chaos.

as the spline chaos with $p = 4$ and one element. Less effective are splines with $p = 2$. Neither lower continuities at the element boundaries (#5) with C^0 continuity nor the introduction of further stochastic elements as in (#1) to (#4) could reach the results for third and fourth order B-splines. It is interesting to note that the location of inner knots has a direct impact on the accuracy in this example. Hence, the errors decreases for more centrally located inner knots, as can be seen from knot vectors (#1) to (#4). These results can be related to the underlying Gaussian measure, where the mass of the distribution is concentrated in the center. This gives rise to the conclusion that a finer discretization in the center leads to increased approximation quality. Moreover, it suggests, on the one hand, using adaptive methods for stochastic mesh refinement is desirable and, on the other side, equidistant partitioning will have an inhibiting effect for more complex stochastic structures.

5.5 Conclusions

The first two sections have introduced polynomial and spline chaos, respectively, in a multi-dimensional abstract framework, with the proof of strong convergence of spline chaos providing the main result. This consideration was accompanied by a one-dimensional description for both cases to make similarities and differences in construction appear obvious, and further strengthens an intuitive notion of the correlation between distribution and polynomial type, the capability of polynomials to represent random variables, and the quality of non-corresponding distribution and polynomial type. Mathematically, this was based on the essential statements from sections 3.1 and 3.2 about polynomial and spline spaces. At the end of this section, the algorithmic

procedure of the newly developed methodology of B-spline chaos was demonstrated, as well as the proof of weak convergence for arbitrary random variables, whose conditions are compatible with most applications.
In the third section, these results were substantiated by first numerical examples. In order to show the versatility and flexibility of spline chaos uniform, beta, normal, and exponential distributed random variables have been approximated. The approximation quality could thus be improved considerably, despite the fact that the distribution was not optimally designed for these bases. The connection between uniform distribution and B-splines, already apparent in the proofs and the construction of section 5.2, were directly consolidated in the first example. So that B-spline chaos can be regarded as a generalization of Legendre chaos. Thus, they are exact from first order on while representing uniform random functions.
In section 5.4, accuracy was examined in more detail. Based on the work of Field and M. Grigoriu (2004), who studied the limits of Hermite chaos, it was found that the methods are complementary for the selected examples. Again, the rich spline space can increase the approximation accuracy by additional elements and flexible continuity. It is important to emphasize the different error type consideration, which has shown the suitability for different application areas, e.g. structural analysis, response variability methods, or methods where the full PDF is used. It is found that the convergence of the spline chaos is very stable, especially for higher moments, which should improve tail probabilities. Besides, picking up the conclusion of Stefanou (2009), the presented results may improve problems involving sharp non-linearities, where Hermite chaos is not a neat choice.
Moreover, multi-dimensional examples were shown in sections 5.4.4 and 5.4.5. The focus was on random vectors and parameterized stationary random processes. The kinked function for the approximation of a random vector confirmed the positive properties of the $\mathcal{C}^0$-continuous elements from the one-dimensional case. The Hermite chaos exhibited a poor convergence behavior. In contrast, the results of the B-spline chaos could be improved by element and continuity fitting, but only with considerably more basis functions than for Hermite chaos, which are optimal for the Gaussian process. Nevertheless, the results are not surprising. Overall, section 5.4 curved out borders to PC expansions, limitations, features, and potentials of possible applications of the new proposed spline chaos.
In the next part, spline chaos is applied to the solution of stochastic differential equations.

6 Applications of B-Spline Chaos

In this chapter the spline chaos is applied in order to solve stochastic differential equations using a Galerkin type approach. At first, the general procedure of the stochastic Galerkin method (SG)Xiu and Karniadakis, 2002 is presented. Then, a stochastic ordinary differential equations ordinary differential equation (ODE) with uniform random input is treated. Convergence rates of Legendre, Hermite, and B-spline chaos are demonstrated by comparing mean and variance with the exact solution. Subsequently, an Euler-Bernoulli beam with random stiffness is processed. Different types of random inputs are analyzed and compared with the exact numerical solution by various error types. Furthermore, the complete density function is validated against the outcome of a MCS. As a multidimensional extension of the beam, namely an infinite plate problem is further examined. The Young's modulus is described as a random field. Beyond all examples, *h*-*p*-convergence is demonstrated.

6.1 General Procedure

Let us consider a system of stochastic PDE in a spatial domain $D \subset \mathbb{R}^{n_x}$ with $n_x = 1, 2, 3$ and a time domain $[0, T] \subset \mathbb{R}_{\geq 0}$

$$\mathcal{L}(x, t, \omega; u(x, t, \omega)) = f(x, t, \omega) \quad \text{in } D \times [0, T] \times \Omega \tag{6.1}$$

with boundary and initial condition

$$u(x, 0, \omega) = h(x, \omega) \qquad \text{on } D \times \{t = 0\} \times \Omega \tag{6.2}$$

$$u(x, t, \omega)\big|_{\partial\Omega} = g(t, \omega) \qquad \text{on } \partial D \times [0, T] \times \Omega. \tag{6.3}$$

$\mathcal{L}$ is a differential operator, which can be non-linear. Equation (6.1) is a deterministic problem with uncertain input conveyed by ω which is defined in an appropriate probability space $(\Omega, \mathcal{F}, \mathcal{P})$. Thus, the solution is given by

$$u : D \times [0, T] \times \Omega \to \mathbb{R}^{n_u} \tag{6.4}$$

where $n_u \in \mathbb{N}$ is the dimension of u. In general, it is not necessary, nor is it relevant, to precisely specify the underlying probability space, because the focus is mostly

on the image space of the random variables of interest. In engineering applications, the uncertainty of the system can be based on material properties, loads, boundary and initial conditions, etc. They can take the form of random parameters or random processes and can decently be parameterized by a set of mutually independent random variables

$$\begin{aligned} Z : (\Omega, \mathcal{F}, \mathcal{P}) &\to (\mathbb{R}^d, \mathcal{B}(\mathbb{R}^d), F_Z) \\ \omega &\mapsto Z(\omega) = (Z_1(\omega), \dots, Z_d(\omega)) \end{aligned}$$

with $d \in \mathbb{N}$. The parametrization for processes can be done by the KLE or PCE, for example. Eq. (6.5) can then be reformulated:

$$\mathcal{L}(x, t, \omega; u(x, t, Z)) = f(x, t, Z) \quad \text{in } D \times [0, T] \times \mathbb{R}^d. \tag{6.5}$$

Consequently, the solution u can also be represented by the random variable Z through a chaos expansion, i.e.

$$\begin{aligned} u : D \times [0, T] \times \mathbb{R}^d &\to \mathbb{R}^{n_u} \\ (x, t, Z) &\mapsto \sum_{i=1}^{N} u_i(x, t) \Psi_i(Z) \end{aligned}$$

where $\{\Psi_i\}$ is a set of basis functions spanning a d-dimensional space and $u_i(x, t) \in \mathbb{R}^d$ are chaos coefficients, which are spatial and time dependent. N is the total number of basis functions.

Applying the Galerkin projection to Eq. (6.5), which forces that the error ε, arising from the truncated PC expansion, is orthogonal in terms of the inner product of $L_2(\Omega, \mathcal{F}, \mathcal{P})$ to the approximating space $\mathcal{P}_p^d$ or $\mathcal{S}_{\mathbf{p}}$, which is finite dimensional, i.e.

$$\langle \varepsilon, \Psi_j \rangle = \mathbf{E}\left(\varepsilon \, \Psi_j\right) = 0 \quad \text{for } j = 1, \dots, N \tag{6.6}$$

with

$$\varepsilon := \mathcal{L}\left(x, t, \omega; \sum_{i=1}^{N} u_i(x, t) \Psi_i(Z)\right) - f(x, t, Z). \tag{6.7}$$

Inserting (6.7) in (6.6) and exploiting the linearity of the expectation leads to

$$\mathbf{E}\left(\mathcal{L}\left(x, t, \omega; \sum_{i=1}^{N} u_i(x, t) \Psi_i(Z)\right) \Psi_j(Z)\right) = \mathbf{E}(f(x, t, Z) \Psi_j(Z)) \tag{6.8}$$

for $j = 1, \dots, N$.

For the Wiener-Askey PC, i.e. the polynomials are orthogonal, we have $N = \binom{p+d}{p}$,

where p is the highest order in the set $\{\Psi_i\}$. As remarked before, when the more flexible B-Splines are used, N depends on the tensor product structure of the basis and is given by $N = n_1 \cdot \ldots \cdot n_d$, where n_i is the number of basis functions of the i-th dimension. However, the randomness is transformed in the space spanned by $\{\Psi_i\}$. Therefore, for a given realization of Z, the PDE (6.5) for a fixed x and t leads to N deterministic problems. Furthermore, the well-posedness of this stochastic system can be reduced to the deterministic case as well Xiu, 2010.

6.2 First order stochastic ordinary differential equation

In the following consider the stochastic ODE presented e.g. from Wan and Karniadakis (2005):

$$\mathcal{L}(t,\omega;y(t,\omega)) = f(t,\omega) \quad \text{in } [0,T]\times\Omega \tag{6.9}$$

$$:\Leftrightarrow \quad \frac{\mathrm{d}\,y(t)}{\mathrm{d}\,t} = -a(\omega)\,y(t) \quad \text{with} \quad y(0)=1, \tag{6.10}$$

where $t \in \mathbb{R}_+$ and the decay rate $a : \Omega \to \mathbb{R}$ is a random variable with mean μ_a and density function f_a. The exact solution of (6.10) is

$$y(t) = \exp(-a(\omega)\,t). \tag{6.11}$$

Then, the stochastic mean solution can be determined by

$$\mathbf{E}\left[y(t)\right] = \int_S \exp(-at) f_a(a)\; da \tag{6.12}$$

with support S of a.
Applying the B-spline chaos to the random variables a and y yields

$$\tilde{a}^N = \sum_{i=1}^{N} a_i B_{i,p}(U) \tag{6.13}$$

and

$$\tilde{y}^N(t) = \sum_{i=1}^{N} y_i(t) B_{i,p}(U), \tag{6.14}$$

where $U \sim \mathrm{unif}([0,1])$ corresponds to the B-spline basis. Substituting Eq. (6.13) in (6.10) leads to

$$\begin{aligned}&\sum_{i=1}^{N} \frac{\mathrm{d}\,y_i(t)}{\mathrm{d}\,t} B_{i,p}(U)\\ &\quad = -\sum_{i=1}^{N}\sum_{j=1}^{N} a_i y_j(t) B_{i,p}(U) B_{j,p}(U).\end{aligned} \tag{6.15}$$

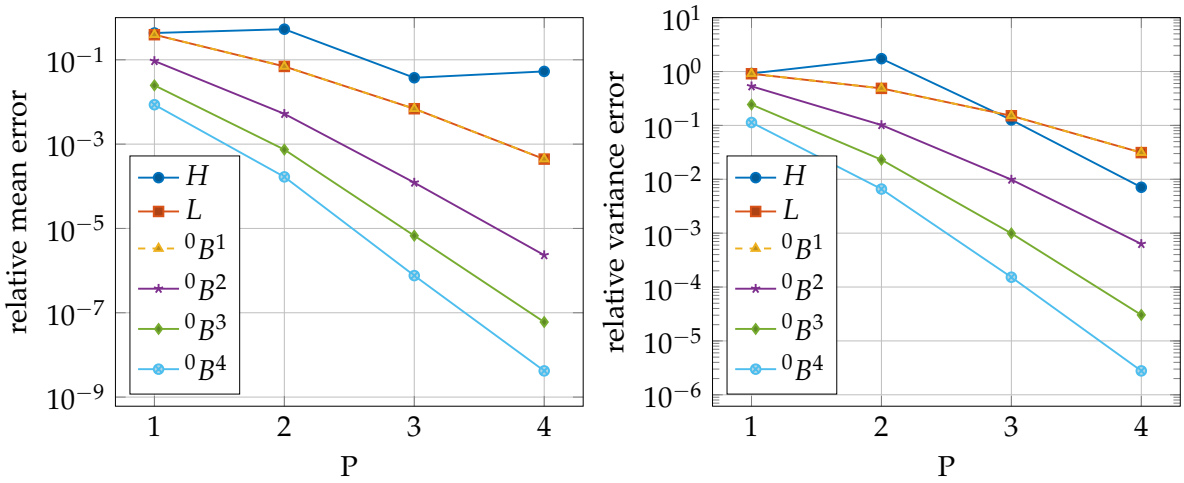

Figure 6.1: Relative mean and variance error of Hermite, Legendre, and B-spline chaos for $t = 5$.

Applying the Galerkin projection to Eq. (6.15) yields

$$\sum_{i=1}^{N} \frac{\mathrm{d}\, y_i(t)}{\mathrm{d}\, t} \mathbf{E}\left[B_{i,p}(U)\, B_{k,p}(U)\right] = -\sum_{i=1}^{N}\sum_{j=1}^{N} a_i y_j(t)\, \mathbf{E}\left[B_{i,p}(U)\, B_{j,p}(U)\, B_{k,p}(U)\right] \tag{6.16}$$

$k = 1, \ldots, N$. The system of equations (6.16) can be solved by any ODE solver. Here, the standard fourth order Runge-Kutta scheme is used. For the mean and variance the errors are defined by

$$\varepsilon_{\text{mean}}(t) = \left| \frac{\mathbf{E}\left[\tilde{y}^N(t)\right] - \mathbf{E}\left[y(t)\right]}{\mathbf{E}\left[y(t)\right]} \right| \tag{6.17}$$

and

$$\varepsilon_{\text{var}}(t) = \left| \frac{\text{Var}\left[\tilde{y}^N(t)\right] - \text{Var}\left[y(t)\right]}{\text{Var}\left[y(t)\right]} \right|, \tag{6.18}$$

where $\text{Var}\left[y(t)\right] = \mathbf{E}\left[y(t) - \mathbf{E}\left[y(t)\right]^2\right]$.
In the sequel, the random decay rate is expected to be uniformly distributed, i.e. $a(\omega) \sim \text{unif}([-1, 1])$. Thus, the exact stochastic mean solution is

$$\mathbf{E}\left[y(t)\right] = \frac{\sinh(t)}{t}. \tag{6.19}$$

Numerical results of Eq. (6.16) are shown in Fig. 6.1. Hermite, Legendre and B-spline

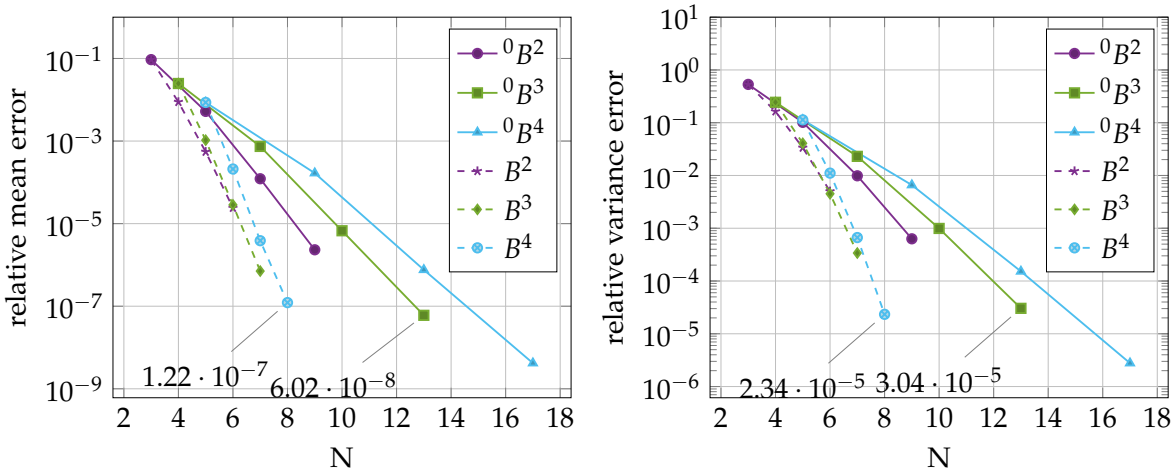

Figure 6.2: Relative mean and variance error of $\mathcal{C}^0$ and $\mathcal{C}^{p-1}$ B-spline chaos for $t = 5$.

representations are opposed against each other. Specifically, the relative mean and variance error of the multi-element generalized polynomial chaos from Wan and Karniadakis, 2005 are reproduced by using Bernstein polynomials, which are equivalent to $\mathcal{C}^0$ B-spline basis functions - see Fig. 3.6 for instance. Exponential p-type convergence for different stochastic meshes, i.e. number of elements in the spectral expansion, are achieved. The Legendre chaos is optimal for the uniform input. Therefore, it generally outperforms the Hermite chaos here, which error is fluctuating and decreases slowly. Furthermore, the Legendre multi-element approach coincides with the $\mathcal{C}^0$ B-spline chaos. Increasing the number of elements validates the results of Wan and Karniadakis (2005, Fig. 2). This means, through the natural structure of B-splines, that the performance of Legendre multi-element chaos is inherited by simply using $\mathcal{C}^0$ B-splines basis functions in the polynomial chaos expansion. Note in addition, it is much easier to implement the B-spline basis in an ordinary PC framework then it is the case with me-gPC.
Further, the capability of $\mathcal{C}^0$ with $\mathcal{C}^{p-1}$ B-spline chaos are compared. The convergence for the error of mean and variance of the solution with respect to the number of basis functions is illustrated in Fig. 6.2. The solid lines represent the same results as in Fig. 6.1, whereas the dashed lines show the errors of the $\mathcal{C}^3$ B-spline chaos. Exponential h-type convergence for both B-spline variants are on hand. Moreover, it can clearly be seen that for $\mathcal{C}^3$-continuity much less basis functions are needed to reach nearly the same accuracy. This crucial point is emphasized distinctly by the marked data sets. The marked data point of B^4 belongs to the basis functions shown in Fig. 3.5 with $N = 8$ and is competitive against the marked data point of $^0B^3$ with $N = 13$ for both error types. The number of basis functions N is directly related to the degrees of freedom of the numerical model. Thus, using smooth B-splines over element boundaries instead of Legendre polynomials in each element leads to a drastic reduction of the degrees of freedom and gain of efficiency. As mentioned above, this improvement is predicated on the smoothness over element boundaries. Note that, the exhibit advantages becomes

even more pronounced if more elements or higher degrees are treated.

6.3 Euler-Bernoulli beam with random stiffness

Next, consider the Euler-Bernoulli beam of length $L = 1$, clamped at $x = 0$, and subjected to a deterministic uniformly distributed load f shown in Fig. 6.3. The governing Eq. is given by

$$\mathcal{L}(x, \omega; u(x, \omega)) = f(x, \omega) \quad \text{in } D \times \Omega \tag{6.20}$$

$$:\Leftrightarrow EI(\omega)\, \frac{d^4}{dx^4} u(x) = f \quad \text{with} \quad u(0) = u'(0) = 0, \tag{6.21}$$

where the beam rigidity $W \equiv EI$ is assumed to be a random variable $W : \Omega \to \mathbb{R}$ with density function f_W, and is specified by the modulus of elasticity E and the area moment of inertia I. The exact solution of (6.21) reads

$$u(x, \omega) = f\, \frac{x^2(6L^2 - 4Lx + x^2)}{24\, EI(\omega)}. \tag{6.22}$$

In order to make Eq. (6.21) numerically feasible the spatial and stochastic space of the solution and the random input must be discretized. Using isogeometric subspace leads to

$$\begin{aligned} \tilde{u}(x, \omega) &= \sum_{l=1}^{n_d} u_l(\omega) N^d_{l,p_d}(u(x)) \\ &= \sum_{l=1}^{n_d} \sum_{i=1}^{n_s} u_{il} N^s_{i,p_s}(U(\omega)) N^d_{l,p_d}(u(x)), \end{aligned} \tag{6.23}$$

and

$$\widetilde{W}(\omega) = \sum_{k=1}^{n_w} w_k N^w_{k,p_w}(U(\omega)), \tag{6.24}$$

where $u(x)$ is a linear mapping from the spatial space $[0, L]$ and the parameter space $[0, 1]$, and $U : \Omega \to [0, 1]$ a uniformly distributed random variable, i.e. $U \sim \text{unif}([0, 1])$. Note, for the deterministic part classical Hermite basis functions can be used in the

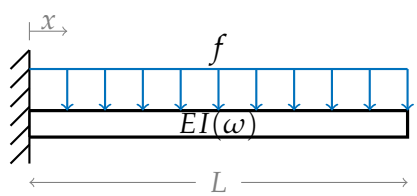

Figure 6.3: Cantilever Euler-Bernoulli beam with deterministic uniformly distributed load f and random beam rigidity $EI(\omega)$.

same way.
Applying the deterministic Galerkin procedure to Eq. (6.21) yields

$$\begin{aligned}
&\sum_{l=1}^{n_d} u_l(\omega) \int_L \frac{d^2}{dx^2} N^d_{l,p_d}(x)\ W(\omega)\ \frac{d^2}{dx^2} N^d_{m,p_d}(x)\ dx \\
&\quad = \int_L f\ N^d_{m,p_d}(x)\ dx \quad m = 1,\dots,n_d \\
&\Leftrightarrow: \quad K^d(\omega) u^d(\omega) = f^d.
\end{aligned} \tag{6.25}$$

Next, using equations (6.23) and (6.24), and applying the stochastic Galerkin procedure gives

$$\begin{aligned}
&\sum_{l=1}^{n_d} \sum_{i=1}^{n_s} \sum_{k=1}^{n_w} u_{il} w_k\, \mathbf{E}_U \left[N^s_{i,p_s}(U) N^s_{j,p_s}(U) N^w_{k,p_w}(U) \right] \\
&\qquad \int_L \frac{d^2}{dx^2} N^d_{l,p_d}(x)\ \frac{d^2}{dx^2} N^d_{m,p_d}(x)\ dx \\
&\qquad = \mathbf{E}_U \left[N^s_{j,p_s}(U) \right] \int_L f N^d_{m,p_d}(x)\ dx
\end{aligned} \tag{6.26}$$

for $j = 1,\dots,n_s$ and $m = 1,\dots,n_d$ which can be reformulated in a matrix scheme of dimension $n_d n_s \times n_d n_s$:

$$Ku = f \tag{6.27}$$

with

$$\begin{aligned}
K_{ijlm} &:= \underbrace{\sum_{k=1}^{n_w} w_k\, \mathbf{E}_U \left[N^s_{i,p_s}(U) N^s_{j,p_s}(U) N^w_{k,p_w}(U) \right]}_{=:K^s_{ijk}} \\
&\qquad \underbrace{\int_L \frac{d^2}{dx^2} N^d_{l,p_d}(x)\ \frac{d^2}{dx^2} N^d_{m,p_d}(x)\ dx}_{=:K^d_{lm}} \\
&= K^s_{ijk} K^d_{lm} \qquad \begin{matrix} i,j = 1,\dots,n_s \\ l,m = 1,\dots,n_d \end{matrix}
\end{aligned} \tag{6.28}$$

and

$$\begin{aligned}
f_{jm} &:= \underbrace{\mathbf{E}_U \left[N^s_{j,p_s}(U) \right]}_{f^s_j} \underbrace{\int_L f N^d_{m,p_d}(x)\ dx}_{f^d_m} \\
&= f^s_j f^d_m \qquad \begin{matrix} j = 1,\dots,n_s \\ m = 1,\dots,n_d \end{matrix}.
\end{aligned} \tag{6.29}$$

Due to the boundary conditions of Eq. (6.21), the first two coefficients of the vector $u_l(\omega)$, i.e. $u_1(\omega)$ and $u_2(\omega)$, are equal to zero, because $u_1(\omega)$ represents the deflection

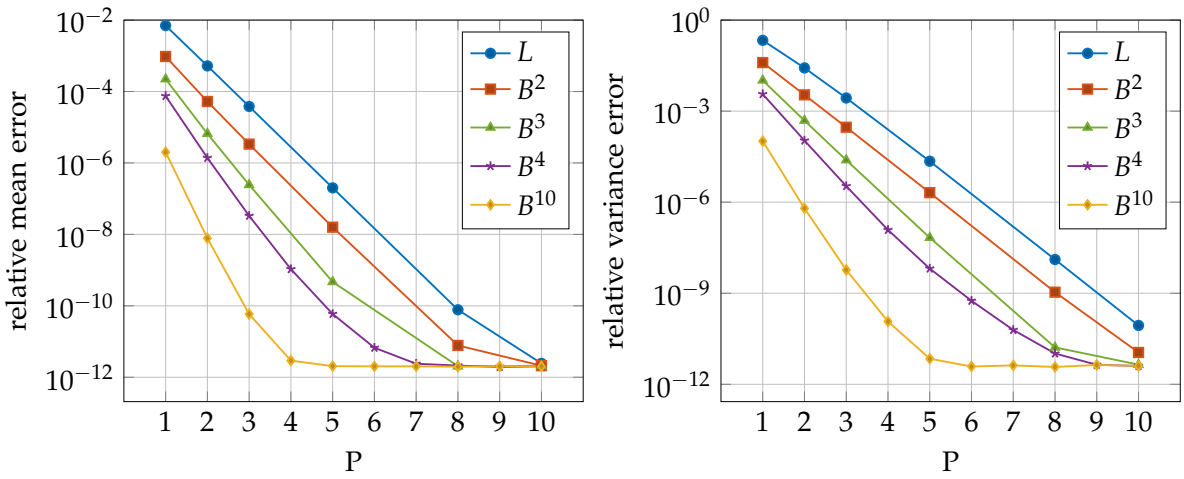

Figure 6.4: Relative mean and variance error at the beam tip solved by Legendre and B-spline chaos with uniformly distributed beam rigidity.

and $u_2(\omega) - u_1(\omega)$ the slope at the clamped end. Thus, for Eq. (6.27) it holds

$$u_{i1} = u_{i2} = 0 \tag{6.30}$$

for $i = 1, \ldots, n_s$,which leads to a reduced system of Eq. (6.27) with dimension $n_d(n_s - 2) \times n_d(n_s - 2)$. Solving the reduced system, $n_d(n_s - 2)$ coefficients of $\tilde{u}(x, \omega)$ are determined, where as the control variables u_{in_d} represents the stochastic beam tip deflection

$$\tilde{u}_L(\omega) = \sum_{i=1}^{n_s} u_{in_d} N^s_{i,p_s}(U(\omega)). \tag{6.31}$$

Further, the relative mean error at the free end can then be computed by

$$\varepsilon_{\text{mean}} = \left| \frac{\mathbf{E}\left[\tilde{u}_L\right] - \mathbf{E}\left[u(L,\omega)\right]}{\mathbf{E}\left[u(L,\omega)\right]} \right| \tag{6.32}$$

with

$$\begin{aligned} \mathbf{E}\left[\tilde{u}_L\right] &= \sum_{i=1}^{n_s} u_{in_d}\, \mathbf{E}\left[N^s_{i,p_s}(U(\omega))\right] \\ &= \sum_{i=1}^{n_s} u_{in_d} \int_{[0,1]} N^s_{i,p_s}(u)\, dF_U(u) \end{aligned} \tag{6.33}$$

and, considering (6.22) with $x = L$,

$$\mathbf{E}\left[u(L,\omega)\right] = \mathbf{E}\left[\frac{f\, L^4}{8\, W(\omega)}\right] = \frac{f\, L^4}{8} \int_{S_W} \frac{1}{w}\, dF_W(w). \tag{6.34}$$

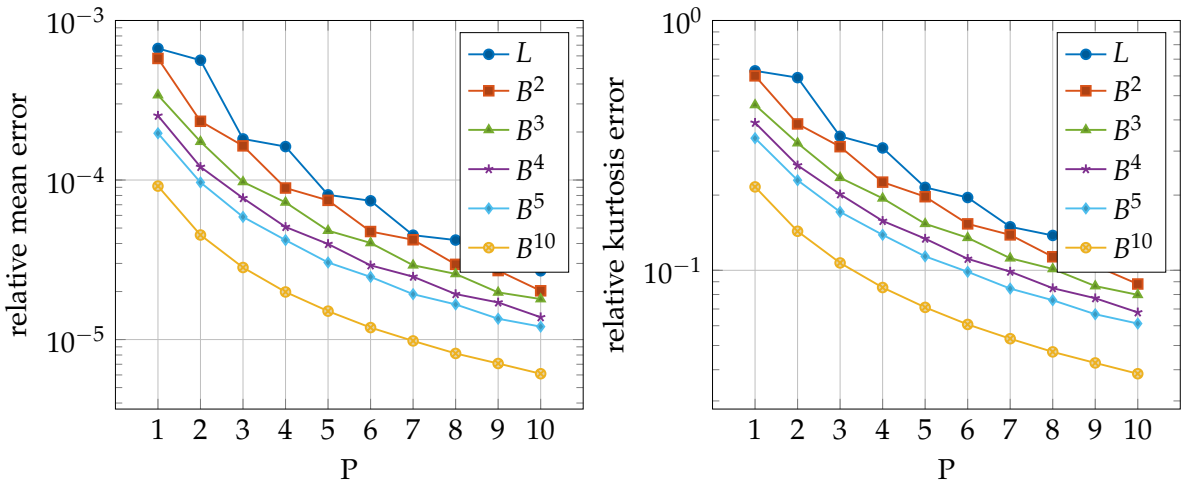

Figure 6.5: Relative mean and kurtosis error at the beam tip solved by Legendre and B-spline chaos with normally distributed beam rigidity.

Analogously, the relative variance and kurtosis error are evaluated in common fashion. For the numerical implementation of the preceding analysis fourth order B-splines with four elements defined by the knot vector

$$\Xi^d = [\ 0\ 0\ 0\ 0\ 0\ 0.25\ 0.5\ 0.75\ 1\ 1\ 1\ 1\ 1\ ]$$

were used, i.e. $p_d = 4$, $nel_d = 4$ and $k_d = p_d - 1$, resulting in eight ($n_d = m_d - p_d - 1 = 8$) degrees of freedom; m_d denotes the number of knots in Ξ^d - compare Fig. 3.5.

Uniformly distributed beam rigidity

Let $W \sim \text{unif}([0.5, 1.5])$ and $f \equiv 1$. Since the B-spline chaos is optimal for a uniform distribution, the approximation (6.24) is exact for $n_w > 1$, e.g.

$$W(\omega) \equiv \widetilde{W}(\omega) = \sum_{k=1}^{2} w_k N_{k,1}^w(U(\omega)) \tag{6.35}$$

with $w_1 = 0.5$, $w_2 = 1.5$ and knot vector $\Xi^w = [\ 0\ 0\ 1\ 1\ ]$. Further, the exact mean solution is given by

$$\begin{aligned} \mathbf{E}\left[u(L,\omega)\right] &= \frac{1}{8}\int_{0.5}^{1} .5\frac{1}{w}\, dw \\ &= \frac{1}{8}\big(\log(1.5) - \log(0.5)\big) \\ &\approx 0.137326536083514. \end{aligned} \tag{6.36}$$

Exponential *h-p* convergence for the first two central moments of the beam tip deflection are shown in Fig. 6.4. The results are found in good agreement with the previous example from section 6.2. The relative mean and variance error are plotted for a different number of stochastic elements as well as the classical Legendre chaos, which performs the worst. The mean error of the four element B-spline chaos (B^4) reach the deterministic approximation error of about 10^{-13} for $p_s \leq 7$. When ten stochastic elements are considered even only fourth order B-splines are required. In general, the relative mean errors converge faster than the errors of higher moments.

Normal distributed beam rigidity

In this section the distribution of the random input W is assumed to be normal, i.e. $W \sim \mathcal{N}(1, 0.1)$, and $f \equiv 1$. As can be seen in section 5.3.3, the B-spline chaos is not optimal for a normal distribution. Thus, the solution quality of $\tilde{u}(x, \omega)$ also depends on the approximation $\widetilde{W}(\omega)$. Therefore, $p_w = 10$, $nel_w = 10$ and $k_w = 0$ are chosen in order to reach high accuracy. Further, the exact mean solution of (6.21) is

$$\begin{aligned} \mathbf{E}\left[u(L,\omega)\right] &= \frac{1}{8}\int_{-\infty}^{\infty} \frac{1}{\sqrt{2\pi\ 0.1^2}\ w} \exp\left(-\tfrac{(w-1)^2}{0.1^2}\right)\, dw \\ &\approx 0.126289521160065, \end{aligned} \tag{6.37}$$

which was solved numerically.
Fig. 6.5 shows the *h-p* convergence in the stochastic space of the first and fourth central moment at the beam tip. The beam rigidity $W(\omega)$ is represented by the non-optimal B-spline chaos which is an indication for the lower convergence rate in comparison with the optimal representation in section 6.3. However, the B-spline chaos still dominates the Legendre chaos. Further, it is remarkable that even for higher orders the high moments do not deteriorates which is a general problem for the Hermite chaos Field and M. Grigoriu, 2004.

Monte Carlo simulation

In order to assess the significance of the numerical results obtained from the B-spline chaos the beam problem is treated by a Monte Carlo simulation. Realizations of the beam rigidity $W(\omega)$ are computed and for each realization the associated deterministic problem (6.25) is solved. The resulting density function of the beam tip deflection for $W \sim \mathcal{N}(1, 0.1)$ and $W \sim \text{unif}([0.5, 1.5])$ are plotted in Fig. 6.6. Comparisons with different B-spline types show a satisfactory level of accuracy for $p_s > 1$ in both cases. Nevertheless, for the uniform input better results are achieved which coincides with the error plots from section 5.3 and 6.2. The probability density functions in Fig. 6.6

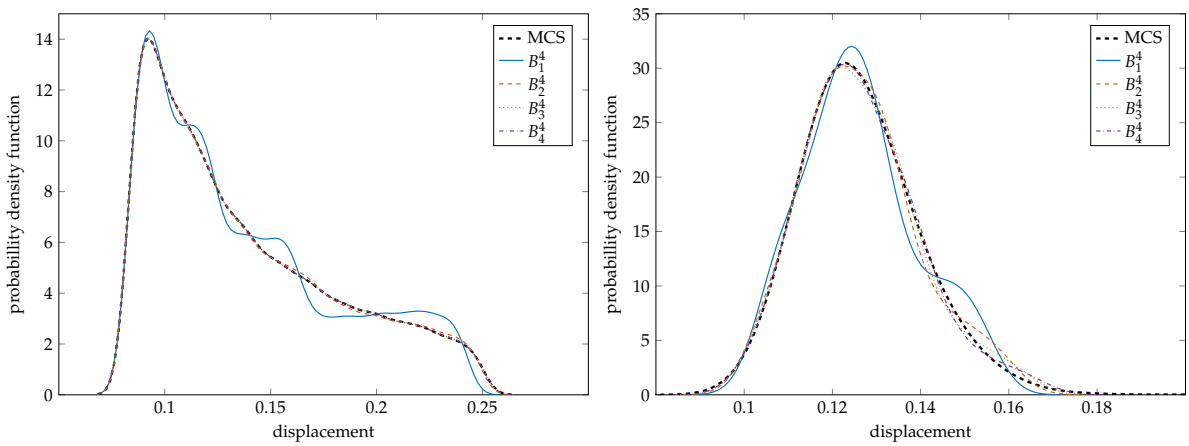

Figure 6.6: Probability density function approximations of the cantilever beam tip deflection with uniformly (left) and normally (right) distributed beam rigidity.

are estimated by a normal kernel smoothing function with bandwidth 0.005 and 10000 samples.

6.4 Infinite Plate with circular hole

The last numerical example is a two-dimensional linear elastostatic problem, namely an infinite plate with circular hole under constant in-plane tension. The governing

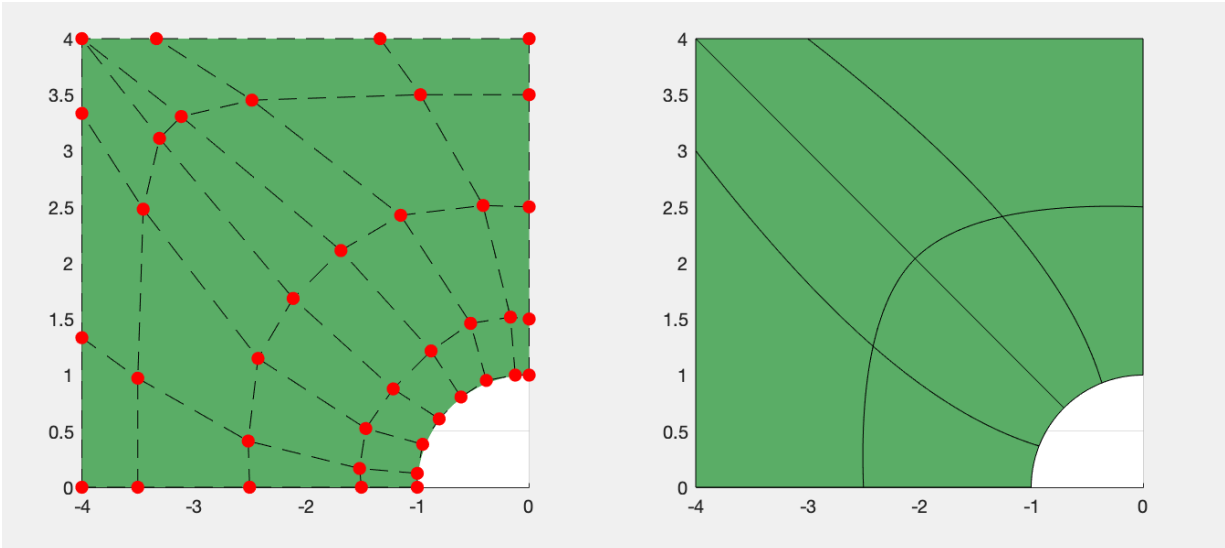

Figure 6.7: Control net and mesh of the finite quarter plate with one h-refinement in each direction.

equations of a linear elastic boundary value problem are given by:

$$\mathcal{L}(x,\omega;u(x,\omega)) = f(x,\omega) \quad \text{in } D\times\Omega \tag{6.38}$$
$$:\Leftrightarrow \quad \operatorname{div}(\sigma(u)) + f = 0 \quad \text{in } D\times\Omega \tag{6.39}$$

and boundary conditions

$$u = g \quad \text{on } \Gamma_D \tag{6.40}$$
$$\sigma\cdot n = h \quad \text{on } \Gamma_N \tag{6.41}$$

with infinitesimal strain tensor

$$\varepsilon = \frac{1}{2}\Big[\nabla u + (\nabla u)^T\Big], \tag{6.42}$$

and constitutive law (generalized Hooke's law)

$$\sigma = \mathbb{C} : \varepsilon\,. \tag{6.43}$$

Further, it is assumed that the material is isotropic, i.e. the elastic coefficients have the form

$$\mathbb{C}_{ijkl} = \lambda\delta_{ij}\delta_{kl} + \mu(\delta_{ik}\delta_{jl} + \delta_{il}\delta_{jk})\,. \tag{6.44}$$

The Lamé parameters λ and μ can be expressed in terms of the Young's modulus E and Poisson's ratio ν as

$$\lambda = \frac{\nu E}{(1+\nu)(1-2\nu)} \tag{6.45}$$
$$\nu = \frac{E}{2(1+\nu)}\,. \tag{6.46}$$

The solution of the stated elastostatic problem is a random field $u : \bar{D}\times\Omega \to \mathbb{R}^{d_u}$.

In this two-dimensional example, a NURBS-based isogeometric analysis with uncertain Young's modulus $E(\omega)$ of an infinite plate with a circular hole under constant in-plane tension at infinity is investigated. For a detailed deterministic description see for example Hughes et al. (2005, p.119). The analytical deterministic solution is given by (Gould (1999, p.120)):

$$\sigma_{rr}(r,\theta) = \frac{T_x}{2}\left(1-\frac{R^2}{r^2}\right) + \frac{T_x}{2}\left(1-4\frac{R^2}{r^2}+3\frac{R^4}{r^4}\right)\cos(2\theta) \tag{6.47}$$
$$\sigma_{\theta\theta}(r,\theta) = \frac{T_x}{2}\left(1+\frac{R^2}{r^2}\right) - \frac{T_x}{2}\left(1+3\frac{R^4}{r^4}\right)\cos(2\theta) \tag{6.48}$$
$$\sigma_{r\theta}(r,\theta) = -\frac{T_x}{2}\left(1+2\frac{R^2}{r^2}-3\frac{R^4}{r^4}\right)\sin(2\theta)\,, \tag{6.49}$$

where T_x is the applied stress as a Neumann boundary condition, and R is the radius

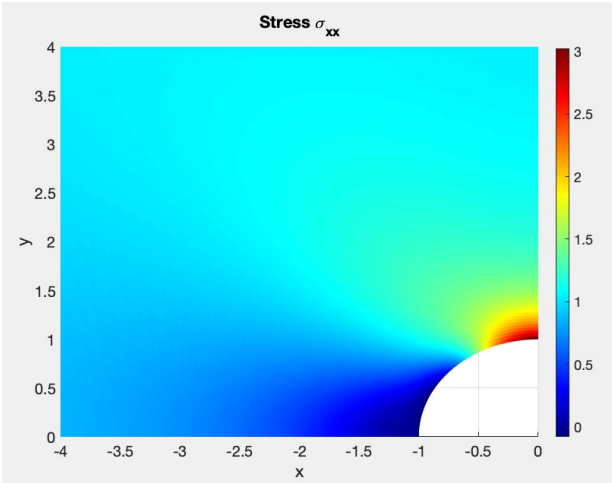

Figure 6.8: Contour plot of σ_{xx} with maximal stress at $r = R$, $\theta = \frac{3}{2}\pi$

of the hole. The geometry of the finite quarter plate, which is solved for investigating the problem, is shown in Fig. 6.7. The geometry is build by B-splines and consequently the approximated spacial space is spanned by the same basis functions. Following the isogeometric approach, the stochastic subspace is also constructed via splines. The infinite plate problem is solved in the same way as the beam example, i.e. the input is expanded in a b-spline chaos, as well as the solution. Applying a Galerkin type procedure for both, the spacial and stochastic space, results in an matrix scheme of the form:

$$Ku = f \tag{6.50}$$

with dimension $n_d \cdot n_s$, where n_d and n_s is the dimension of the deterministic and stochastic space, respectively. For the numerical implementation of the preceding stochastic analysis third order B-spline basis functions with varying elements and continuity are used. The stress concentration of $\sigma_{xx} = 3\ T_x$ is located at the edge of the hole and obtained when the mesh is properly refined - see Fig. 6.8. The displacement at this point is zero, whereas the maximal displacement in x-direction is at the lower corner on the opposite edge - see Fig. 6.9.

One-dimensional Random Input

First, the uncertainty is modeled as a one-dimensional uniform random input over the material parameter, i.e. the Young's modulus E is uniformly distributed around the mean value $\mu_E = 10^5$. The results in Fig. 6.10 confirm h-p convergence for the first two central moments of the maximal displacement in x-direction and are found in good agreement with the previous examples. The relative mean and variance error are plotted for multi-element Legendre chaos and B-spline chaos with different continuities and increasing number of stochastic elements. Here again, spline-chaos outperforms

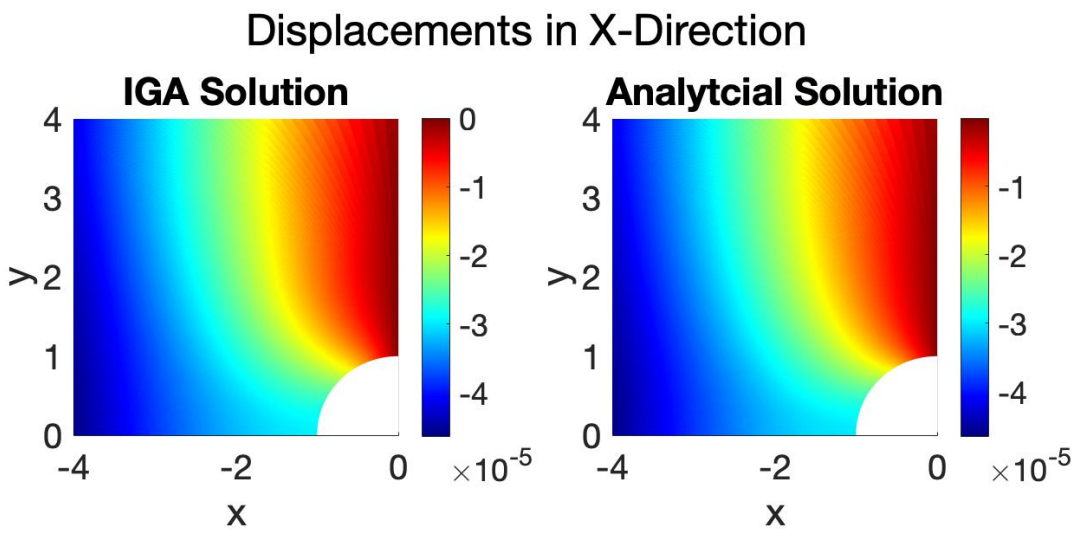

Figure 6.9: Analytical and numerical solution of u in x-direction.

multi-element Legendre chaos. In general, the relative mean errors converge faster than the errors of higher moments. Fig. 6.11 illustrates the probability function of the maximal displacement in x-direction. The reference solution was generated using MCS. Due to the optimal correspondence between uniform density and Legendre and Bernstein polynomials, satisfactory coincidence is obtained for both chaos expansions. The probability density functions in Fig. 6.11 is estimated by a normal kernel smoothing function with bandwidth 0.005 and 10000 samples.

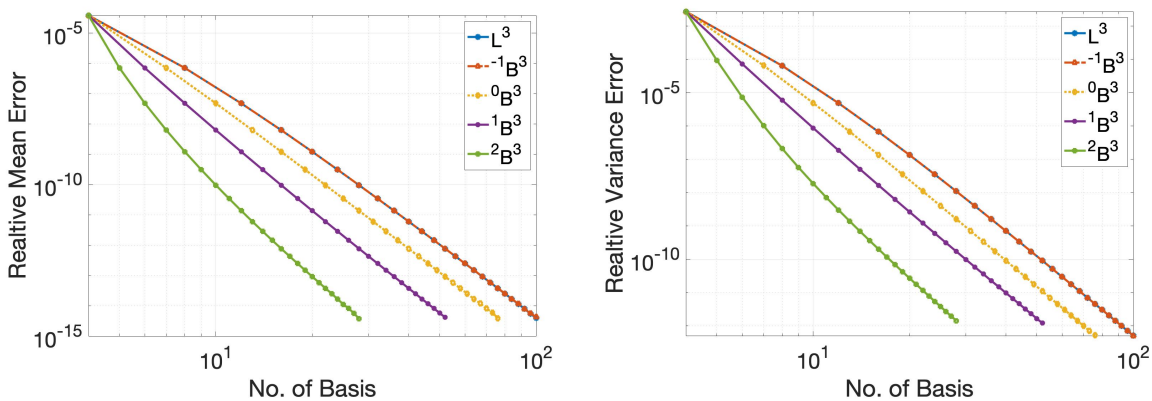

Figure 6.10: Relative mean and variance order for the infinite plate problem.

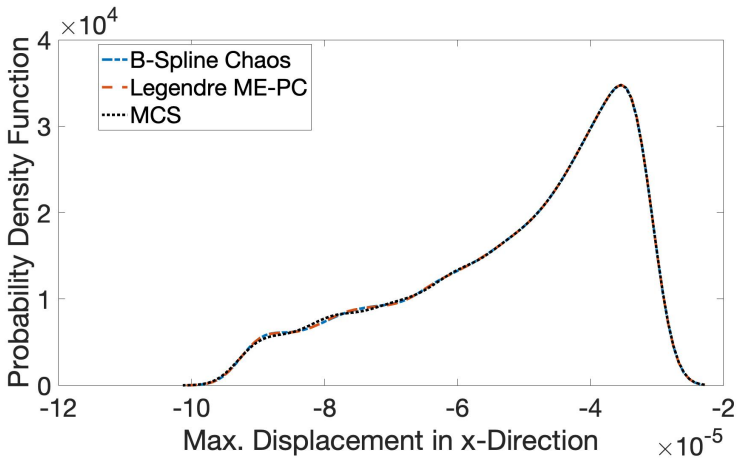

Figure 6.11: PDF approximation with 1D random input and MCS.

Random Field Input

In the last step, the Young's modulus is represented by a harmonic uniform random field, i.e.:

$$E(x,y) = \mu_E + \sigma_E(\sin(a_1 x)\sin(a_2 y)U_1 + \cos(b_1 x)\cos(b_2 y)U_2) \tag{6.51}$$

with $\mu_E = 10^5$, $\sigma_E = 3 \cdot 10^3$, $U_1, U_2 \sim$ unif, and algebraic constants $a_1 = a_2 = b_1 = b_2 = 1$. The analysis is performed in the same way as before, except that multi-dimensional chaos expansions are utilized.
To assess the validity of the numerical results obtained with the B-spline chaos, the

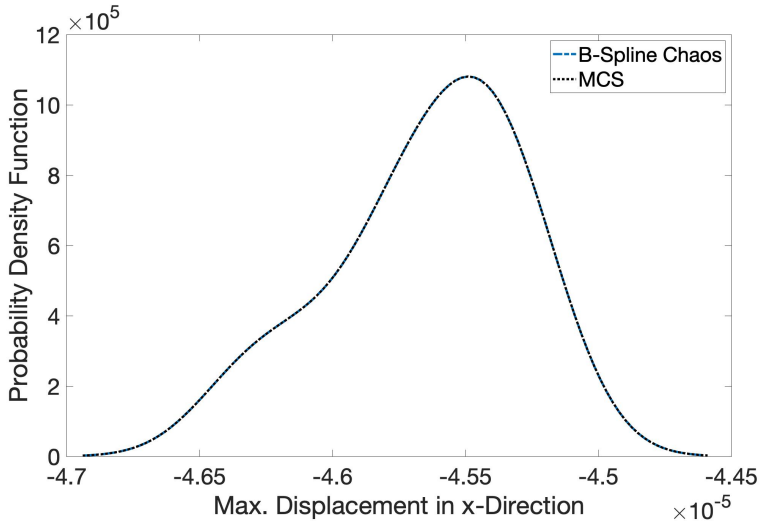

Figure 6.12: PDF approximation with random field input and MCS.

beam problem is treated by a MCS. Realizations of the Young's modulus $E(\omega)$ are computed and for each realization the associated deterministic elastostatic problem is solved. The resulting density function of the maximum displacement in x-direction are plotted in Fig. 6.12. B-spline chaos show a satisfactory level of accuracy. The probability density functions in Fig. 6.12 is estimated by a normal kernel smoothing function with bandwidth 0.005 and 10000 samples.

7 Stochastic Galerkin Isogeometric Analysis

This chapter defines and analyzes the SGIGA for linear elliptic PDEs with stochastic coefficients and homogeneous Dirichlet boundary condition. The aim is the representation of the complete solution by splines and the application of isogeometric solvers. This can be realized by finite dimensional approximations of the stochastic coefficients leading to a deterministic parametric elliptic problem Ivo Babuška, Raúl Tempone, et al., 2004. Subsequently, a Galerkin type isogeometric technique describes the corresponding deterministic solution. The chapter closes with an a priori error estimation for the computation of the expected value of the solution.
The method of SGIGA is derived from the stochastic Galerkin finite element method (SGFEM) first proposed by Babuŝka et al. (2005). They show an alternative approach to the SSFEM of R.G. Ghanem and P. Spanos (2003). Instead of using orthogonal polynomials to represent the stochastic components, Lagrangian functions are used, which also describe the deterministic components and the geometry. In the same paper also an a priori error estimation is stated, which includes estimates for Lagrangian functions and thus polynomials. This notion is adopted here to the isogeometric approach, where splines are considered. The recently published estimations for splines, which also take into account their flexibility in terms of continuity and number of elements, derived by Sande et al. (2019), contribute significantly to the fact that such a sharp a priori error estimations can be stated here. This, in turn, can be very beneficial for practical applications. For example, it is previously evident, what influence does the h-refinement have on the reduction of the error in comparison to the p-refinement.

7.1 Mathematical model

The starting point is the end of section 4.2, i.e., consider the problem:

$$\begin{aligned} \mathcal{L}(x, Y(\omega); u(x, Y(\omega))) &= f(x, Y(\omega)) \quad \text{on } D \times \mathbb{R}^{d_s} \\ u(x, Y(\omega)) &= 0 \quad \text{on } \partial D \times \mathbb{R}^{d_s}. \end{aligned} \tag{7.1}$$

with $u : \bar{D} \times \mathbb{R}^{d_s} \to \mathbb{R}^{d_u}$ by the use of the Doob-Dynkin lemma, e.g. Rao and Swift, 2006b, p.7, and $Y_1, \ldots, Y_{d_s}$ are independent and identically distributed. Remember,

assumption 1 and 2 hold. Thus, for each realization of $Y(\omega)$ Eq. (7.1) is well-posed in its deterministic sense. Next, the random vector Y is transformed into a uniformly distributed random vector by the isoprobabilistic Rosenblatt transformation Rosenblatt, 1952. Denote by F_{Y_i} the marginal distribution function of Y_i, $i = 1, \dots, d_s$, and by C_Y the copula of Y. Then,

$$Z := T^R(Y) \tag{7.2}$$

with

$$\begin{aligned} T^R &: \mathbb{R}^{d_s} \to [0,1]^{d_s} \\ Y \mapsto Z &= \begin{pmatrix} F_{Y_1}(Y_1) \\ F_{Y_2|Y_1}(Y_2|Y_1) \\ \vdots \\ F_{Y_{d_s}|Y_1,\dots,Y_{d_s-1}}(Y_{d_s}|Y_1,\dots,Y_{d_s-1}) \end{pmatrix} \end{aligned} \tag{7.3}$$

is a uniformly distributed random vector over $[0,1]^{d_s}$ with independent copula, where $Y_i|Y_1,\dots,Y_{i-1}$ is the cumulative distribution function of the conditional random variable $Y_i|Y_1,\dots,Y_{i-1}$. Because of assumption 1 Eq. (7.2) simplifies to

$$Y(\omega) = (F_{Y_1}^{-1}(Z(\omega)),\dots,F_{Y_{d_s}}^{-1}(Z(\omega))) := F_Y^{-1}(Z(\omega)). \tag{7.4}$$

Thus, Eq. (7.1) can further be rewritten as

$$\begin{aligned} &\mathcal{L}(x, F_Y^{-1}(Z(\omega); u(x, F_Y^{-1}(Z(\omega))) = f(x, F_Y^{-1}(Z(\omega)) \quad \text{on } D \times [0,1]^{d_s} \\ &u(x, F_Y^{-1}(Z(\omega)) = 0 \quad \text{on } \partial D \times [0,1]^{d_s}. \end{aligned} \tag{7.5}$$

with $u : \bar{D} \times \mathbb{R}^{d_s} \to \mathbb{R}^{d_u}$ by the use of the Doob-Dynkin lemma, e.g. Rao and Swift, 2006b, p.7, and $Z(\omega) = (Z_1, \dots, Z_{d_s})$ are independent and identically distributed with $Z_i \sim \text{unif}([0,1])$.
For the next part, remember from section 2.4, a function $\phi : \bar{D} \times \Omega \to \mathbb{R}^{d_\phi}$ is called a random function (process or field), if it is jointly measurable on $\mathcal{B}(D) \otimes \mathcal{F}$ and it holds

$$\mathbf{E}\left[\int_D \phi(x,\omega)dx\right] < \infty. \tag{7.6}$$

7.2 Elliptic model problem

In the following, the stochastic diffusion equation

$$\begin{aligned} \nabla_x \cdot (k(x,\omega)\nabla_x(u(x,\omega))) &= f(x,\omega) \quad \text{in } D \times \Omega \\ u(x,\omega) &= 0 \quad \text{on } \partial D \times \Omega \end{aligned} \tag{7.7}$$

is considered, where the diffusivity field k and source term f are assumed to be random functions, which can be parameterized by a truncated Karhunen-Loève expansion (or any chaos expansion) (assumption 1), i.e.

$$k(x,\omega) \approx k(x,Y) = \mu_k(x) + \sum_{i=1}^{d_s} k_i(x) Y_i(\omega), \tag{7.8}$$

$$f(x,\omega) \approx f(x,Y) = \mu_f(x) + \sum_{i=1}^{d_s} f_i(x) Y_i(\omega), \tag{7.9}$$

where $k_i(x)$ and $f_i(x)$ are determined by the eigenvalues and eigenfunctions of their covariance function, respectively, c.f. Ivo Babuška, Raúl Tempone, et al., 2004, sectionn 2.4. Furthermore, define

$$Y = (Y_1, \dots, Y_{d_s}) \equiv F_Y^{-1}(Z). \tag{7.10}$$

According to Eq. (7.5), Eq. (7.7) can be expressed by Eq. (7.2) and Eq. (7.10) as

$$\begin{aligned} \nabla_x \cdot (k(x, F_Y^{-1}(Z)) \nabla_x (u(x, F_Y^{-1}(Z)))) &= f(x, F_Y^{-1}(Z)) \quad \text{in } D \times I_Z \\ u(x, F_Y^{-1}(Z)) &= 0 \quad \text{on } \partial D \times I_Z \end{aligned} \tag{7.11}$$

with $I_Z = [0,1]^{d_s}$ the support of Z. Define the tensor product Hilbert Space $H := H_0^1(D) \otimes L_P^2(\Omega)$ Ivo Babuška, Raúl Tempone, et al., 2004. Then, Eq. (7.7) is equivalent to: Find $u \in H$ such that:

$$\mathbf{E}\left[\int_D k(x,\omega) \nabla u(x,\omega) \cdot \nabla v(x,\omega) dx\right] = \mathbf{E}\left[\int_D f v dx\right] \quad \forall v \in H\,. \tag{7.12}$$

Eq. (7.12) is referred to as the stochastic variational formulation of Eq. (7.7) and gives the basis for the stochastic Galerkin isogeometric analysis. Define the spaces Ivo Babuška and Chatzipantelidis, 2002:

$$V(D; I_Z) := \{v(x, F_Y^{-1}(Z)) \mid \|v\|_V < \infty \wedge v(x, F_Y^{-1}(Z)) = 0 \text{ on } \partial D\} \tag{7.13}$$

and

$$\|v\|_V := \int_{I_Z} \int_D k(x, F_Y^{-1}(z)) |\nabla v(x, F_Y^{-1}(z))|^2 dx f_Z(z) dz. \tag{7.14}$$

Then, with the previously required assumptions, Eq. (7.12) is equivalent to - c.f. Ivo Babuška and Chatzipantelidis, 2002; Ivo Babuška, Raúl Tempone, et al., 2004; Deb et al., 2001: Find $u \in V$ such that

$$\begin{aligned} &\int_{I_Z} \int_D k(x, F_Y^{-1}(z)) \nabla u(x, F_Y^{-1}(z)) \cdot \nabla v(x, F_Y^{-1}(z)) dx f_Z(z) dz \\ &\quad = \int_{I_Z} \int_D f(x, F_Y^{-1}(z)) v(x, F_Y^{-1}(z)) dx f_Z(z) dz \quad \forall v \in V \end{aligned} \tag{7.15}$$

Now, Eq. (7.15) is a deterministic variational formulation with d_s-dimensional parameter and is the deterministic equivalent of the stochastic variational formulation (7.12) - c.f. Ivo Babuška and Chatzipantelidis, 2002; Ivo Babuška, Raúl Tempone, et al., 2004; Deb et al., 2001 and is the. The finite noise assumption 1, is responsible for turning the stochastic equation in a deterministic one Ivo Babuška, Raúl Tempone, et al., 2004. For the more interested reader, existence and uniqueness is proven in e.g. Ivo Babuška, Raúl Tempone, et al. (2004, sectionn 2.2). However, here, the focus lies on the rigorous formulation of SGIGA and the a priori error estimation. In order to make the difference to SGFEM clear, the transformation $F_Y^{-1}(z)$ was written down so far continuously. For the sake of clarity, the variable z is written instead from now on, if nothing else is mentioned.

7.3 Isogeometric Approximation

Eq. (7.15) is suitable for a Galerkin based isogeometric analysis, i.e. define isogeometric approximation spaces over $D \times [0,1]^{d_s}$ Ivo Babuška, Raúl Tempone, et al., 2004. Intensive use of the already introduced spline spaces and estimations from section 3.2, for both the deterministic and stochastic cases, are required in the sequel.

7.3.1 Spatial Space

Consider a family of NURBS spaces on the spatial domain $\{\mathcal{V}_{h_d,0}\}_{h_d}$ with $\mathcal{V}_{h_d,0} \subset H_0^1(D)$ with conforming and shape regular mesh $\mathcal{K}_{h_d} = F(\mathcal{Q}_{h_d})$ such that $\bigcup_{K\in\mathcal{K}_{h_d}} K = D$ with deterministic mesh parameter $h_d = \max\{h_K\}$. sectionn 3.2, in particular Lemma 3.2.2, delivers the following approximation estimation for NURBS spaces $\mathcal{V}_{h_d,0}$ with homogeneous Dirichlet boundary conditions, i.e. for all $v \in H^2(D) \cap H_0^1(D)$ it holds

$$\min_{\chi\in\mathcal{V}_{h_d,0}} |v-\chi|_{\mathcal{H}^1_{h_d,0}(D)} \leq C_d(\mathbf{W},F)\, h_d \sum_{K\in\mathcal{K}_{h_d}} \|v\|_{H^2(\tilde{K})} \ . \tag{7.16}$$

7.3.2 Spectral Space

Consider the spline spaces $\mathcal{S}_{h_s}^{p_s}$ with $\mathcal{S}_{h_s}^{p_s} \subset L^2(I_Z)$, stochastic degree $p_s = \{p_1,\ldots,p_{d_s}\}$, and stochastic mesh parameter $h_s = \max_i\{h_{s_i}\}$ with $i = 1,\ldots,d_s$ and h_{s_i} is the maximal distance between inner knots in the i-th direction. Again, section 3.2, in particular

Eq. (3.45) and theorem 3.2.4, delivers the following approximation estimation for spline spaces in d_s dimensions, i.e. for all $v \in H^{p_s+1}(I_Z)$ it holds

$$\min_{\psi \in \mathcal{S}_{h_s}^{p_s}} \|v - \psi\|_{L^2(I_Z)} \leq \sum_{i=1}^{d_s} \left(\frac{2eh}{e\pi + 4h(p_{s_i}+1)} \right)^{p_{s_i}+1} \|\partial_{z_i}^{p_{s_i}+1} v\|_{L^2(I_Z)}. \tag{7.17}$$

If Eq. (7.17) is compared with Eq. (3.2) in Ivo Babuška, Raúl Tempone, et al., 2004, where the space I_Z is approximated by polynomials, the factor $\frac{1}{p_{s_i}+1}$ is missing. This is corrected in the next section, when the tensor product space is defined. Note, $\|\partial_{z_i}^{p_{s_i}+1} v\|_{L^2(I_Z)}$ denotes the $p_{s_i}+1$ partial derivative in the i-th stochastic dimension z_i of the function v, e.g. Ivo Babuška, Raúl Tempone, et al., 2004; Sande et al., 2020.

7.3.3 Tensor Product Space

Now, consider approximations of the tensor product space $D \times I_Z$. Hence, define the space composed of tensor product splines, for both the deterministic and stochastic part:

$$\begin{aligned} \mathcal{V}_{h_d,0} \otimes \mathcal{S}_{h_s}^{p_s} := \{ \phi(x,z) \in L^2(D \times I_Z) \\ \mid \phi \in \operatorname{span}\{ \chi(x)\psi(z) \mid \chi \in \mathcal{V}_{h_d,0}, \psi \in \mathcal{S}_{h_s}^{p_s} \} \} \end{aligned} \tag{7.18}$$

The following proposition provides a first approximation quantification for the tensor product isogeometric space in Eq. (7.18).

Proposition 7.3.1 (cf. Prop. 3.1 in Ivo Babuška, Raúl Tempone, et al., 2004)**.** *For all $v \in C^{p_s+1}(H^2(D) \cap H_0^1(D); I_Z)$, there exists a constant $C > 0$ independent of h_d, h_s, d_s and v, such that*

$$\begin{aligned} \min_{\phi \in \mathcal{V}_{h_d,0} \otimes \mathcal{S}_{h_s}^{p_s}} \|v - \phi\|_{L^2(H_0^1(D);I_Z)} \leq C(F, \mathbf{W}) \Bigg(h_d \sum_{K \in \mathcal{K}_{h_d}} \|v\|_{L^2(H^2(\tilde{K});I_Z)} + \\ \sum_{i=1}^{d_s} \left(\frac{2eh}{\frac{e\pi}{p_{s_i}+1} + 4h} \right)^{p_{s_i}+1} \frac{\|\partial_{z_i}^{p_{s_i}+1} v\|_{L^2(H_0^1(D);I_Z)}}{(p_{s_i}+1)!} \Bigg), \end{aligned} \tag{7.19}$$

where F and , $\mathbf{W}$ are defined in Lemma 3.2.2 and coming from the deterministic part.

Proof. Cf. Prop. 3.1 in Ivo Babuška, Raúl Tempone, et al., 2004. For the projectors

$\Pi_{\mathcal{V}h_d,0} : H_0^1(D) \to \mathcal{V}_{h_d,0}$ and $\Pi_{\mathcal{S}_{h_s}^{p_s}} : L^2(I_Z) \to \mathcal{S}_{h_s}^{p_s}$ with

$$(\nabla(\Pi_{\mathcal{V}h_d,0}v - v), \nabla\chi)_{L^2(D)} = 0 \quad \forall\psi \in \mathcal{V}_{h_d,0} \quad \forall v \in H_0^1(D) \tag{7.20}$$

$$(\Pi_{\mathcal{S}_{h_s}^{p_s}}v - v, \psi)_{L^2(I_Z)} = 0 \quad \forall\psi \in \mathcal{S}_{h_s}^{p_s} \quad \forall v \in L^2(I_Z). \tag{7.21}$$

Eq. (7.16) and (7.17) imply

$$\left\|\Pi_{\mathcal{V}_{h_d,0}}v - v\right\|_{H_0^1(D)} \leq C_d(\mathbf{W}, F)\, h_d \sum_{K\in\mathcal{K}_{h_d}} \|v\|_{H^2(\tilde{K})} \tag{7.22}$$

for all $v \in H^2(D) \cap H_0^1(D)$ and

$$\left\|\Pi_{\mathcal{S}_{h_s}^{p_s}}v - v\right\|_{L^2(I_Z)} \leq \sum_{i=1}^{d_s} \left(\frac{2eh}{\frac{e\pi}{p_{s_i}+1} + 4h}\right)^{p_{s_i}+1} \frac{\|\partial_{z_i}^{p_{s_i}+1}v\|_{L^2(I_Z)}}{(p_{s_i}+1)!} \tag{7.23}$$

for all $v \in H^{p_s+1}(I_Z)$. In Eq. 7.23 it was exploited that

$$(p_{s_i}+1)! \leq (p_{s_i}+1)^{p_{s_i}+1} \quad \forall p_{s_i} \geq 0\,. \tag{7.24}$$

Then, with $\Pi_{\mathcal{V}_{h_d,0}}(\Pi_{\mathcal{S}_{h_s}^{p_s}}v) \in \mathcal{V}_{h_d,0} \otimes \mathcal{S}_{h_s}^{p_s}$, using Eq. (7.22) and Eq. (7.23), and the boundedness of $\Pi_{\mathcal{V}_{h_d,0}}$ in $H_0^1(D)$ Bazilevs et al., 2006, it holds

$$\begin{aligned}
\min_{\phi\in\mathcal{V}_{h_d,0}\otimes\mathcal{S}_{h_s}^{p_s}} \|v-\phi\|_{L^2(H_0^1(D);I_Z)} &\leq \left\|v - \Pi_{\mathcal{V}_{h_d,0}}(\Pi_{\mathcal{S}_{h_s}^{p_s}}v)\right\|_{L^2(H_0^1(D);I_Z)} \\
&\leq \left\|v - \Pi_{\mathcal{V}_{h_d,0}}v\right\|_{L^2(H_0^1(D);I_Z)} \\
&+ \left\|\Pi_{\mathcal{V}_{h_d,0}}v - \Pi_{\mathcal{V}_{h_d,0}}(\Pi_{\mathcal{S}_{h_s}^{p_s}}v)\right\|_{L^2(H_0^1(D);I_Z)} \\
&\leq C_d(\mathbf{W}, F)\, h_d \sum_{K\in\mathcal{K}_{h_d}} \|v\|_{L^2(H^2(\tilde{K});I_Z)} \\
&+ \left\|v - \Pi_{\mathcal{S}_{h_s}^{p_s}}v\right\|_{L^2(H_0^1(D);I_Z)} \\
&\leq C_d(\mathbf{W}, F)\, h_d \sum_{K\in\mathcal{K}_{h_d}} \|v\|_{L^2(H^2(\tilde{K});I_Z)} \\
&+ \sum_{i=1}^{d_s} \left(\frac{2eh}{\frac{e\pi}{p_{s_i}+1} + 4h}\right)^{p_{s_i}+1} \frac{\|\partial_{z_i}^{p_{s_i}+1}v\|_{L^2(H_0^1(D);I_Z)}}{(p_{s_i}+1)!}
\end{aligned} \tag{7.25}$$

□

Eq. (7.19) is structurally identical to Eq. (3.7) in Ivo Babuška, Raúl Tempone, et al., 2004, but is specified for splines. In fact, this astonishing similarity is the reason why the following a priori error estimation can be directly adopted for splines.

7.4 Formulation

In the following, the general procedure of the SGIGA is introduced, which delivers a Galerkin variational formulation based approximation, $u_{ds} \in \mathcal{V}_{h_d,0} \otimes \mathcal{S}_{h_s}^{p_s}$, of the solution u of the corresponding strong formulation (7.11), which is an elliptic partial differential equation with d_s-dimensional parameter - cf. chapter 5 in Ivo Babuška, Raúl Tempone, et al., 2004 for the case of SGFEM.

Formulation of the $h-p-k$-SGIGA: The $h-p-k$-SGIGA is the tensor product solution $u_{ds} \in \mathcal{V}_{h_d,0} \otimes \mathcal{S}_{h_s}^{p_s}$, i.e. isogeometric approximations for both the deterministic and stochastic part, such that

$$(u_{ds}, \phi)_E = (f, \phi)_{L^2(D;I_Z)} \quad \forall \phi \in \mathcal{V}_{h_d,0} \otimes \mathcal{S}_{h_s}^{p_s} \tag{7.26}$$

with

$$(u_{ds}, \phi)_E := \int_{I_Z} \int_D k(x,z) \nabla u_{ds}(x,z) \cdot \nabla \phi(x,z) dx f_Z(z) dz \tag{7.27}$$

and

$$(f, \phi)_{L^2(D;I_Z)} := \int_{I_Z} \int_D f(x,z) \phi(x,z) dx f_Z(z) dz \, . \tag{7.28}$$

For practical reasons, the diffusion coefficient $k(x,z)$ and the load coefficient $f(x,z)$ are assumed to be truncated KLE, although the analysis can be generalized Ivo Babuška and Chatzipantelidis, 2002, e.g. PCE could be used instead Ivo Babuška, Raúl Tempone, et al., 2004. Thus, by assumption 1 the diffusion coefficient is bounded, i.e. Ivo Babuška and Chatzipantelidis, 2002; Ivo Babuška, Raúl Tempone, et al., 2004; Deb et al., 2001:

$$k(x,z) \in [k_{min}, k_{max}] \quad \forall (x,y) \in D \bar{\times} I_Z \, . \tag{7.29}$$

7.5 A Priori Error Estimation

Now, the h-p a priori error estimation adopted from Ivo Babuška, Raúl Tempone, et al. (2004) for isogeometric basis function is proposed - the case for maximal-smooth splines is treated. The thoroughly introduced spaces and estimations from chapter 3 for both the deterministic and the stochastic case are now proving to be an advantage. Built on the foundations of section 3.2, proposition 7.3.1 is structurally identical to theorem 3.1

in Ivo Babuška, Raúl Tempone, et al., 2004. Thus, the corresponding error estimates for polynomials and splines, can be easily substituted. In the following, proposition 5.1 and theorem 5.1 from Ivo Babuška, Raúl Tempone, et al. (2004) are rewritten for the isogeometric case. Since the random quantity Z in SGIGA is always an uniformly distributed random vector, the conditions on the density function are satisfied.

Theorem 7.5.1. *Let u be the solution of problem (7.11) and $u_{ds} \in \mathcal{V}_{h_d,0} \otimes \mathcal{S}_{h_s}^{p_s}$ be the $h-p-k$-SGIGA approximation of u defined in (7.26). If $f_Z \in L^\infty$, then for $l = 0, 1$ it holds*

$$\frac{\|E[u(\cdot, Z)] - E[u_{ds}(\cdot, Z)]\|}{\|k f_Z\|_{L^\infty(I_Z \times D)}} \leq C \left(h_d^{2-l} + \sum_{i=1}^{d_s} (c_i)^{2-l} (c_i r_i)^{(2-l)p_{s_i}} \right) \tag{7.30}$$

with

$$c_i(h_{s_i}, p_{s_i}) := \frac{2eh_{s_i}}{\frac{e\pi}{p_{s_i}+1} + 4h_{s_i}} \tag{7.31}$$

and

$$r_i := \sqrt{\lambda_i} \| \frac{\hat{k}_i(x)}{k} \|_{L^\infty}(D; I_Z) \,, \tag{7.32}$$

where λ_i and $\hat{k}_i(x)$ are the eigenvalues and -functions of the KLE of the diffusivity field k. The constant C depends on the domain D, load coefficient f, and diffusion coefficient k, and is independent of deterministic (spatial) grid size h_d, stochastic (spectral) grid size h_s, and stochastic (spectral) order p_s.

Proof. Following the proof in Ivo Babuška, Raúl Tempone, et al. (2004, theorem 5.1) together with proposition 7.3.1, the adjusted spline estimation, results in Eq. 7.30 - attention was paid to ensure compatibility. □

The a priori error estimation assists in choosing the initial parameters for constructing the splines chaos that approximate the stochastic solution. Especially, this is extremely useful for more complex computational models. In general, the question '*which adjustment is most appropriate for the problem posed*' is unsettled for spline approximations due to their versatility. In the context of this contribution, it has been demonstrated pertinently that splines can efficiently approximate random functions in a wide variety of settings. For the one problem, increasing the degree is the appropriate choice, while the other problem is solved more efficiently by knot insertion. It was also shown that continuity over element boundaries is valuable, as well as irregular grids by moving the inner knots. However, determining a sharp approximation constant with respect to all the flexibilities that splines have to offer is a challenging and open problem, which remains the subject of current research Sande et al., 2019, 2020. Also the estimation used here was found only recently Sande et al., 2020. In theorem 7.5.1, a simplified version from the mentioned publication was actually used, which considers maximal-smooth splines and provides an estimate for the simultaneous convergence of p and h. Consequently,

a sharper estimation, say for h only, could be easily derived using the tools already presented. Another point of interest would be the consideration of continuity in the constant in Eq. (7.31).

Coming back to stochastic elliptic PDEs, theorem 7.5.1 can help to decide either an h- or p-refinement is valuable and that for each stochastic dimension, respectively. Everything that must be available for this is the KLE of the diffusion coefficient $k(x, y)$ in order to calculate r_i, given in Eq. (7.32), for each stochastic dimension $i = 1, \ldots, d_s$. Assuming r_i is equal to one, Fig. (7.1) shows the computation of $c_i^{(p_{s_i}+1)}$ in terms of number of refinements for p_{s_i} and h_{s_i}. As can be seen by the slightly slanted ascent, there is a preferred choice in each refinement step. Assuming the same effort, p_{s_i}-refinement is globally preferable to h_{s_i}-refinement here. Locally, this is different in each step. So the strategy here seems to be after 4 p_{s_i}-refinements, to perform h_{s_i}-refinement. In the absence of decision tools like a priori error estimations, guessing would be mandatory unless expert knowledge is available.
To reinforce the need for problem dependent a priori error estimation, consider Fig. 7.2. Number of p_{s_i}- and h_{s_i}-refinements are plotted against the coefficient of the simple error estimation - see Eq. (3.43). The strategy analyst would rather follow the h_{s_i}-

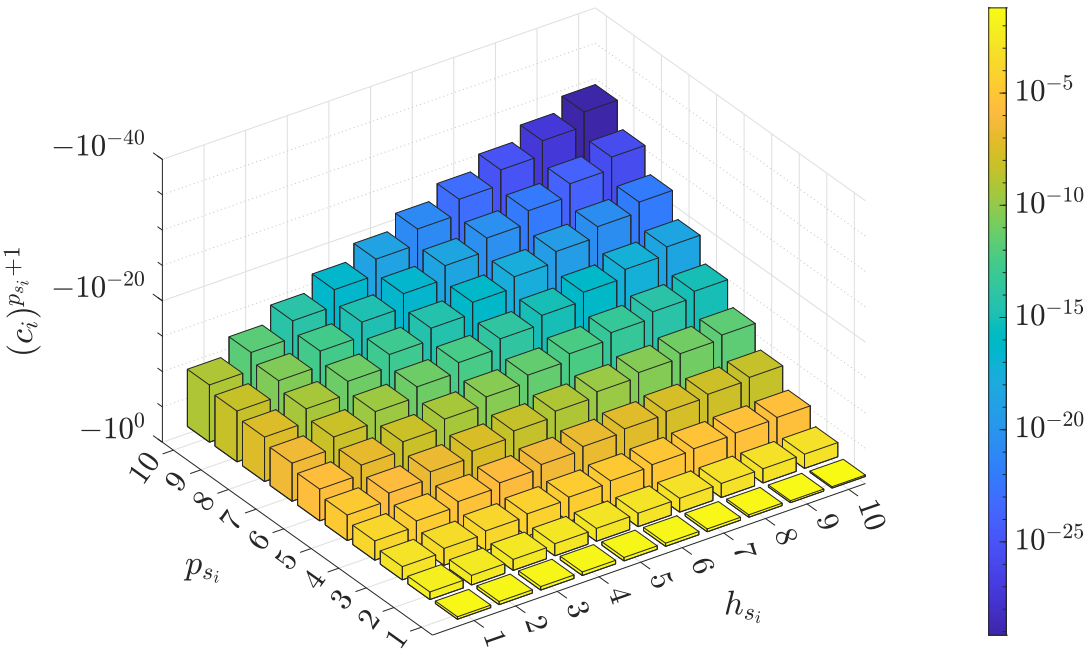

Figure 7.1: A priori error estimation for stochastic elliptic PDEs. Number of p_{s_i}-and h_{s_i}-refinements are plotted against the error constant $c_i^{(p_{s_i}+1)}$.

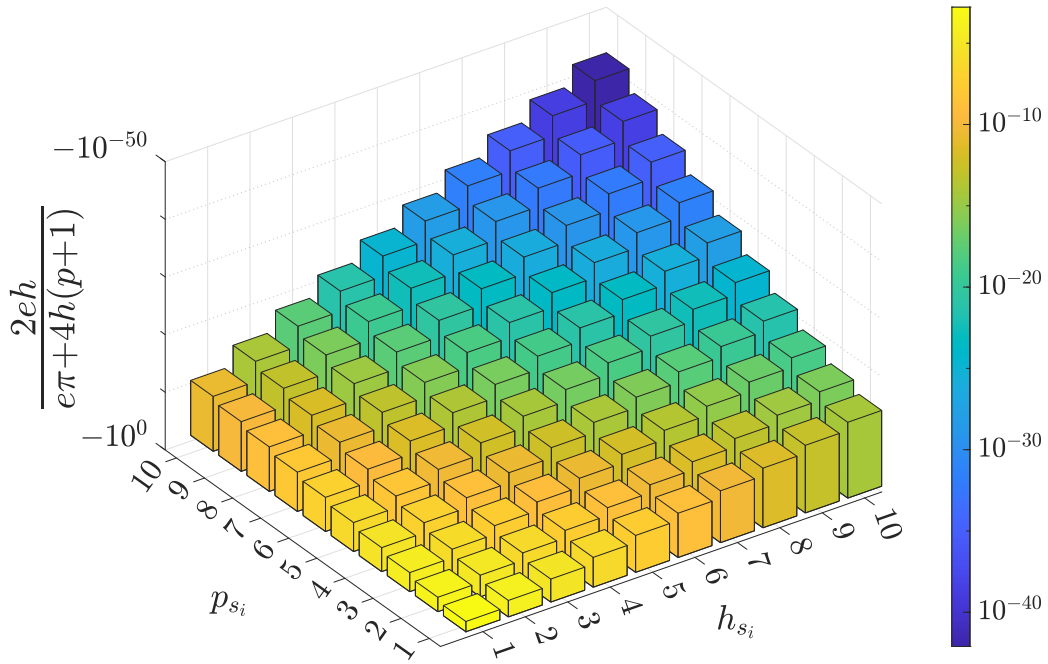

Figure 7.2: Number of p_{s_i}-and h_{s_i}-refinements are plotted against the coefficient of the simple error estimation Eq. (3.43).

refinement in this particular case. This manifests, as well as the many examples in this thesis, refinement strategies cannot be solved in general, but depend on the problem structure and must be decided on a case-by-case basis to achieve highest efficiency. For elliptic problems with random coefficients, the proven error estimation contributes to a more efficient solution procedure in the framework of the new stochastic Galerkin isogeometric analysis.

8 Summary and Conclusions

The present work intends the rigorous development of spline chaos for the purpose of a more efficient stochastic analysis. In this context, the method augments the well-established framework of Wiener-Askey polynomial chaos expansions with the primary goal of uncertainty analysis in practical applications, i.e. the mathematical properties of spline chaos are investigated. In addition, the methodology is applied to the representation of random quantities and solution of various differential equations subjected to different random sources. The main results can be summarized as follows:

- The multidimensional spline chaos for representing stochastic processes has been rigorously introduced, as well as strong convergence proved according to the theorem of Cameron and Martin (1947). For this purpose the space of polynomials $\mathcal{P}_p^d$ of the Wiener-Askey chaos is extended to the space of splines $\mathcal{S}_{\mathbf{p}}$.
- A detailed construction procedure of the one-dimensional spline chaos for the determination of the coefficients was presented. Furthermore, weak convergence was shown, which justifies the general use for practical applications.
- Several random variables are approximated by different chaos expansions and are juxtaposed with each other. It could be shown by numerical examples that spline chaos is a generalization of the Legendre chaos, and thus corresponds to uniform distribution, leading to optimal convergence rates, i.e. exponential.
- The advantage of spline chaos lies in the flexibility of adapting the order, number of stochastic elements, and continuity over element boundaries, which can be quite powerful, especially if the underlying distribution is not specified.
- Afterwards, the accuracy of spline chaos was intensively studied. On the one hand, the connectivity to the uniform distribution could be confirmed. On the other hand, the versatile examples show that the B-spline chaos is competitive by goal-oriented configuration despite Gaussian input. In particular, it could be noted that the B-spline chaos performs well where the Hermite suffers and vice versa. This has also been shown for multi-dimensional random vectors, and applies in particular to the stability of the computation of higher moments. The realization of a stationary Gaussian process by B-spline chaos was also presented.
- It has been found that the smoothness property of B-spline basis functions improves significantly the efficiency when decomposing the random space, which comes to a greater extent if the dimensionality is increased.
- The spline chaos was applied in order to solve stochastic differential equations using a Galerkin type approach. A general procedure of the stochastic Galerkin

method (SG) was presented. In- and Output randomness was modeled by B-spline chaos.

- Then, a stochastic ordinary differential equation with uniform random input was treated. Convergence rates of Legendre, Hermite, and B-spline chaos were evaluated by comparing mean and variance with the exact solution. It was found that, similar to multi-element chaos expansions, the B-spline chaos is suitable for long-term integration problems. Furthermore, it was confirmed that it is a generalization of the multi-element Legendre chaos and is more efficient due to the continuity property over stochastic elements.
- Two examples from the field of stochastic mechanics with one- and multi-dimensional random input type were considered and h-p-convergence were demonstrated. Moreover, the superiority of spline chaos over multi-element Legendre chaos was confirmed due to a higher accuracy with a lower number of basis functions.
- A new method to solve stochastic elliptic boundary value problems (BVP) was rigorously introduced, namely stochastic Galerkin isogeometric analysis (SGIGA). A general procedure was presented were the same function describing the geometry are used to approximate the spatial and stochastic space. The aforementioned spline chaos is involved. The problem was transformed in a multi-parametric deterministic BVP. Note, the method was derived for, but is far from limited to, elliptic BVPs.
- A first sharp a priori error estimation of the mean solution for stochastic elliptic problems for SGIGA was derived. This assists in the efficient use of splines when representing stochastic quantities.
- The method allows $h - p - k$ refinement and can thus surpass the classical polynomial approach. It takes advantage of the fact that smoother splines lead to higher accuracy per degree of freedom.

All shown applications were extensively validated by comparing spline chaos to exact solutions if known, or results from Monte Carlo simulations. On the one hand, this thesis supports the statement that existing PC expansions may fail or converge poorly. On the other hand, it has been pointed out that spline chaos, with appropriately chosen bases, provides significant enhancements and achieves exponential convergence. In particular, for certain problems such as long-term integration, which has already been demonstrated, but also for stochastic discontinuities, sharp non-linearities, abrupt slope changes, or bifurcations, this could be of significant value Stefanou, 2009.
In general, polynomial chaos is shown to be highly efficient compared to sampling methods, in many cases, by two to three orders Xiu, 2010, which justifies the general proliferation of new non-sampling methods such as spline chaos. However, it is a new concept and there remain some open issues. We mention only the most important of them here:

- Like many other numerical methods, spline chaos suffers from the 'curse of dimensionality'. As the dimensionality increases, the number of basis functions

increases rapidly and so do the computational efforts - the efficiency decreases drastically for high dimensional expansions. Sparse spline chaos could be an answer and are currently being investigated. Thereby, the bases that contribute the most are identified and the rest are neglected. But other dimension reduction techniques could be relevant, too.

- Exploiting the role of quadrature formulas has turned out to be very promising. This is underlined by the intensive research in the deterministic field and in efficient spline evaluation in general Giancarlo Sangalli and Tani, 2018. In fact, numerical examples, investigated by the author, have already shown that spline chaos and Hermite chaos provide the same approximation quality for Gaussian inputs if the quadrature points are adjusted in the former case. This is more noteworthy, as spline chaos is not optimized for Gaussian random variables, whereas the Hermite chaos corresponds to them.
- Beta distributions, from whose specialization the uniform distribution emerges, can be a reasonable distribution for parameters due to the limited definition range. An investigation whether there is an extension of the spline chaos, so that it corresponds with the beta distribution, would be interesting.
- Broaden the B-Spline approximation to Non-Uniform Rational B-Splines (NURBS) - commonly used in computer aided design (CAD) and IGA. This may lead to further improvement through increased flexibility and consequently to a reduction in the degrees of freedom.
- Restoring the orthogonality by constructing a dual basis of $B_i(u)$ Bellucci, 2014, i.e. build orthogonal functions $\Psi_{j,p}$, $j = 1, \ldots, N$, such that

$$E_X(N_i(u)\psi_{j,p}(u)) = 0 \quad \text{for } i, j = 1, \ldots, N \; i \neq j \; .$$

  A different approach can be found in the work of Sharif Rahman (2020).
- To let the full potential of spline chaos unfold, it is necessary to clarify exactly which problems can be solved, where polynomials fail. From a current perspective, this is the case where more complex stochastic fields can no longer be well represented via conventional distributions.

In conclusion, B-spline chaos has been shown to be a very promising tool for uncertainty quantification in real applications, as many of the examples in this thesis have demonstrated. From a historical perspective, the long-term goal may be a general spline chaos with sparse structure. The development from Hermite space, over general polynomial spaces to B-spline space indicates this. However, it remains a new concept, and much more research efforts are needed to further exploit its potential.

Bibliography

Adler, Robert J (2010). *The geometry of random fields*. SIAM (cit. on pp. 23, 49).

Anderson, Theodore Wilbur (1958). *An introduction to multivariate statistical analysis*. Vol. 2. Wiley New York (cit. on p. 48).

Askey, Richard and Wilson, James Arthur (1985). *Some basic hypergeometric orthogonal polynomials that generalize Jacobi polynomials*. Vol. 319. American Mathematical Soc. (cit. on p. 26).

Atkinson, Kendall E and Han, Weimin (2009). *Theoretical Numerical Analysis: A Functional Analysis Framework*. Springer (cit. on pp. 33, 34).

Auricchio, F., Beirão da Veiga, L., Hughes, T.J.R., and Reali, A. (2012). "Isogeometric collocation for elastostatics and explicit dynamics". In: *Computer Methods in Applied Mechanics and Engineering* 249-252, pp. 2–14. ISSN: 0045-7825. DOI: 10.1016/J.CMA.2012.03.026 (cit. on p. 4).

Babuška, I., Baumann, C. E., and Oden, J. T. (1999). "Discontinuous hp finite element method for diffusion problems: 1-D analysis". In: *Computers and Mathematics with Applications* 37.9, pp. 103–122. DOI: 10.1016/S0898-1221(99)00117-0 (cit. on p. 42).

Babuška, Ivo and Chatzipantelidis, Panagiotis (2002). "On solving elliptic stochastic partial differential equations". In: *Computer Methods in Applied Mechanics and Engineering* 191.37-38, pp. 4093–4122. ISSN: 00457825. DOI: 10.1016/S0045-7825(02)00354-7. URL: https://linkinghub.elsevier.com/retrieve/pii/S0045782502003547 (cit. on pp. 47, 105, 106, 109).

Babuška, Ivo, Tempone, Raúl, and Zouraris, Georgios E. (2005). "Solving elliptic boundary value problems with uncertain coefficients by the finite element method: The stochastic formulation". In: *Computer Methods in Applied Mechanics and Engineering* 194.12-16, pp. 1251–1294. ISSN: 00457825. DOI: 10.1016/j.cma.2004.02.026 (cit. on p. 103).

Babuška, Ivo, Tempone, Raúl, and Zouraris, Georgios E. (2004). "Galerkin Finite Element Approximations of Stochastic Elliptic Partial Differential Equations". In: *SIAM Journal on Numerical Analysis* 42.2, pp. 800–825. ISSN: 0036-1429. DOI: 10.1137/S0036142902418680 (cit. on pp. 79, 103, 105–107, 109, 110).

Bazilevs, Y, Beirão Da Veiga, L., Cottrell, J A, Hughes, T. J.R., and Sangalli, G (2006). "Isogeometric analysis: Approximation, stability and error estimates for h-refined meshes". In: *Mathematical Models and Methods in Applied Sciences* 16.7, pp. 1031–1090. ISSN: 02182025. DOI: 10.1142/S0218202506001455 (cit. on pp. 25, 39, 41–43, 45, 108).

Bazilevs, Y., Calo, V. M., Hughes, T. J R, and Zhang, Y. (2008). "Isogeometric fluid-structure interaction: Theory, algorithms, and computations". In: *Computational Mechanics* 43.1, pp. 3–37. ISSN: 01787675. DOI: 10.1007/s00466-008-0315-x (cit. on p. 4).

Beck, Joakim, Tamellini, Lorenzo, and Tempone, Raúl (2019). "IGA-based multi-index stochastic collocation for random PDEs on arbitrary domains". In: *Computer Methods in Applied Mechanics and Engineering* 351, pp. 330–350. ISSN: 00457825. DOI: 10.1016/j.cma.2019.03.042. arXiv: 1810.01661 (cit. on pp. 3, 4).

Beck, Joakim, Tempone, Raul, Nobile, Fabio, and Tamellini, Lorenzo (2012). "On the optimal polynomial approximation of stochastic PDEs by Galerkin and collocation methods". In: *Mathematical Models and Methods in Applied Sciences* 22.09, p. 1250023 (cit. on p. 3).

Beckmann, Petr (1973). *Orthogonal polynomials for engineers and physicists*. Golem Press, Boulder, Colorado (cit. on p. 25).

Bellman, Richard (1966). "Dynamic programming". In: *Science* 153.3731, pp. 34–37 (cit. on p. 3).

Bellucci, Michael A. (2014). "On the explicit representation of orthonormal Bernstein Polynomials". In: arXiv: 1404.2293 (cit. on pp. 31, 115).

Boor, Carl de (1972). "On calculating with B-splines". In: *Journal of Approximation Theory* 6.1, pp. 50–62. DOI: 10.1016/0021-9045(72)90080-9 (cit. on p. 37).

Bressan, Andrea and Sande, Espen (2019). "Approximation in FEM, DG and IGA: a theoretical comparison". In: *Numerische Mathematik* 143.4, pp. 923–942 (cit. on p. 44).

Cameron, R. H. and Martin, W. T. (1947). "The Orthogonal Development of Non-Linear Functionals in Series of Fourier-Hermite Functionals". In: *The Annals of Mathematics* 48.2, p. 385. ISSN: 0003486X. DOI: 10.2307/1969178 (cit. on pp. 50, 55, 56, 113).

Cheney, Elliott Ward (1966). *Introduction to approximation theory*. McGraw-Hill (cit. on p. 33).

Chihara, Theodore S (2014). *An Introduction to Orthogonal Polynomials*. Courier Corporation (cit. on pp. 25, 26).

Cottrell, J.A., Evans, J.A., Lipton, S., Scott, M.A., and Sederberg, T.W. (2010). "Isogeometric analysis using T-splines". In: *Computer Methods in Applied Mechanics and Engineering* 199.5-8, pp. 229–263. ISSN: 0045-7825. DOI: 10.1016/J.CMA.2009.02.036 (cit. on p. 4).

Cottrell, J.A., Reali, A., and Bazilevs, Y. (2006). "Isogeometric analysis of structural vibrations". In: *Computer Methods in Applied Mechanics and Engineering* 195.41-43, pp. 5257–5296. ISSN: 0045-7825. DOI: 10.1016/J.CMA.2005.09.027 (cit. on p. 4).

Courant, Richard and Hilbert, David (2008). *Methods of Mathematical Physics: Partial Differential Equations*. John Wiley & Sons (cit. on p. 34).

COX, M. G. (1972). "The Numerical Evaluation of B-Splines". In: *IMA Journal of Applied Mathematics* 10.2, pp. 134–149. DOI: 10.1093/imamat/10.2.134 (cit. on p. 37).

Da Veiga, L Beirao, Buffa, Annalisa, Rivas, Judith, and Sangalli, Giancarlo (2011). "Some estimates for h–p–k-refinement in isogeometric analysis". In: *Numerische Mathematik* 118.2, pp. 271–305 (cit. on p. 36).

Da Veiga, L Beirao, Buffa, Annalisa, Sangalli, Giancarlo, and Vázquez, Rafael (2014). "Mathematical analysis of variational isogeometric methods". In: *Acta Numerica* 23, p. 157 (cit. on pp. 36, 45).

Da Veiga, L Beirao, Cho, Durkbin, and Sangalli, Giancarlo (2012). "Anisotropic NURBS approximation in isogeometric analysis". In: *Computer Methods in Applied Mechanics and Engineering* 209, pp. 1–11 (cit. on pp. 36, 45).

Davis, Philip J and Rabinowitz, Philip (2007). *Methods of numerical integration*. Courier Corporation (cit. on p. 3).

Deb, Manas K., Babuška, Ivo M., and Oden, J.Tinsley (2001). "Solution of stochastic partial differential equations using Galerkin finite element techniques". In: *Computer Methods in Applied Mechanics and Engineering* 190.48, pp. 6359–6372. ISSN: 0045-7825. DOI: 10.1016/S0045-7825(01)00237-7 (cit. on pp. 105, 106, 109).

Deodatis, George (1991). "Weighted integral method. I: stochastic stiffness matrix". In: *Journal of Engineering Mechanics* 117.8, pp. 1851–1864 (cit. on p. 52).

Deodatis, George and Shinozuka, Masanobu (1991). "Weighted integral method. II: response variability and reliability". In: *Journal of Engineering Mechanics* 117.8, pp. 1865–1877 (cit. on p. 52).

Devroye, Luc (1986). *Non-Uniform Random Variate Generation*. Springer New York. DOI: 10.1007/978-1-4613-8643-8 (cit. on p. 16).

Ding, Chensen, Cui, Xiangyang, Deokar, Rohit. R., Li, Guangyao, Cai, Yong, and Tamma, Kumar. K. (2018). "Modeling and simulation of steady heat transfer analysis with material uncertainty: Generalized n th order perturbation isogeometric stochastic method". In: *Numerical Heat Transfer, Part A: Applications* 74.9, pp. 1565–1582. ISSN: 1040-7782. DOI: 10.1080/10407782.2018.1538296. URL: https://www.tandfonline.com/doi/full/10.1080/10407782.2018.1538296 (cit. on p. 4).

Ding, Chensen, Deokar, Rohit R., Cui, Xiangyang, Li, Guangyao, Cai, Yong, and Tamma, Kumar K. (2019). "Proper orthogonal decomposition and Monte Carlo based isogeometric stochastic method for material, geometric and force multi-dimensional uncertainties". In: *Computational Mechanics* 63.3, pp. 521–533. ISSN: 01787675. DOI: 10.1007/s00466-018-1607-4 (cit. on p. 4).

Ding, Chensen, Deokar, Rohit R., Ding, Yanjun, Li, Guangyao, Cui, Xiangyang, Tamma, Kumar K., and Bordas, Stéphane P.A. (2019). "Model order reduction accelerated Monte Carlo stochastic isogeometric method for the analysis of structures with high-dimensional and independent material uncertainties". In: *Computer Methods in Applied Mechanics and Engineering* 349, pp. 266–284. ISSN: 00457825. DOI: 10.1016/j.cma.2019.02.004 (cit. on p. 4).

Ding, Chensen, Tamma, Kumar K., Cui, Xiangyang, Ding, Yanjun, Li, Guangyao, and Bordas, Stéphane P.A. (2020). "An nth high order perturbation-based stochastic isogeometric method and implementation for quantifying geometric uncertainty in shell structures". In: *Advances in Engineering Software* 148. ISSN: 18735339. DOI: 10.1016/j.advengsoft.2020.102866. URL: https://www.sciencedirect.com/science/article/pii/S096599781931186X (cit. on p. 4).

Ding, Chensen, Tamma, Kumar K., Lian, Haojie, Ding, Yanjun, Dodwell, Timothy J., and Bordas, Stéphane P.A. (2021). "Uncertainty quantification of spatially uncorrelated loads with a reduced-order stochastic isogeometric method". In: *Computational Mechanics*. ISSN: 14320924. DOI: 10.1007/s00466-020-01944-9 (cit. on p. 5).

Ditlevsen, Ove and Madsen, Henrik O (1996a). *Structural reliability methods*. Vol. 178. Wiley New York (cit. on p. 2).

Ditlevsen, Ove and Madsen, Henrik O (1996b). *Structural reliability methods*. Vol. 178. Wiley New York (cit. on p. 52).

Dsouza, Shaima M., Varghese, Tittu Mathew, Budarapu, P. R., and Natarajan, S. (2020). "A non-intrusive stochastic isogeometric analysis of functionally graded plates with material uncertainty". In: *Axioms* 9.3. ISSN: 20751680. DOI: 10.3390/AXIOMS9030092. URL: https://www.mdpi.com/784258 (cit. on p. 5).

Engel, David Douglas (1982). *The multiple stochastic integral*. Vol. 265. American Mathematical Soc. (cit. on p. 51).

Evans, John A, Bazilevs, Yuri, Babuška, Ivo, and Hughes, Thomas JR (2009). "n-Widths, sup–infs, and optimality ratios for the k-version of the isogeometric finite element method". In: *Computer Methods in Applied Mechanics and Engineering* 198.21-26, pp. 1726–1741 (cit. on p. 44).

Farin, Gerald E. (1995). *NURB Curves and Surfaces: From Projective Geometry to Practical Use*. USA: A. K. Peters, Ltd. ISBN: 1568810385 (cit. on p. 40).

Farouki, Rida T. (2000). "Legendre–Bernstein basis transformations". In: *Journal of Computational and Applied Mathematics* 119, pp. 145–160. ISSN: 03770427. DOI: 10.1016/S0377-0427(00)00376-9 (cit. on pp. 31, 65).

Feller, William (1968). *An introduction to probability theory and its applications*. 3rd Edition. John Wiley & Sons (cit. on p. 9).

Field, R. V. and Grigoriu, M. (2004). "On the accuracy of the polynomial chaos approximation". In: *Probabilistic Engineering Mechanics*. Vol. 19. Elsevier, pp. 65–80. DOI: 10.1016/j.probengmech.2003.11.017 (cit. on pp. 55, 67–70, 81, 82, 85, 96).

Funaro, Daniele (2008). *Polynomial approximation of differential equations*. Vol. 8. Springer Science & Business Media (cit. on p. 34).

Gardiner, Crispin W et al. (1985). *Handbook of stochastic methods*. Vol. 3. Springer Berlin (cit. on p. 22).

Gentle, James E (2006). *Random number generation and Monte Carlo methods*. Springer Science & Business Media (cit. on pp. 15, 16).

Ghanem, R. and Spanos, P.D. (1993). "A stochastic Galerkin expansion for nonlinear random vibration analysis". In: *Probabilistic Engineering Mechanics* 8.3-4, pp. 255–264. ISSN: 0266-8920. DOI: 10.1016/0266-8920(93)90019-R (cit. on p. 52).

Ghanem, R.G. and Spanos, P.D. (2003). *Stochastic Finite Elements: A Spectral Approach*. revised. Mineola, New York: Dover Publications, INC., p. 222 (cit. on pp. 3, 47–51, 55, 60, 103).

Ghanem, Roger (1999). "Ingredients for a general purpose stochastic finite elements implementation". In: *Computer Methods in Applied Mechanics and Engineering* 168.1-4, pp. 19–34 (cit. on p. 51).

Ghanem, Roger and Spanos, P D (1990). "Polynomial Chaos in Stochastic Finite Elements". In: *Journal of Applied Mechanics* 57.1, pp. 197–202. ISSN: 0021-8936. DOI: 10.1115/1.2888303 (cit. on p. 55).

Gómez, Héctor, Calo, Victor M, Bazilevs, Yuri, and Hughes, Thomas JR (2008). "Isogeometric analysis of the Cahn–Hilliard phase-field model". In: *Computer methods in applied mechanics and engineering* 197.49-50, pp. 4333–4352 (cit. on p. 4).

Gould, Phillip L (1999). *Introduction to Linear Elasticity*. Springer-Verlag (cit. on p. 98).

Grigoriu, Mircea (1995). *Applied non-gaussian processes: Examples, theory, simulation, linear random vibration, and MATLAB solutions(Book)*. Englewood Cliffs, NJ: Prentice Hall, Inc, 1995. (cit. on pp. 22, 81).

Grigoriu, Mircea (2003). *Stochastic Calculus: Applications in Science and Engineering*. Birkhäuser, p. 774. ISBN: 0-8176-4242-0 (cit. on pp. 9, 21–23, 47–49, 57).

Grigoriu, Mircea (2006). "Evaluation of Karhunen–Loève, Spectral, and Sampling Representations for Stochastic Processes". In: *Journal of Engineering Mechanics* 132.2, pp. 179–189. ISSN: 0733-9399. DOI: 10.1061/(ASCE)0733-9399(2006)132:2(179) (cit. on p. 70).

Haji-Ali, Abdul-Lateef, Nobile, Fabio, Tempone, Raúl, and Wolfers, Sören (2020). "Multilevel weighted least squares polynomial approximation". In: *ESAIM: Mathematical Modelling and Numerical Analysis* 54.2, pp. 649–677 (cit. on p. 3).

Hastings Jr, Cecil, Wayward, Jeanne T, and Wong Jr, James P (2015). *Approximations for digital computers*. Princeton University Press (cit. on p. 16).

Hien, T D and Lam, N N (2016). "Investigation into the effect of random load on the variability of response of plate by using Monte Carlo simulation". In: *International Journal of Civil Engineering and Technology* 7.5, pp. 169–176. ISSN: 0976-6316. URL: http://www.iaeme.com/IJCIET/index.asp169http://www.iaeme.com/IJCIET/issues.asp?JType=IJCIET&VType=7&IType=5http://www.iaeme.com/IJCIET/issues.asp?JType=IJCIET&VType=7&IType=5 (cit. on p. 4).

Hien, Ta Duy and Nguyen, Phu Cuong (2020). "Perturbation based stochastic isogeometric analysis for bending of functionally graded plates with the randomness of elastic modulus". In: *Latin American Journal of Solids and Structures* 17.7, pp. 1–19. ISSN: 16797825. DOI: 10.1590/1679-78256066. URL: https://www.scielo.br/j/lajss/a/6KDXj5b4ZMfpLGcKMYyFXzS/abstract/?lang=en (cit. on p. 4).

Hien, Ta Duy and Noh, Hyuk Chun (2017). "Stochastic isogeometric analysis of free vibration of functionally graded plates considering material randomness". In: *Computer Methods in Applied Mechanics and Engineering* 318, pp. 845–863. ISSN: 00457825. DOI: 10.1016/j.cma.2017.02.007 (cit. on p. 4).

Hörmann, Wolfgang, Leydold, Josef, and Derflinger, Gerhard (2013). *Automatic nonuniform random variate generation*. Springer Science & Business Media (cit. on p. 16).

Hughes, T.J.R., Cottrell, J.A., and Bazilevs, Y. (2005). "Isogeometric analysis: CAD, finite elements, NURBS, exact geometry and mesh refinement". In: *Computer Methods in Applied Mechanics and Engineering* 194.39, pp. 4135–4195. ISSN: 0045-7825. DOI: 10.1016/j.cma.2004.10.008 (cit. on pp. 3, 40, 98).

Itô, K. (1951). "Multiple Wiener Integral". In: *Journal of the Mathematical Society of Japan* 2.1 (cit. on p. 51).

Itô, Kiyosi et al. (1984). *An Introduction to Probability Theory*. Cambridge University Press (cit. on p. 9).

Jackson, Dunham (2012). *Fourier series and orthogonal polynomials*. Courier Corporation (cit. on p. 25).

Jahanbin, Ramin and Rahman, S. (2021). "Isogeometric methods for karhunen-loÈve representation of random fields on arbitrary multipatch domains". In: *International*

Journal for Uncertainty Quantification 11.3, pp. 27–57. ISSN: 21525099. DOI: 10.1615/Int.J.UncertaintyQuantification.2020035185. URL: https://www.dl.begellhouse.com/journals/52034eb04b657aea,6849ac9f50c363c1,54f797055666cd22.html (cit. on p. 4).

Jahanbin, Ramin and Rahman, Sharif (2020). "Stochastic isogeometric analysis in linear elasticity". In: *Computer Methods in Applied Mechanics and Engineering* 364. ISSN: 00457825. DOI: 10.1016/j.cma.2020.112928. URL: https://www.sciencedirect.com/science/article/pii/S0045782520301110 (cit. on p. 5).

Jakeman, John D, Franzelin, Fabian, Narayan, Akil, Eldred, Michael, and Plfüger, Dirk (2019). "Polynomial chaos expansions for dependent random variables". In: *Computer Methods in Applied Mechanics and Engineering* 351, pp. 643–666 (cit. on p. 47).

Kaintura, Arun, Dhaene, Tom, and Spina, Domenico (2018). "Review of polynomial chaos-based methods for uncertainty quantification in modern integrated circuits". In: *Electronics* 7.3, p. 30 (cit. on p. 52).

Karatzas, Ioannis and Shreve, Steven (2014). *Brownian motion and stochastic calculus*. Vol. 113. Springer (cit. on pp. 9, 22).

Karhunen, Kari (1947). "Über lineare Methoden in der Wahrscheinlichkeitsrechnung". In: *Amer. Acad. Sci.* 37.I, pp. 3–97 (cit. on p. 49).

Knuth, Donald E (1998). *The art of computer programming: Volume 3: Sorting and Searching*. Addison-Wesley Professional (cit. on p. 15).

Koekoek, Roelof, Lesky, Peter A, and Swarttouw, René F (2010). *Hypergeometric orthogonal polynomials and their q-analogues*. Springer Science & Business Media (cit. on p. 26).

Koekoek, Roelof and Swarttouw, Rene F (1996). "The Askey-scheme of hypergeometric orthogonal polynomials and its q-analogue". In: *arXiv preprint math/9602214* (cit. on p. 26).

L'Ecuyer, Pierre (1994). "Uniform random number generation". In: *Annals of Operations Research* 53.1, pp. 77–120 (cit. on p. 15).

Lemaire, Maurice (2013). *Structural reliability*. John Wiley & Sons (cit. on p. 2).

Li, Keyan, Gao, Wei, Wu, Di, Song, Chongmin, and Chen, Taicong (2018). "Spectral stochastic isogeometric analysis of linear elasticity". In: *Computer Methods in Applied Mechanics and Engineering* 332, pp. 157–190. ISSN: 00457825. DOI: 10.1016/j.cma.2017.12.012 (cit. on pp. 4, 50).

Li, Keyan, Wu, Di, and Gao, Wei (2018). "Spectral stochastic isogeometric analysis for static response of FGM plate with material uncertainty". In: *Thin-Walled Structures* 132, pp. 504–521. ISSN: 02638231. DOI: 10.1016/j.tws.2018.08.028 (cit. on pp. 4, 50).

Li, Keyan, Wu, Di, and Gao, Wei (2019). "Spectral stochastic isogeometric analysis for near stabity analysis of plate". In: *Computer Methods in Apped Mechanics and Engineering* 352, pp. 1–31. ISSN: 00457825. DOI: 10.1016/j.cma.2019.04.009 (cit. on pp. 4, 50).

Li, Keyan, Wu, Di, Gao, Wei, and Song, Chongmin (2019). "Spectral stochastic isogeometric analysis of free vibration". In: *Computer Methods in Applied Mechanics and Engineering* 350, pp. 1–27. ISSN: 00457825. DOI: 10.1016/j.cma.2019.03.008 (cit. on pp. 4, 50).

Liu, Wing Kam, Belytschko, Ted, and Mani, A (1986). "Random field finite elements". In: *International journal for numerical methods in engineering* 23.10, pp. 1831–1845 (cit. on p. 52).

Liu, WK, Belytschko, T, and Mani, A (1986). "Probabilistic finite elements for nonlinear structural dynamics". In: *Computer Methods in Applied Mechanics* (cit. on p. 52).

Liu, Zhenyu, Yang, Minglong, Cheng, Jin, and Tan, Jianrong (2021). "A new stochastic isogeometric analysis method based on reduced basis vectors for engineering structures with random field uncertainties". In: *Applied Mathematical Modelling* 89, pp. 966–990. ISSN: 0307904X. DOI: 10.1016/j.apm.2020.08.006. URL: https://www.sciencedirect.com/science/article/pii/S0307904X20304352 (cit. on p. 5).

Liu, Zhenyu, Yang, Minglong, Cheng, Jin, Wu, Di, and Tan, Jianrong (2020). "Stochastic isogeometric analysis for the linear stability assessment of plate structures using a Kriging enhanced Neural Network". In: *Thin-Walled Structures* 157. ISSN: 02638231. DOI: 10.1016/j.tws.2020.107120. URL: https://www.sciencedirect.com/science/article/pii/S0263823120309940 (cit. on p. 5).

Liu, Zhenyu, Yang, Minglong, Cheng, Jin, Wu, Di, and Tan, Jianrong (2021). "Meta-model based stochastic isogeometric analysis of composite plates". In: *International Journal of Mechanical Sciences* 194. ISSN: 00207403. DOI: 10.1016/j.ijmecsci.2020.106194. URL: https://www.sciencedirect.com/science/article/pii/S0020740320342995 (cit. on p. 5).

Loève, Michel (1948). "Functions aleatoires du second ordre". In: *Processus stochastique et mouvement Brownien*, pp. 366–420 (cit. on p. 49).

Loève, Michel (1977). *Probability Theory*. 4th edition. Springer-Verlag, Berlin (cit. on p. 49).

Luis, Alamilla-López Jorge (2015). "An Approximation to the Probability Normal Distribution and its Inverse". In: *Ingeniería, Investigación y Tecnología* 16.4, pp. 605–611. ISSN: 1405-7743. DOI: https://doi.org/10.1016/j.riit.2015.09.012 (cit. on p. 16).

Lüthen, Nora, Marelli, Stefano, and Sudret, Bruno (2021). "Sparse polynomial chaos expansions: Literature survey and benchmark". In: *SIAM/ASA Journal on Uncertainty Quantification* 9.2, pp. 593–649 (cit. on pp. 3, 48).

Mack, Chris A (2011). "Fifty years of Moore's law". In: *IEEE Transactions on semiconductor manufacturing* 24.2, pp. 202–207 (cit. on p. 1).

Mika, Michal L, Hughes, Thomas JR, Schillinger, Dominik, Wriggers, Peter, and Hiemstra, René R (2021). "A matrix-free isogeometric Galerkin method for Karhunen–Loève approximation of random fields using tensor product splines, tensor contraction and interpolation based quadrature". In: *Computer Methods in Applied Mechanics and Engineering* 379, p. 113730 (cit. on pp. 4, 50).

Moore, Gordon (1965). "Moore's law". In: *Electronics Magazine* 38.8, p. 114 (cit. on p. 1).

Nguyen, HX, Hien, TD, Lee, J, And, H Nguyen-Xuan - Aerospace Science, and 2017, Undefined (2017). "Stochastic buckling behaviour of laminated composite structures with uncertain material properties". In: *Aerospace Science and Technology* 66, pp. 274–283. URL: https://www.sciencedirect.com/science/article/pii/S1270963816305855 (cit. on p. 4).

Ogura, Hisanao (1972). "Orthogonal functionals of the Poisson process". In: *IEEE Transactions on Information Theory* 18.4, pp. 473–481 (cit. on p. 56).

Pavlack, Bruna, Paixão, Jessé, Da Silva, Samuel, Cunha Jr, Americo, and Garcıéa Cava, David (2021). "Polynomial Chaos-Kriging metamodel for quantification of the debonding area in large wind turbine blades". In: *Structural Health Monitoring*, p. 14759217211007956 (cit. on p. 52).

Petromichelakis, Ioannis, Psaros, Apostolos F, and Kougioumtzoglou, Ioannis A (2018). "Stochastic response determination and optimization of a class of nonlinear electromechanical energy harvesters: A Wiener path integral approach". In: *Probabilistic Engineering Mechanics* 53, pp. 116–125 (cit. on p. 53).

Pinkus, Allan (2012). *N-widths in Approximation Theory*. Vol. 7. Springer Science & Business Media (cit. on p. 36).

Rahman, Sharif (2018). "A polynomial chaos expansion in dependent random variables". In: *Journal of Mathematical Analysis and Applications* 464.1, pp. 749–775 (cit. on p. 47).

Rahman, Sharif (2020). "A spline chaos expansion". In: *SIAM/ASA Journal on Uncertainty Quantification* 8.1, pp. 27–57 (cit. on pp. 5, 115).

Rao, Malempati M and Swift, Randall J (2006a). *Probability theory with applications*. Vol. 582. Springer Science & Business Media (cit. on p. 9).

Rao, Malempati M and Swift, Randall J (2006b). *Probability theory with applications*. Vol. 582. Springer Science & Business Media (cit. on pp. 52, 103, 104).

Ripley, Brian D (2009a). *Stochastic simulation*. Vol. 316. John Wiley & Sons (cit. on p. 3).

Ripley, Brian D (2009b). *Stochastic simulation*. Vol. 316. John Wiley & Sons (cit. on p. 15).

Rosenblatt, Murray (1952). "Remarks on a multivariate transformation". In: *The annals of mathematical statistics* 23.3, pp. 470–472 (cit. on pp. 48, 104).

Ross, Sheldon M (1996). *Stochastic Processes*. 2nd Edition. John Wiley & Sons (cit. on p. 22).

Sakamoto, Shigehiro and Ghanem, Roger (2002). "Polynomial Chaos Decomposition for the Simulation of Non-Gaussian Nonstationary Stochastic Processes". In: *Journal of Engineering Mechanics* 128.2, pp. 190–201. ISSN: 0733-9399. DOI: 10.1061/(ASCE)0733-9399(2002)128:2(190) (cit. on p. 81).

Sande, Espen, Manni, Carla, and Speleers, Hendrik (2019). "Sharp error estimates for spline approximation: Explicit constants, n-widths, and eigenfunction convergence". In: *Mathematical Models and Methods in Applied Sciences* 29.06, pp. 1175–1205 (cit. on pp. 6, 36, 44, 45, 103, 110).

Sande, Espen, Manni, Carla, and Speleers, Hendrik (2020). "Explicit error estimates for spline approximation of arbitrary smoothness in isogeometric analysis". In: *Numerische Mathematik* 144.4, pp. 889–929 (cit. on pp. 25, 36, 44, 45, 107, 110).

Sangalli, G., Hughes, T.J.R., Beirão da Veiga, L., Auricchio, F., and Reali, A. (2010). "Isogeometric Collocation Methods". In: *Mathematical Models and Methods in Applied Sciences* 20.11, pp. 2075–2107. ISSN: 0218-2025. DOI: 10.1142/s0218202510004878 (cit. on p. 4).

Sangalli, Giancarlo and Tani, Mattia (2018). "Matrix-free weighted quadrature for a computationally efficient isogeometric k-method". In: *Computer Methods in Applied Mechanics and Engineering* 338, pp. 117–133 (cit. on p. 115).

Schillinger, Dominik, Dedè, Luca, Scott, Michael A., Evans, John A., Borden, Michael J., Rank, Ernst, and Hughes, Thomas J.R. (2012). "An isogeometric design-through-analysis methodology based on adaptive hierarchical refinement of NURBS, immersed boundary methods, and T-spline CAD surfaces". In: *Computer Methods in Applied Mechanics and Engineering* 249-252. Higher Order Finite Element and Isogeometric Methods, pp. 116–150. ISSN: 0045-7825. DOI: https://doi.org/10.1016/j.cma.2012.03.017. URL: https://www.sciencedirect.com/science/article/pii/S004578251200093X (cit. on p. 4).

Schoutens, Wim (2012). *Stochastic processes and orthogonal polynomials*. Vol. 146. Springer Science & Business Media (cit. on p. 26).

Schumaker, Larry (2007). *Spline functions: Basic theory, third edition*. Cambridge University Press, pp. 1–582. DOI: 10.1017/CBO9780511618994 (cit. on pp. 33, 37, 39, 43, 59).

Schwab, Christoph, Schwab, Ch, and Schwab, CH (1998). *p-and hp-finite element methods: Theory and applications in solid and fluid mechanics*. Oxford University Press (cit. on p. 45).

Schwab, Christoph and Todor, Radu Alexandru (2006). "Karhunen–Loève approximation of random fields by generalized fast multipole methods". In: *Journal of Computational Physics* 217.1, pp. 100–122 (cit. on p. 50).

Spanos, P. D. and Ghanem, Roger (1989). "Stochastic Finite Element Expansion for Random Media". In: *Journal of Engineering Mechanics* 115.5, pp. 1035–1053. ISSN: 0733-9399. DOI: 10.1061/(ASCE)0733-9399(1989)115:5(1035) (cit. on pp. 3, 81).

Spanos, Pol D., Beer, Michael, and Red-Horse, John (2007). "Karhunen–Loéve Expansion of Stochastic Processes with a Modified Exponential Covariance Kernel". In: *Journal of Engineering Mechanics* 133.7, pp. 773–779. ISSN: 0733-9399. DOI: 10.1061/(ASCE)0733-9399(2007)133:7(773) (cit. on p. 81).

Stefanou, George (2009). *The stochastic finite element method: Past, present and future*. DOI: 10.1016/j.cma.2008.11.007 (cit. on pp. 49, 55, 70, 85, 114).

Sudret, B and Der Kiureghian, A (2000). "Stochastic finite element methods and reliability. A state-of-the-art-report". In: *Technical Rep. UCB/SEMM-2000/08, Univ. of California, Berkeley, CA* November (cit. on p. 48).

Sudret, Bruno (2007). "Uncertainty propagation and sensitivity analysis in mechanical models–Contributions to structural reliability and stochastic spectral methods". In: *Habilitationa diriger des recherches, Université Blaise Pascal, Clermont-Ferrand, France* 147 (cit. on pp. 1, 2).

Sun, Xiang, Pan, Xiaomin, and Choi, Jung-Il (2021). "Non-intrusive framework of reduced-order modeling based on proper orthogonal decomposition and polynomial chaos expansion". In: *Journal of Computational and Applied Mathematics* 390, p. 113372 (cit. on p. 52).

Szegö, G. (1939). *Orthogonal Polynomials*. Vol. 23. 213. ISBN: 9780821810231. DOI: 10.1090/coll/023 (cit. on p. 25).

Takacs, Stefan and Takacs, Thomas (2016). "Approximation error estimates and inverse inequalities for B-splines of maximum smoothness". In: *Mathematical Models and Methods in Applied Sciences* 26.07, pp. 1411–1445 (cit. on p. 36).

Takada, Tsuyoshi (1990). "Weighted integral method in stochastic finite element analysis". In: *Probabilistic Engineering Mechanics* 5.3, pp. 146–156 (cit. on p. 52).

Tao, Tianyou, Wang, Hao, and Zhao, Kaiyong (2021). "Efficient simulation of fully non-stationary random wind field based on reduced 2D hermite interpolation". In: *Mechanical Systems and Signal Processing* 150, p. 107265 (cit. on p. 49).

Timan, A F (1963). *Theory of approximation of functions of a real variable*. Pergamon Press, Oxford (cit. on p. 33).

Todd, J. (1963). *Introduction to the constructive theory of functions*. Birkhäuser Verlag, Basel (cit. on p. 33).

Van Trees, Harry L (2004). *Detection, estimation, and modulation theory, part I: detection, estimation, and linear modulation theory*. John Wiley & Sons (cit. on p. 50).

Wan, Xiaoliang and Karniadakis, George Em (2005). "An adaptive multi-element generalized polynomial chaos method for stochastic differential equations". In: *Journal of Computational Physics* 209.2, pp. 617–642. ISSN: 0021-9991. DOI: 10.1016/J.JCP.2005.03.023 (cit. on pp. 89, 91).

Wang, Wenpei, Chen, Guohai, Yang, Dixiong, and Kang, Zhan (2019). "Stochastic isogeometric analysis method for plate structures with random uncertainty". In: *Computer Aided Geometric Design* 74. ISSN: 01678396. DOI: 10.1016/j.cagd.2019.101772 (cit. on p. 4).

Wang, Zhiheng and Ghanem, Roger (2021). "An extended polynomial chaos expansion for PDF characterization and variation with aleatory and epistemic uncertainties". In: *Computer Methods in Applied Mechanics and Engineering* 382, p. 113854 (cit. on p. 52).

Wiener, Norbert (1938). "The homogeneous chaos." In: *Amer. J. Math* 60897.4, p. 936. ISSN: 00029327. DOI: 10.2307/2371268 (cit. on pp. 3, 50, 51).

Xiu, Dongbin (2010). *Numerical Methods for Stochastic Computations: A Spectral Method Approach*. Princeton University Press, p. 142. ISBN: 9780691142128 (cit. on pp. 25, 26, 32–35, 47, 48, 51, 55, 60, 61, 64, 89, 114).

Xiu, Dongbin and Karniadakis, George Em (2002). "The Wiener–Askey Polynomial Chaos for Stochastic Differential Equations". In: *SIAM Journal on Scientific Computing* 24.2, pp. 619–644. ISSN: 1064-8275. DOI: 10.1137/S1064827501387826 (cit. on pp. 3, 26, 55–58, 61, 87).

Xiu, Dongbin and Karniadakis, George Em (2003). "Modeling uncertainty in flow simulations via generalized polynomial chaos". In: *Journal of Computational Physics* 187.1, pp. 137–167. ISSN: 0021-9991. DOI: 10.1016/S0021-9991(03)00092-5 (cit. on p. 56).

Zhang, Hongguan and Shibutani, Tadahiro (2019). "Development of stochastic isogeometric analysis (SIGA) method for uncertainty in shape". In: *International Journal for Numerical Methods in Engineering* 118.1, pp. 18–37. ISSN: 10970207. DOI: 10.1002/nme.6008. URL: https://onlinelibrary.wiley.com/doi/abs/10.1002/nme.6008 (cit. on p. 4).

Zhang, Jian, Yue, Xinxin, Qiu, Jiajia, Zhuo, Lijun, and Zhu, Jianguo (2021). "Sparse polynomial chaos expansion based on Bregman-iterative greedy coordinate descent for global sensitivity analysis". In: *Mechanical Systems and Signal Processing* 157, p. 107727 (cit. on p. 52).

Christoph Eckert

Research Assistant

Contact

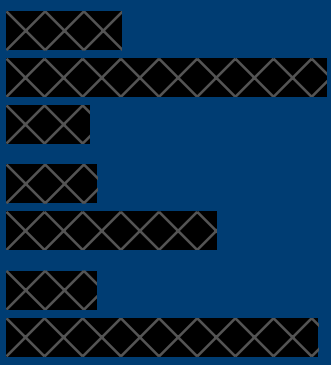

Skills

- Applied mathematics
- Uncertainty Quantification
- Isogeometric Analysis
- Object-orientated programming and modeling
- Mixed dimensional problems in structural analysis
- Evolutionary algorithms (AI)

Software

- Java
- Phython
- JavaScript
- Julia
- C/C++
- MATLAB

Proficient Research Assistant skilled in performing **uncertainty quantification** to facilitate research for **efficient representation and analysis of stochastic fields in partial differential equations**. Versed in completing diverse range of computational research tasks under strict schedules. Familiar with documentation requirements and bringing an organized and precision-minded approach.

Work History

2016-10 - Current

Research Assistant

Institute for Risk and Reliability, Hannover, Germany

- Derived new methods and generated object-orientated frameworks for performing stochastic analysis.
- Attended seminars, symposiums and international conferences to improve overall knowledge and present of own research progresses including one key note.
- Demonstrated strong writing skills to published one paper plus two in preparation, eleven conference papers, two posters.

2014-02 - 2016-10

Teaching Assistant

Institute for Computer Science in Civil Engineering, Hannover

- Lectureship for 'Database systems for engineers', and 'Isogeometric Analysis'.
- Exercise instructor for 'Geometric Modeling & Visualization', 'Stochastic for Engineers', 'Numerics for Engineers'.
- Extensive knowledge in preparation and execution of online and distance learning materials.
- Supervision of 4 master's theses, 5 bachelor's theses, 2 practical projects, 4 seminar papers, 3 project papers.

2010-10 - 2014-01

Student Assistant

Leibniz University Hannover, Hannover

- Supported student learning objectives through personalized and small group assistance in many different institutes.

Languages

German

English

Education

2015-10 - Current

Master of Science: Mathematics

Leibniz University Hannover - Hannover

2012-10 - 2014-10

Master of Science: Computational Engineering

Leibniz University Hannover - Hannover

- Graduated summa cum laude
- Six month at Cardiff University, Wales

2010-10 - 2015-05

Bachelor of Science: Mathematics

Leibniz University Hannover - Hannover

2009-10 - 2013-02

Bachelor of Science: Computational Engineering

Leibniz University Hannover - Hannover

2008-10 - 2009-10

Mathematics in Business

Universität Bielefeld - Bielefeld

Certifications

2019-06 Professionalization of teaching 'Pro Lehre' - 120 working hours

Committee work

Deputy of the research assistants in the faculty council since 2016-01. Voting member on various committees.

Publications and Conferences

Journal Publications:

1. **Eckert, C., Beer, M.; Spanos, P.D. (2020):** A Polynomial Chaos Method for Arbitrary Random Inputs using B-Splines, Probabilistic Engineering Mechanics, 60, Article 103051.
   DOI: **10.1016/j.probengmech.2020.103051**

2. **Eckert, C., Beer, M.; Spanos, P.D.:** On the accuracy of spline chaos approximation. In preparation.

3. **Eckert, C., Beer, M.; Spanos, P.D.:** Stochastic Galerkin Isogeometric Analysis of Elliptic Partial Differential Equations. In preparation.

Conference Proceedings & Abstracts:

1. **Eckert, C.; Beer, M.; Spanos, P. D. (2018):** B-Spline based Polynomial Chaos Approximation for Random Variables, 8th Conference on Computational Stochastic Mechanics, Paros, Greece. (Proceedings)

2. **Eckert, C.; Beer, M.; Spanos, P. D. (2018):** Polynomial Chaos Approximation Using B-Splines, World Congress in Computational Mechanics, New York, USA. (Proceedings & Poster submitted)

3. **Eckert, C.; Beer, M.; Spanos, P. D. (2019):** B-Spline based Polynomial Chaos for Stochastic Galerkin Methods, 2019 EMI International Conference, Lyon, France.

4. **Eckert, C.; Beer, M.; Spanos, P. D. (2019):** On Solving Euler-Bernoulli Beams using a B-Spline based Representation for Random Variables, 8th GACM, Kassel, Germany. (Proceedings & Key Note)

5. **Eckert, C. (2019):** B-Spline Chaos for Random Quantities, 8th GACM, Kassel, Germany. (Poster)

6. **Eckert, C.; Beer, M. (2019):** Systemic Risk Measure in Structural Mechanics, ESREL 2019, Hanover, Germany.

7. **Eckert, C.; Beer, M.; Spanos, P. D. (2020):** B-Spline Chaos: An Isogeometric Approach for Uncertainty Quantification, Eccomas Congress 2020 & 14th WCCM, Virtual Conference.

8. **Eckert, C.; Beer, M.; Spanos, P. D. (2022):** Spline Chaos: An efficient representation of stochastic processes, SIAM Conference on Uncertainty Quantification, Atlanta, Georgia, U.S. (Invited Talk)